THE UNIVERSITY *of* EDINBURGH

The Effect of LS3 Peptide on the Structure of Dioleoylphosphatidylethanolamine Lipid Membrane Formations

by

Farid Sa'adedin

Thesis presented for the degree of Doctor of Philosophy

University of Edinburgh

2014

Abstract

In an attempt to understand the anti-bacterial action of LS3, a synthetic helical peptide (LS3), the interaction of the peptide with a non-lamellar forming lipid dioleoylphosphatidylethanolamine (DOPE) was studied.

Using Differential Scanning Calorimetry (DSC) it was found that the introduction of LS3 at increasing concentrations decreased the phase transition temperature of the DOPE lipid from the lamellar to inverse hexagonal phase by 3°C (Sa'adedin, Bradshaw., 2010). Further studies on the effect that LS3 concentration had on the DOPE lipid system were conducted using Small Angle X-ray diffraction at the ELETTRA Synchrotron in Trieste, Italy. The introduction of LS3 on the DOPE membrane showed that the peptide actively induced or stabilised a number of non-biological lipid structures. In particular, it was clearly shown that two different structures were formed and stabilised in the presence of the peptide over a wide range of temperatures. The level of destabilisation of the biologically stable phase was found to be substantial, with increasing concentration of peptide in the membrane almost eliminating the lamellar phase entirely in the sample. The two different structures that were formed as a result of the introduction of the LS3 peptide varied in size depending on the concentration of LS3 peptide introduced.

LS3 stabilises the inverse hexagonal phase and cubic phases, by reducing the negative curvature stress of these structures, and at high concentrations of LS3 the size of cubic and inverse hexagonal structure is reduced. This can be explained by: the water being removed from the surrounding lipids, resulting in a more

tightly packed inverse hexagonal structure. This is an unexpected result, as LS3 is a peptide that has associated water with it due to the serine amino acids present.

Lastly, I studied the positioning of the LS3 peptide on DOPE bilayers at a molecular level. In order to do this, I used the Membrane Diffractometer (D16) at the Institut Laue-Langevin (ILL) in Grenoble. Testing at two separate LS3 concentrations, I used deuterated labelled LS3 peptide (a heavy Hydrogen) in order to identify the positioning and orientation of the peptide on the DOPE bilayer system. It was found that, at both concentrations, the peptide resided at the lipid/water interface of the membrane at an angle between 4°-6°.

The insertion of the peptide into the lipid, disrupts bilayer stability. The current model in peptide/membrane destabilisation, states that membrane destabilisation correlates to the depth of insertion of a peptide in a bilayer. My results show that the depth of a peptide in the membrane is not required for increased membrane curvature/membrane destabilisation at the lamellar phase as LS3 was located at the lipid/water interface.

ACKNOWLEDGEMENTS

The Royal (Dick) School of Veterinary Studies at Edinburgh University provided the necessary support, guidance and resources for this project.

Data collection was conducted at the Institute Laue-Langevin (ILL), France, ELETTRA Synchrotron Light source, Italy, The National Synchrotron Radiation Center, Taiwan and the Harroun Laboratory, Brock University, Canada and the Roser Membrane Biophysics laboratory, Bath University.

I would like to thank Edinburgh University and Pfizer for sponsoring me and providing the funding for me to carry out this research.

I would like to personally thank the various instrument scientists and fellow colleagues for their invaluable advice and assistance in discussing ideas, data collection and generally being able to tolerate my constant questions during my PhD.

Dr Bruno Deme, the main D16 scientist responsible for maintaining and providing technical and experimental support for the membrane diffractometer.

Prof Michael Rappolt, the main small angle X-ray scientist for maintaining and providing technical and experimental support for the membrane diffractometer

Dr Arwel Hughes, Dr Steve Roser and Dr Robert Barker for being able to use their respective Brewster Angle Microscopy setups at ISIS and Bath University.

Dr Ming-Tao Lee for putting my prepared samples in his X-ray membrane diffractometer instrument in Taiwan and providing me images of said samples.

Special mentions must be made to Dr Heinz Amenitsch, his time and help was invaluable in helping me understand how to use Igor Pro with regards to X-ray analysis. The Harroun laboratory, Prof Thad Harroun and his student Brad Van Oosten for being able to perform energy minimisations on my peptide location results and give a cartoon representation of the orientation and location of the peptide on the membrane.

I am also indebted to all my fellow colleagues at Edinburgh University for all the assistance provided in my research:

Dr Daniel Baptista-Hon: with regards to the preliminary Black Membrane studies that I performed.

Dr Lijing Ke: Lijing has helped me greatly during our time performing experiments together. We worked as a team for our respective projects, providing technical support for each other and being able to cover shifts during our X-ray and neutron diffraction experiments. His kindness, friendship and great humour have brought me constant relief during my time conducting this research.

Prof Jeremy Bradshaw: I have been honoured to have Jeremy as a supervisor and mentor for many years now. He has allowed me to go around the world performing experiments and to be based in China for several months on a PhD exchange program. He has provided great support and encouragement during our years together. His constant compassion, consideration, guidance and patience have been a beacon of strength to me during my PhD studies. It is safe to say, that without his help I would have never been able to reach this stage and submit.

Suffice to say, I am indebted to him for the rest of my life for everything he has done for me.

Finally, I would like to thank my friends and family for being able to put up with me, I know I am not easy at the best of times! A special mention to two friends of mine Dr Khodor Fawaz, he has been able to be there for me, giving me inspiration and hope in me finishing my studies. Dr Donald Thomson, a very old family friend who has known me since I was 5 years old. He has been an incredible source of support and advice over the years, providing wise words of advice on how to best deal with the trial and tribulations of life and has especially helped me a great deal personally over the last few years.

Last but certainly not least; I would especially like to thank my incredible wife Aliaa. She has sacrificed a tremendous amount for me to be able to get to this stage. Without her help and motivation, I would very much doubt I would be at this stage right now and I am able to submit this thesis due to her constant love and support.

So, I humbly dedicate this work to the two most incredible people in my life,

Aliaa and Jeremy.

Thank you both so much for everything.

DECLARATION

I declare that this work in this thesis and how it has been presented is wholly original and written by myself. Any contributions made by others in the thesis have been clearly indicated and acknowledged, either by being referenced in the literature or via research collaborations and engagements. The research was performed under the supervision of Professor Jeremy P. Bradshaw at the University of Edinburgh, United Kingdom and the work has not been submitted to any other institution for any other degrees.

Mr Farid Sa'adedin

Date: 28th April 2014

Table of Contents

Abbreviations

Å – Angstrom

AA – Amino Acid

AgBH – Silver Behenate

AMP - Antimicrobial Peptides

apo A-I - Apolipoprotein A-I

APD – Antimicrobial Peptide Database

BAM – Brewster Angle Microscopy

B. subtilis – Bacillus subtilitis

cis DOPE – 1,2-dioleoyl-*sn*-glycero-3-phosphotidylethanolamine

CL – Cardiolipin

ΔH – Change in Enthalpy

DOPE - 1,2-dioleoyl –*sn*- glycero-3-phosphatidylethanolamine

DOPE-Me – N-monomethylated-dioleoyl-phosphatidylethanolamine

DPoPE - dipalmitoleoylphosphatidylethanolamine

DPPG - 1,2-dipalmitoyl-*sn*-glycero-3-phosphoglycerol

DPPGOG - 1,2-dipalmitoyl-*sn*-glycero-3-phosphoglyceroglycerol

DSC - Differential Scanning Calorimetry

E. coli – *Escherichia coli*

fm – Femto meter

GUV - Giant Unilamellar Vesicles

H_I – Hexagonal phase

H_{II} – Inverse Hexagonal phase

HDL - High Density Lipoprotein

HPLC - High Performance Liquid Chromatography

Ia3d – Inverse Body Centred Cubic

ILL - Institute Laue-Langevin

Im3m – Body Centred Cubic

kHz – Kilo Hertz

L_α - Lamellar phase

L_β - Gel phase

LS3 - LSSLLSLLSSLLSLLSSLLSL

LUV - Large Unilamellar Vesicles

LXD – Lamellar X-ray diffraction

μm – Micro meter

MALDI – TOF – Matrix-assisted Laser Desorption/Ionization – Time-of-Flight

Mass Spectrometer

MLV - Multilamellar Vesicles

MRSA – Methicillin-resistant *Staphylococcus Aureus*

mV - Milli Volts

MVV - Multivesicular Vesicles

NIPAM - Poly(N-isopropylacrylamide)

nm - Nano meter

pA - Pico Amps

PC - Phosphatidylcholine

PE – Phosphatidylethanolamine

PEG - Polyethylene Glycol

PG – Phosphatylglycine

PIPES – Piperazine-N,N'-bis(2-ethanesulfonic acid)

P/L – Peptide/Lipid

Pn3m – Primitive Cubic

P_s – Pico Siemens

PS - Phosphatidylserine

Q – Cubic

q – Momentum Transfer

Q_{II} – Inverse Bicontinuous Cubic Phases

rh – Relative Humidity

σ - Standard Deviation

SAM - Self Assembled Monolayer

SAXD – Small Angle X-Ray Diffraction

SAXS – Small Angle X-Ray

SM - Sphingomyelin

SUV - Small Unilamellar Vesicles

T_h– Lamellar to Non-lamellar phase transition

T_m – Gel to fluid lamellar phase transition

trans DOPE – 1,2-dielaidoyl-*sn*-glycero-3-phosphotidylethanolamine

VdWs – Van der Waals

Chapter 1: Introduction

Background and General Premise to the PhD

The initial idea of this project was founded on a relatively simple concept.

Is it possible to use liposomes to contain, transport and release anti-microbial peptides?

This question is important, due to the limited antibiotics that are currently available. There are worldwide reports of bacteria becoming resistant to the antibiotics. The prevalence of methicillin-resistant *Staphylococcus aureus* (MRSA) bacteria has become a major worry for hospitals, prisons and nursing homes worldwide and includes resistance to various antibiotics including penicillins (methicillin, dicloxacillin, nafcillin, oxacillin) and cephalosporins. Besides taking many years to develop new antibiotics, the cost effectiveness in manufacturing and producing antibiotics means it is not financially viable for many pharmaceutical companies.

Liposomes in Drug Delivery

Initially described in 1961, by Dr Alec Bangham (Bangham and Horne., 1964) when researching blood clotting, liposomes or lipid vesicles are composed of phospholipid molecules of enclosed hydrated lipid bilayers between 15nm to 3000nm in diameter (**Figure 1.1**). There are five main structural classes of liposomes that can be prepared (**Table 1.1**).

Liposomes are unique in that they can be used to encase drugs in an aqueous and lipid phase, which makes liposomes an ideal vehicle for the delivery of hydrophobic and hydrophilic drugs as they can retain their size and shape. Liposomes have already been used as a mechanism of drug delivery in the treatment of cancer, fungal infections, metabolic disorders and gene therapy (Kulkarni, Jaydeep, & Kumar., 2011). They have an advantage of being biodegradable, non-toxic and provide little or no immune response.

Liposome Classification	***Size***	***Lamellae Number***
SUV: Small/sonicated unilamellar vesicles	20nm to 100nm	One
LUV: Large unilamellar vesicles	100nm to 10μm	One
GUV: Giant unilamellar vesicles	1μm plus	One
MLV: Multi lamellar vesicles	200nm to 3μm	Multiple
MVV: Multi vesicular vesicles	200nm to 3μm	Multiple

Table 1.1: The five main classifications of liposomes ranging from nm to μm in diameter, with either a single or multiple lamellae (Leimannova., 2006 pg 283).

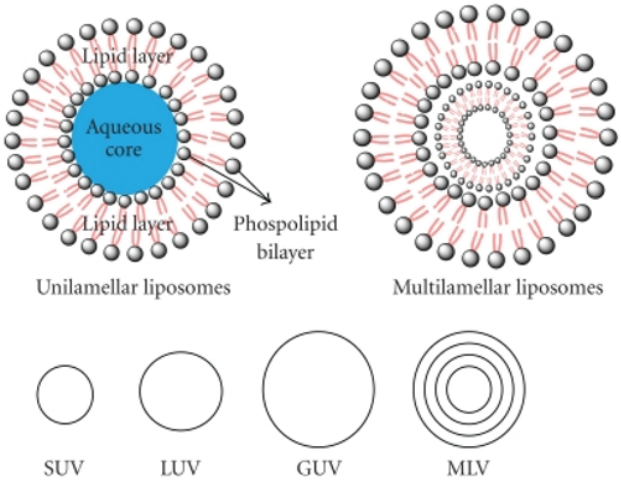

Figure 1.1: Cartoon representation of SUV, LUV, GUV, MLV liposomes. (Taken from: Mishra, et al., 2011)

In order to increase the specificity of liposomes as drug delivery vesicles, the lipid composition can be modified to release its contents at the desired location. Three major examples of lipid modification that have been developed:

1. pH sensitive liposomes
2. Polymer modified liposomes
3. Temperature sensitive liposomes

With regards to pH sensitive liposomes, two mechanisms have predominantly been used. A synthetic polymer, such as poly(2-ethlacrylic acid), or a modified peptide with a carbonyl group is introduced into the membrane (Maeda, Kumano and Tirrell., 1988, Thomas et al., 1994, Kono, Zenitani, and Takagishi., 1994, Meyer et al., 1998 and Bailey et al., 1997).

Further polymer modifications have been used to increase membrane fluidity and stability in the preparation of polymer coated liposomes, for example poloxamer (Jamshaid et al*.,* 1988) and chitosan (Guo et al., 2003). One of the current methods of increasing liposomal circulation time is through the creation of "stealth" liposomes by the addition of poly(ethylene glycol) (PEG) (Klibanov et al*.,* 1990*)*. The addition of polymers into liposome surfaces were used in both pH and temperature modified liposomes.

A History of Temperature Sensitive Liposomes:

First described by Yatvin, (Yatvin. et al., 1980), current liposome formulations have phase transitions between 43°C-45°C. Modification of lipid headgroups has shown promising results in developing a universal thermally-regulated liposome. Lindner (Lindner, et al., 2004) modified the headgroup of 1,2-dipalmitoyl-*sn*-glycero-3-phosphglycerol (DPPG) and added glycerol to make 1,2-dipalmitoyl-*sn*-glycero-3-phosphoglyceroglycerol (DPPGOG). It was shown that incorporation of DPPGOG into the liposome increased circulation time. It has been postulated that this is because the DPPGOG contains free hydroxyl groups that provides stronger hydrophobicity than PEG. The phase transition temperature for this system is close to 40°C which has a narrow transition range like DPPG; unlike PEGlated lipids which have a wider transition range (Lindner et al. 2004).

Using homopolymers and copolymers of poly(N-isopropylacrylamide) NIPAM, they were (Kitano et al., 1994) bound to the liposome surface. They showed that liposomal content release can be activated by increasing the temperature above their lower critical solution temperature of approximately 32°C (Kono, et al., 1999, Hayashi et al., 1996, Hayashi, et al., 1999). The addition of the thermosensitive polymers to the liposomes allowed the hydrophobic and surface charge density to be controlled by the ambient temperature (Hayashi et al., 1998, Kono et al., 1999).

In this study, I focused on modifying the lipid content in the membrane in order to create a temperature sensitive liposome. I wanted to design a liposome system that would be stable at normal body temperature (36.8°C ± 0.4°C) but would become unstable under pyretic temperatures at sites of infection (38.0°C to

41.0°C). In order to construct a viable system, the lipids are required to rearrange in orientation with an increase in temperature. The rearrangement in orientation is associated with a change of phase of the lipid system.

Phospholipids

Phospholipids are one of the major lipid components of a membrane. They are composed of hydrophobic hydrocarbon tails that are connected to a glycerol molecule, which is attached to a hydrophilic phosphate group (**Figure 1.2**).

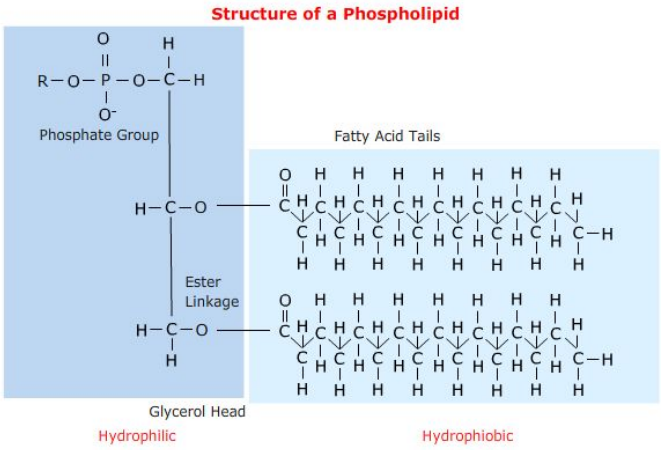

Figure 1.2: Phospholipid basic chemical structure. The hydrophillic section of the lipid contains the phosphate group whereas the fatty acid tails are the hydrophobic part of the lipid. Image taken from (Carnegie Mellon: Department of Biological Sciences) http://telstar.ote.cmu.edu/biology/MembranePage/index2.html (last accessed on 29th October 2013)

In this study, I am using non-lamellar lipids to create temperature sensitive liposomes. This is done so that even a small change in temperature can result in a phase transition of the liposome system from the lamellar phase to inverse hexagonal phase. The non-lamellar lipid I used is 1,2-dioleoyl-*sn*-glycero-3-phosphatidylethanolamine (DOPE) it is a non-lamellar lipid that is known to bend negatively with relative ease and form inverse hexagonal structures (Marsh, 2013., page 383). Specifically, I created liposome systems that have a mixture of *cis* and *trans* DOPE (**Figures 1.3** and **1.4)**. The different isoforms of DOPE have very different T_h (lamellar to non-lamellar) phase transition temperatures. With

trans DOPE, the acyl chains are reoriented; as a result, each acyl chain is relatively parallel to one another. This increases the packing order within the lipid molecules, resulting in greater VdWs attraction between the lipids, therefore increasing the T_h temperature of the *trans* DOPE.

Cis DOPE	*Trans* DOPE
T_h = 10°C	T_h = 64°C

In order to create a liposome system that has a phase transition temperature of around 39°C, a range of liposome mixtures was created with various amounts of *cis* and *trans* DOPE. Using differential scanning calorimetry (DSC), I found that a 50:50 mixture of both isoforms of DOPE was used to create a liposome system that had the desired phase transition temperature. Further details on the liposome creation can be found in the DSC chapter.

Trans Phosphatidylethanolamine:

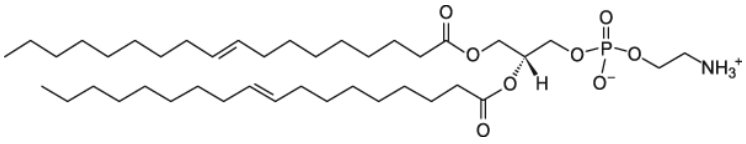

Figure 1.3: Molecular representation of 18:1 (Δ9-*Trans*) PE 1,2-dielaidoyl-sn-glycero-3-phosphoethanolamine. Image taken from Avanti lipids http://avantilipids.com/index.php?option=com_content&view=article&id=566&Itemid=228&catnumber=850726 last accessed on 29th Oct 2013.

Cis Phosphatidylethanolamine:

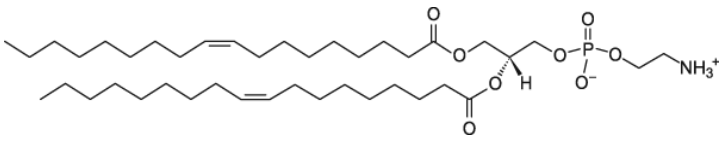

Figure 1.4: Molecular representation of 18:1 (Δ9-*Cis*) PE (DOPE) 1,2-dioleoyl-sn-glycero-3-phosphoethanolamine (image from Avanti lipids http://avantilipids.com/index.php?option=com_content&view=article&id=565&Itemid=228&catnumber=850725) last accessed on 29th October 2013.

Brewster Angle Microscopy:

Using planar lipid systems in order to study lipid interaction on monolayers are ideal for studying the dynamics of LS3 as in general, planar systems mimic the lateral arrangement of lipid in a membrane. The 'flat' surface obtained with this type of system; it can be seen as molecularly comparable to cell surfaces on a membrane as minimal curvature is observed on the system.

Using a Langmuir trough, one can study the air/water interface of the aqueous solutions as models of peptide organisation, membrane interactions with LS3, organisation and disruption of the lipid layers with the interaction of the LS3. To observe the interactions of LS3 on the monolayer, Brewster Angle Microscopy (BAM) is used to capture images of the monolayer at different pressures.

Principle of BAM, using a beam of p-polarised light (p = parallel to the plane of incidence) there is an angle of incidence α, at where no reflection of the p-polarised light occurs. The Brewster Angle is defined as $\tan \theta = n_1/n_2$ where n_1 and n_2 are the respective refractive indices of air and water (Volinsky et al., 2006). When this occurs, the angle of incidence that the light is travelling is transmitted through a surface without any reflection (**Figure 1.5**).

At the Brewster angle, a low reflectivity occurs which shows the image against a dark background. The incident p-polarised light at the Brewster angle is sensitive to the various interfacial structures that are formed, especially the structures observed by a lipid monolayer rearrangement. The p-polarised light illuminates a pure water surface at an angle of 53.1°, which has no reflection (Hönig and

Möbius., 1992). With the introduction of a lipid monolayer, the illumination of the polarised light at the Brewster angle results in the formation of an image (**Figure 1.6**).

BAM is a good visualisation tool for understanding the dynamics of peptide/lipid interaction and behaviour. But one of the limitations of the technique is that it is difficult to analyse quantitively and you have to use the images along with the appropriate surface pressure-area isotherm.

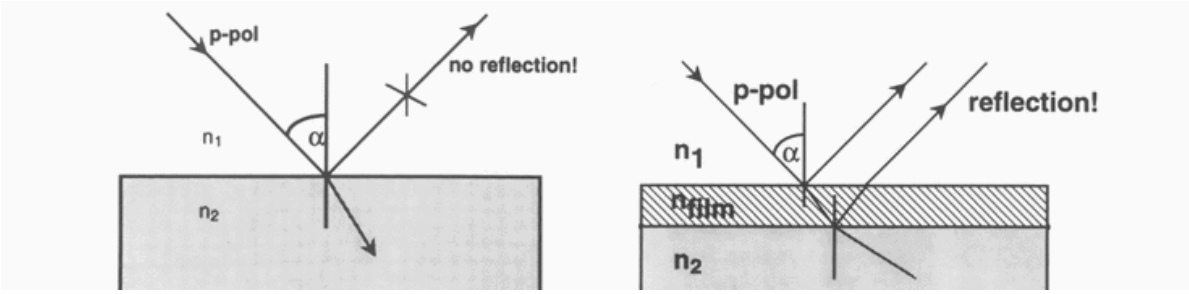

Figure 1.5: Cartoon on the left demonstrates the principle of BAM. The p-polarised light is incident at the interface of the two refractive indicies. When light is reflected at the Brewster angle then no visible light is reflected. The cartoon on the right represents the introduction of a thin lipid film at the n_1/n_2 interface; the angle α is now not at the Brewster angle. Image taken from Kaercher et al., 1993

Materials and Methods:

Synthetic 1,2-Dioleoyl –sn- glycero-3-phosphoethanolamine and 1,2-dielaidoyl –sn- glycero-3-phosphoethanolamine (DOPE *cis*/*trans*; Avanti Polar Lipids, Alabaster, AL) were dissolved in $CHCl_3$ mixed in a 1:1 ratio at a concentration of

1mg/ml. 100µl of lipid solution was added to PIPES buffer (20mM, 150mM NaCl, 1mM EDTA and 0.3mM Sodium Azide at pH 7.4 18.2 Ω) in a 300cm^2 Langmuir trough (NIMA) and measured using a Brewster Angle Microscope at a Brewster angle of 53.15^o. Surface pressure was monitored using a 1cm wide filter paper. Compression was conducted at 10cm^2/min.

LS3 peptide was dissolved in methanol at a 1:25 peptide:lipid molar concentration and added underneath the trough barrier in order for the peptide to associate on the phospholipid head group region of the lipid. Lipid and peptide were allowed to equilibrate for 20 minutes. Experimental runs were carried at 37°C. **Figure 1.6** shows the images of the *cis* DOPE and *cis*/*trans* DOPE monolayers observed using Brewster Angle Microscopy (BAM) the black round domains on the right, are the result of the formation of an uneven monolayer due to aggregation of the more densely packed *cis* DOPE lipid domains on the surface of the monolayer (**Figure 1.7**).

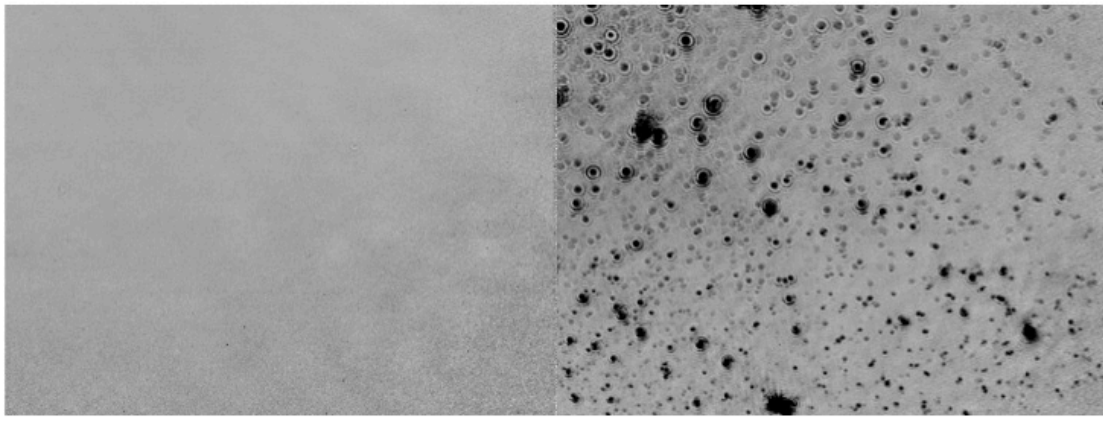

Figure 1.6: Brewster Angle Microscopy image of monolayers of *cis* and *trans* DOPE at 30mN. *Cis* DOPE monolayer displayed on the left. *Cis*/*trans* DOPE monolayer displayed on the right. The horizontal edge of each image corresponds to 430 microns.

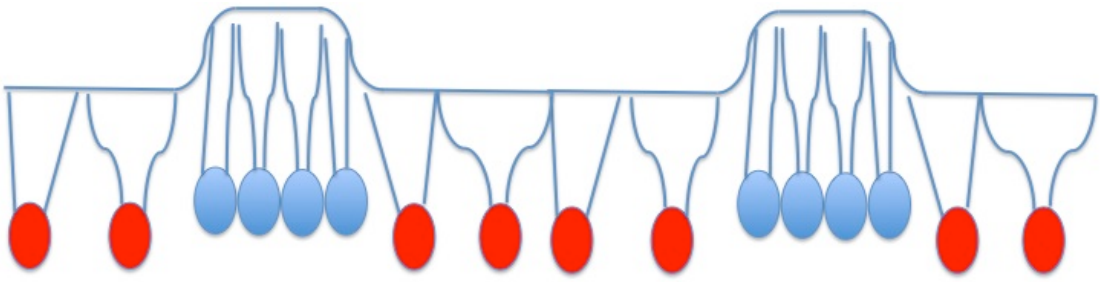

Figure 1.7: Detailed cartoon representation of BAM image of a mixed *cis* and *trans* DOPE monolayer. In the *trans* configuration, the C=C at position 9 of the acyl chain has resulted in a kink in the hydrophobic tail which spreads the tails further apart from each other as compared to its cis configuration. The *cis* DOPE lipids can aggregate close together, due to the tails being able to remain relatively parallel to each other. With the lipid mixture, the *cis* lipids can move up in the monolayer with respect to the *trans* DOPE. The resultant uneven monolayer can be observed using BAM images that I performed as darkened round spots (**Figure 1.6**).

Lipid Phases

Lipids can form different structures during specific temperature ranges; the temperature that is required for the lipid to change structures is called the phase transition temperature (Tristram-Nagle and Nagle., 2004 and Nagle., 1980).

Lipids have a variety of phases and structures that can be formed depending on the type of lipid, temperature, humidity, ions and pressure (**Figure 1.9**).

All lipids can form a solid-state system; a regularly aligned, extremely closely packed structure. This is known as the gel phase (L_β). Upon heating the gel phase, lipids would melt and become more fluid and dynamic because the acyl chains can change into a *trans*/*gauche* confirmation. This is termed the liquid phase/liquid crystalline phase. This particular phase is the most relevant biologically active in membrane biology, as it represents a standard lipid bilayer structure (Israelachvili et al., 1980, Israelachvili et al., 1976,).

Luzzati described the different phases that are observed in lipid systems using small angle X-ray diffraction studies (Luzzati & Husson., 1962 and. Luzzati, and Tardieu., 1974). Upon observation they found that the lipid phases formed highly ordered long ranged symmetrical structures. The flexibility of the dihedral angles on the hydrocarbon tails of the lipid molecules allows multiple orientations; as a result, multiple lipid structures can be formed (**Figures 1.9, 1.10 and 1.11)**.

Lamellar phase

The first structure observed was the lamellar ($L\alpha$) phase, which showed the hydrocarbon chain perpendicular to the lipid/water interface. L denotes the long-range order; in this case it is for a one-dimensional lamellar lattice. The short-range order is denoted by α, which represents a disordered fluid. The lamellar phase is also known as the biologically relevant phase as it represents the majority of stable lipid membranes in prokaryotic and eukaryotic cells (Cullis, Kruijff., 1979) and (Helfrich., 1973).

The lipid chains are continually going through conformational changes (*trans*/*gauche* isomerisations) and on average they are aligned perpendicularly to the membrane plane (Rappolt & Pabst., 2008). As a result, the lipid molecules are free to diffuse laterally, which leads to membrane fluidity. The hydrophobic effect provides membrane stability, as a result this minimises the polar/apolar interface area of each monolayer and counteracts the lateral chain and headgroup pressure respectively. This flexibility in membrane fluidity allows the substantial deformation in the bilayer like bending, stretching, shearing, compression and intermonolayer slip as shown in **Figure 1.8**.

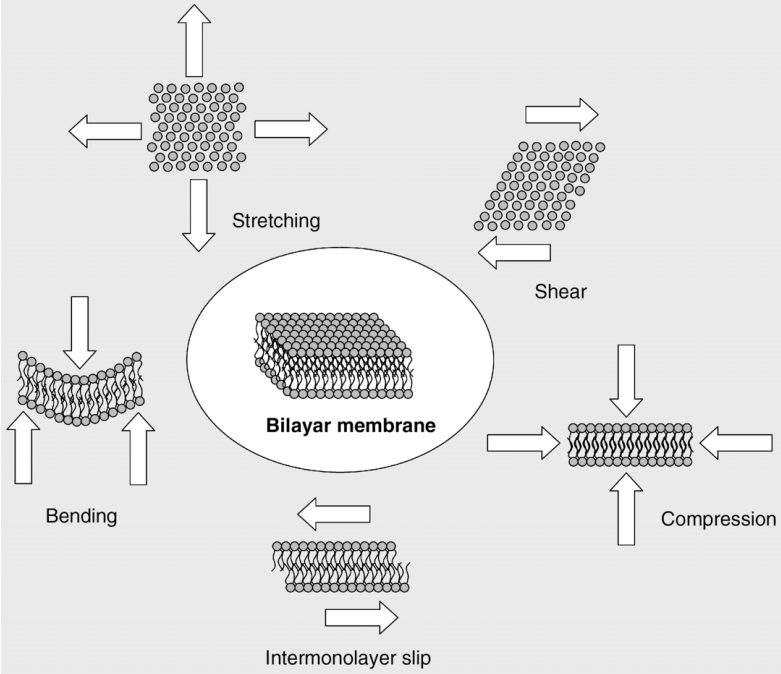

Figure 1.8: Cartoon representation of membrane deformation (Image taken from Rappolt & Pabst., 2008).

Hexagonal Phases

The formation of hexagonal phases is mainly due to lipids with small, relatively weak, hydrated headgroups compared to their wide hydrophobic tails. The shape of the lipid is similar to the shape of an inverted cone (**Figure 1.13**). With the increase in temperature, the bilayer curves negatively (**Figures 1.15** and **1.16**) and this results in an energetically unfavourable orientation that leads to the creation of a more energetically stable inverse hexagonal phase (**Figure 1.9**). The lipid headgroups become closer together and the area per headgroup decreases. This results in the formation of a water pore in between the headgroup. The resultant chains of the lipid molecules are allowed to splay in an outward exposed manner (**Figures 1.13** and **1.14**).

Conversely, if the lipid molecule has a relatively large headgroup region in relation to their acyl chain, then the lipid molecule is in a shape of a cone (***Figures* 1.14** and **1.15**). The lipids bend in a positive direction (***Figure* 1.16**) and the acyl chains come closer together reducing their area whereas the headgroup area has increased and forms circular lipid tubes (Hexagonal phase, H_I) (***Figure* 1.9**).

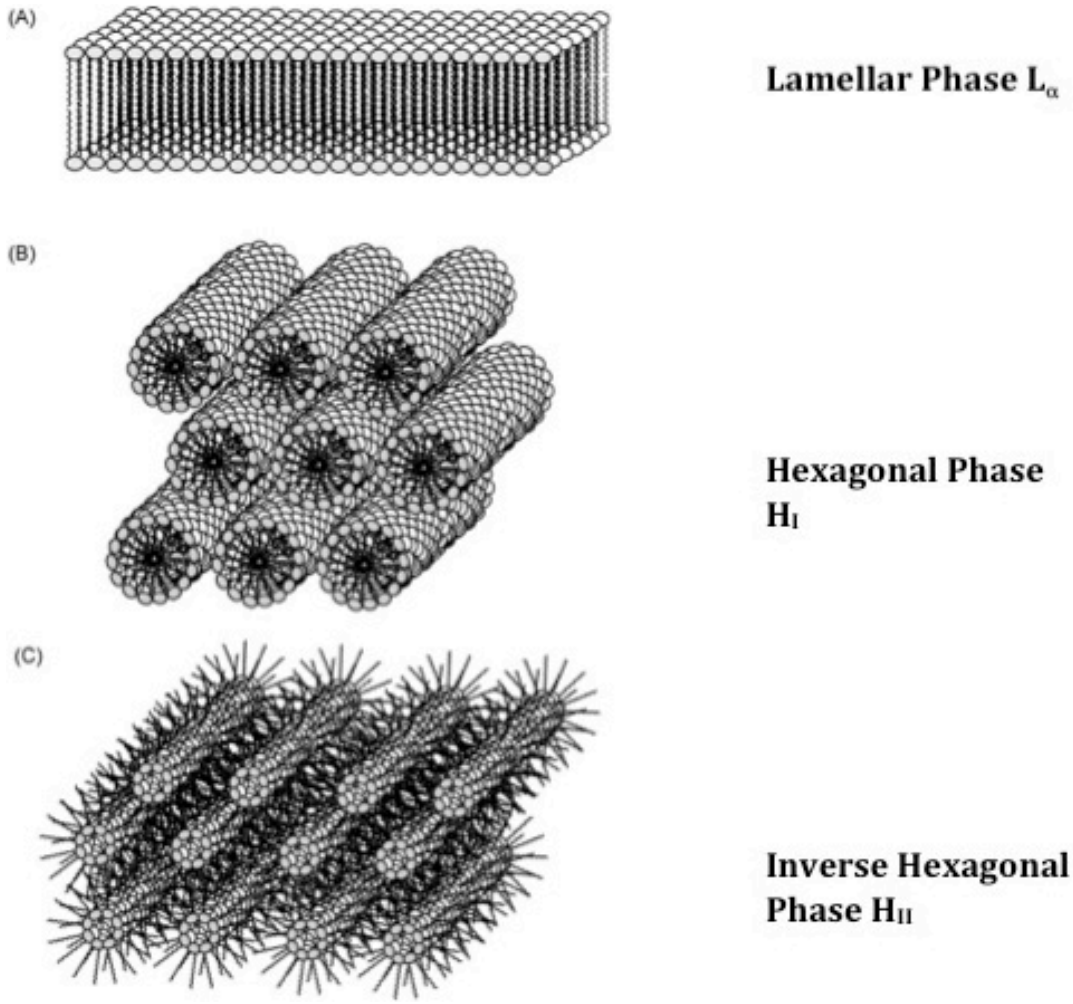

Figure 1.9: The L_α lipid phase (A) has a similar structure to that of a lipid bilayer. The H_I phase (B) and the H_{II} phase (C) are non-lamellar lipid phases. Image taken from (Haney et al., 2009)

Cubic phases

More complicated lipid structures can be formed with non-lamellar forming lipids, such as the inverse bicontinuous cubic phases (Q_{II}). But the most common of cubic phases (Q) that are formed are known as Body Centred Cubic (*Im3m)*, Primitive Cubic (*Pn3m)* and Inverse Body Centred Cubic (*Ia3d)* (**Figures 1.10**, **1.11 1.12)**. With all three cubic phases, the water channel moves through a single-continuous bilayer, which separates equally into two connected but distinct water regions (Gruner., 1989 and Shearman et al., 2006) (**Figure 1.11**).

It had been thought that the formation of cubic phases by non-lamellar forming lipids was a way of minimising the interaction of the water on the headgroups when in the lamellar phase. In reality, the headgroups are even more hydrated than in the lamellar phase. This is because the water is flowing through the channels of the various cubic phases.

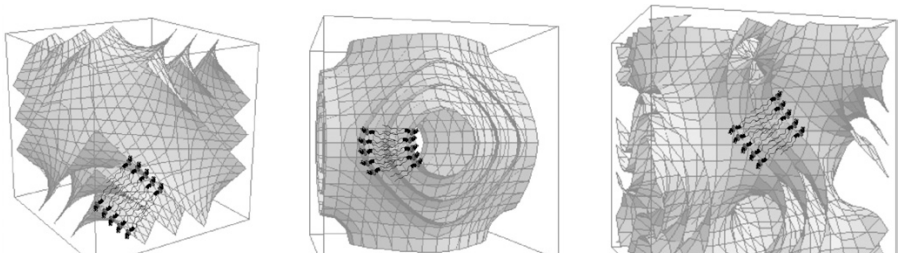

Figure 1.10: Cartoon representations of bicontinuous cubic phases in order of increasingly negative interfacial mean curvature from left to right: (*Pn3m*, *Im3m*, *Ia3d*). Image taken from (Shearman et al., 2006)

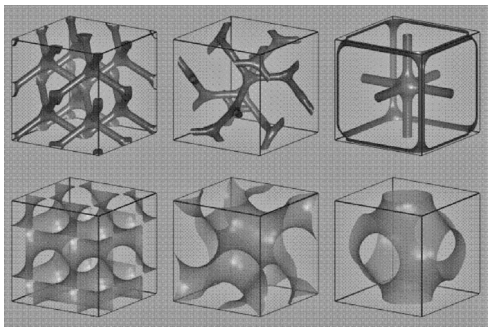

Figure 1.11: Cartoon representation of the three major bicontinuous cubic phases (bottom) and their respective water channels (above). *Pn3m* (left) *Im3m* right and *Ia3d* middle. Image taken from (Marsh., 2013) page 1091

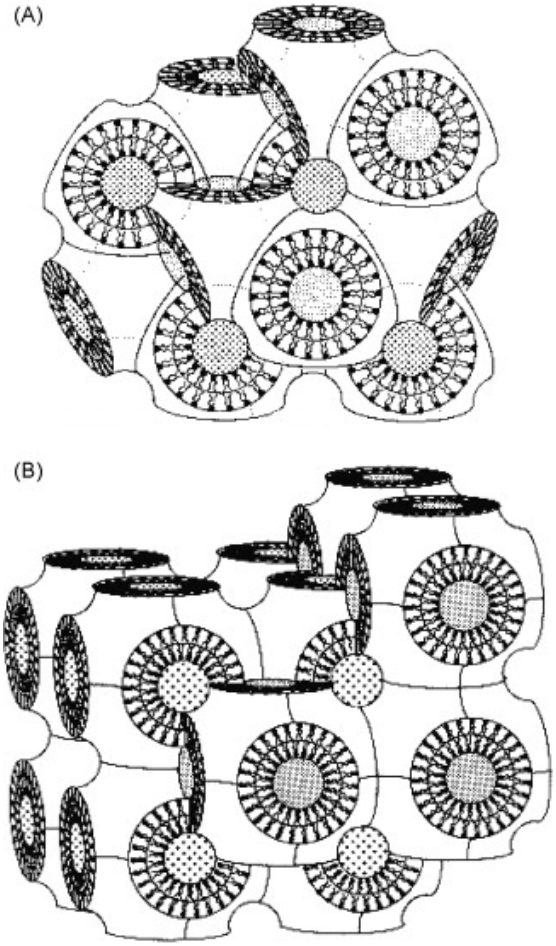

Primitive Cubic:

Pn3m

Body Centered Cubic:

Im3m

Figure 1.12: Three dimensional lattice structure of *Pn3m* (A) and *Im3m* (B) cubic lipid phases. (Image taken from Haney et al. 2009)

Lipid packing variables

What is lipid packing? Simply put, it is how "well" the lipids interact with one another when put in close proximity to each other. To determine how well the lipids can pack together, the shape of the lipid is key. The shape of the lipids is determined by their packing parameter (*S*) (**Equation 1.1**).

Calculating packing parameter

The lipids can be organised by their packing parameters. Packing parameter is defined by:

$$S = \frac{v}{a_0 l_c}$$

S = Packing parameter

v = molecular volume of the chains

a_0 = optimum surface area of the headgroup

l_c = maximum length of the chains

Equation 1.1 (Gruner., 1985)

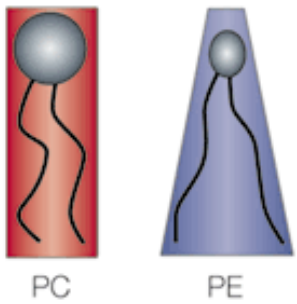

Figure 1.13: Lipid shape depends on relative size of the phosphate group region to the acyl chains. Specifically, if the cross-sectional area of the phosphate group and tail regions are similar, then the lipid shape is similar to a rod as is the case with phosphatidylcholine lipids. In the example of small phosphate group with respect to their acyl chains like phosphatidylethanolamine lipids (PE), then the lipids are shaped like a cone. Image taken from (Sprong et al., 2001).

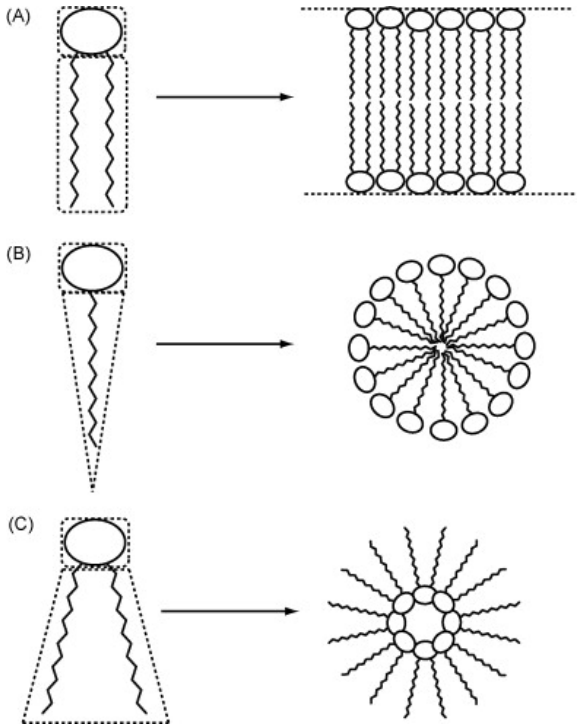

The relationship between lipid shape and the formation of different lipid phases

Figure 1.14: Representation of lipid shape in relation to lipid aggregated structure. Rod shaped lipid molecules (A) form bilayer structures. Cone shaped lipids (B) form micelles or structures with a high positive curvature. Splayed acyl chains in comparison to the lipid head (C) form inverted hexagonal lipid structures with negative membrane curvature (Image taken from Haney, et al., 2010).

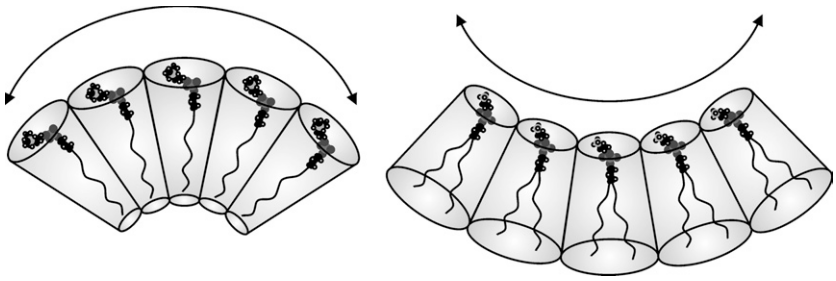

Figure 1.15: Cartoon representing the different shapes of lipids. The shape of the lipids is determined by their packing parameter. If S is less than 1 then a cone shaped lipid (far left) forms. If S is equal to 1 then lipid would be cylindrical in shape (middle). When S is less than 1, then an inverted cone shaped lipid will be formed (Image from Shearman et al., 2006).

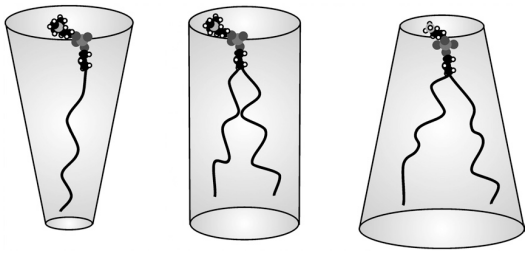

Figure 1.16: Cartoon illustrating the effect of lipid shape on membrane curvature positive (left) and negative (right). (Shearman, et al., 2006)

Since the lipids I am using form curved inverse phases, this is as a result of the packing parameter (*S*) being less than 1, due to the small headgroup area in relation to the tails.

Natural Antimicrobials

The Antimicrobial Peptide Database (APD) contains 2287 antimicrobial peptides (AMPs) (http://aps.unmc.edu/AP/main.php last accessed 23rd April 2014). They are found on the moist skins of amphibians, insects and fish and even on the skin of humans. These are classes of peptides that have various antimicrobial activities on bacteria, fungi and viruses. The problem with using these classes of peptides in clinical use is that, there is no practical mechanism of delivery, because they would be broken down by an immune response and by various proteases. This project was conceived in order to devise a possible stable mechanism of delivery of antimicrobial peptides.

Antimicrobial peptide key facts:

Antimicrobial peptides interact with a membrane forming mainly β-sheet structures or α helicies, the peptides form a secondary structure which may span the thickness of the membrane (Huang., 2000). It has also been shown that both native L-amino acids and D-amino acid enantiomers produced peptides that have antimicrobial properties (Huang., 2000). The mechanism of action of the peptide is not linked to direct interaction to membrane proteins, but instead, with the membrane surface directly. The majority of the antimicrobial peptides that have been classified are anionic; it has been hypothesised that the positive charge on the peptide binds preferentially to the negatively charged membranes of prokaryotes. However, the electrostatic interaction between the peptide and the membrane is not the determining factor of the efficacy of the peptide on the

prokaryotic cell (Almeida & Pokorny., 2009). Using orientated circular dichroism analysis of alamethicin, magainin, protegin-1 and melittin, it showed that the most important feature of the peptides upon binding was the folded helical secondary structures formed with two sides, a hydrophobic and hydrophilic side (Chen, Lee, & Huang., 2002).

Proposed mechanism of action of AMP

Two State Model

The orientation and structure of the peptide was tested at various peptide/lipid (P/L) concentrations using orientated circular dichroism. This resulted in two outcomes:

1) Low P/L concentrations; the peptide is in a helical confirmation, parallel to the bilayer. (**S** state)
2) High P/L concentrations; peptide remains in helical confirmation, but the peptide is reoriented perpendicular to the bilayer. (**I** state)

P/L concentrations that require the change in reorientation of the peptide in the membrane depend on: lipid and peptide composition, hydration, ionic concentration and temperature (Huang., 2000).

In order to do this, I have used a "model" peptide that has very similar chemical and physiological properties to various types of antimicrobial peptides. Initially described by Degrado (Degrado and Lear., 1989), I have used a synthetic peptide 21 amino acids in length. Composed of a repeating sequence of leucine and serine (LSSLLSLLSSLLSLLSSLLSL), the peptide forms a helical structure when bound to

the bilayer (Chung et al. 1992) and a random coil in solution. The resultant helix shows the leucine residues on the hydrophobic side and the serine residues on the hydrophillic side of the helix (**Figure 1.16**).

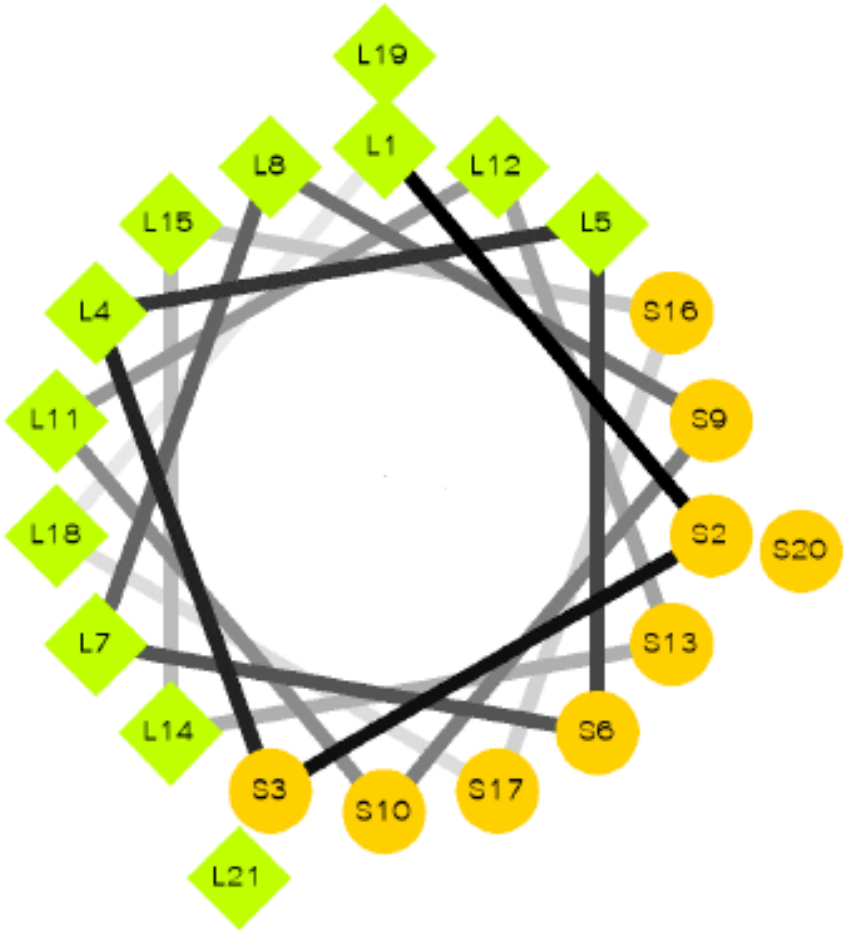

Figure 1.17: Cartoon helical representation of LS3 peptide. Hydrophobic leucine in green and hydrophilic serine in orange.

The benefits of using a leucine/serine repeat peptide in this way is that, when in helical form, the peptide is amphipathic. One side is completely hydrophobic due to the leucine resides, and the other side is hydrophilic due to the serine residues.

Naturally occurring amphipathic helices have been classified into seven separate groups. These groups are selected on the size and charge distribution of the hydrophilic region (Segrest et al. 1990). Focusing on two peptide groups:

1) A class L peptide (Lytic) are classified by having a wide and bulky hydrophobic face with a narrow hydrophilic area containing cationic residues. 2) The other category of peptide is a class A (Apolipoprotein) peptide that contains a narrow apolar region, a narrow anionic region and a wide cationic region.

LS3 is a mixture between the two classes of peptide because with just over 50% of the peptide is apolar and the remainder is cationic. Whereas with class A peptides, they have been shown to stabilise lamellae curvature by removing any positive curvature on the system (Polozov et al. 1997) by residing on the surface of the bilayer. Class L peptides on the other hand has been shown to have the opposite effect to class A peptides and destabilises the bilayer by promoting increased negative curvature on the membrane (Tytler et al. 1993). Simply put, class L peptides are buried into the bilayer and act as a wedge in the lipid. The increase in the negative curvature on the bilayer system and the increase in the membrane disorder, is as a result of the decreasing phase transition temperature between the lamellar to inverse hexagonal phase. Class A amphipathic peptides reside on the surface and act as a supporting rod on the bilayer membrane surface. The peptide essentially flattens the surface of the bilayer and eliminates positive curvature on the lipid system and increases the stability and order of the

membrane, this would result in an increased phase transition temperature between the lamellar and inverse hexagonal phase.

The synthetic antimicrobial peptide I used in my studies, commonly known as LS3 (serine-leucine repeat), was first synthesised by Regan (Regan, and Degrado., 1988) . It was designed to show the most prominent behaviour of AMPs using a simple repetitive structure. It has been shown that the peptide action is voltage dependant and previous studies has proposed that the peptide lies parallel to the bilayer at the headgroup/alkyl chain interface as to minimise hydrophilic/hydrophobic interactions. It is believed that the peptide 'flips' trans-bilayer upon an applied potential difference and aggregates into ion channels to allow ion flow (**Figure 1.18**) (Lear, et al., 1997). I confirmed this flipping behaviour by conducting experiments on black membranes by slowly ramping a potential difference (ramped to -50mV) across a membrane and found that the peptide formed multiple ion channels in the membrane (observed three separate ion channels) (**Figure 1.17**). Measurement of single channels proved difficult, as the lipid bilayer was easily breaking down at low voltage. The results obtained were in agreement to Lear (Lear et al., 1997) but there was insufficient data to produce a stable I/V trace.

Black Membrane

Developed by Mueller and Rudin (Mueller and Rudin., 1962), the black membrane system allows electrodes to be placed either side of a single phospholipid bilayer to measure the electrical conductivity across a membrane. The membrane is

created by painting a phospholipid (I used 50% mixed *cis*/*trans* DOPE) with ethanol across a small opening on a Teflon cup that has immersed in a PIPES buffer solution (1mM EDTA, 150mM NaCl and 0.3 NaN_3 pH 7.4). The single bilayer forms in the hole and electrodes can be placed inside and outside the Teflon cup in order to measure the flow of ions across the system. This system allows for the buffer composition to be modified, as a result the black membrane system can measure the electrical properties of a membrane. The problem with this method in comparison to patch clamping is that there are traces of the solvent in the membrane, which can change the properties and characteristics of the lipid membrane. The other challenges with using the Black Membrane technique are:

1) The bilayer is unstable, as the membrane easily breaks down.
2) The results obtained cannot be compared to results obtained with liposomes systems.

With my lipid preparation, the membrane would readily breakdown before the introduction of the LS3 peptide into the solution. As a result, it was only possible to obtain a maximum 10 second recording of ion channel formation in the membrane, before the bilayer ruptured.

The reason I conducted a preliminary black membrane study was to check the formation of ion channels from my synthesised peptide, by measuring the flow of ions across the membrane. Another reason was to find out more information on the pore formation stability, when an applied potential difference is put across the membrane.

Previous ion channel mathematical modelling studies (Lear et al., 1997., Kienker et al 1994., Kienker and Lear., 1995., Dieckman et al., 1999) have shown that the peptide can insert into a bilayer and aggregate into a voltage sensitive channel under an applied potential difference. A high voltage (±200mV) was used to get to measure single channel peptide recordings through the membrane (Lear et al., 1997). It is unusual to use such a high potential difference to measure single channel recordings because at this voltage the bilayer would break down. The reason why their system was able to take the high potential difference was that they used an incredibly stable lipid to conduct this study (1,2-diphytanoyl-sn-glycero-3-phosphocholine). With my proposed model of peptide delivery and action I wanted to test if a channel formed and was stable under a more physiologically appropriate potential difference of -70mV.

Materials and Method:

Bilayer membranes were formed by the monolayer apposition technique (Kienker et al 1994) across a 50-80μM hole in a Teflon cylinder separating two Teflon chambers. The hole was pre-treated with 1mg/ml solution of L_α PE (this lipid was used in creating the artificial bilayer as it has been known to create a stable bilayer easily) (Avanti Polar Lipids) that was dissolved in N-decane and dried under a stream of N_2(g). 1M solution of KCl filled both of the chambers the Teflon hole was further brushed with L_α PE in-order to form a stable bilayer. Once a stable bilayer had formed (remained intact for 20minutes without breaking down). LS3 peptide

(dissolved in methanol) was added at a concentration of 1:50 of the lipid was added to the outside chamber. LS3 was given 5 minutes to incorporate onto the bilayer, and the voltage was slowly ramped to -50mV. All experiments we conducted at room temperature, 21-23^{o}C, pH 7 at a filtering frequency of 2000Hz.

Results:

Measurement of single channels proved to be difficult because the bilayer kept breaking down at low voltage. This may be because the charges on the N-termini of the helix on our LS3 peptide are unblocked, Kienker et al 1994 and Lear et al., 1997 believed that blocking the N-terminal of the peptide with the acetyl group would stabilise channel formation by reducing the electrostatic repulsion between helices in the pore formation.

The recording seems to indicate that there is more than one channel present in our membrane (represented by O1, O2 and O3 as each of the downward inflections are approximately the same magnitude (O1 = -3.44pA, O2 = -6.69pA O3 = -9.55pA) (**Figure 5**). It indicates that three channels are present, but it could also represent various sub-states of the channel that can be formed due to peptide aggregation. The conductance of the primary opening is 68.8pS (conductance is a measure of ion permeability across a membrane). The results obtained from this trace is in agreement with Lear et al., 1997, but there was insufficient data to produce an I/V trace as the bilayer broke down at a voltage higher than -50mV.

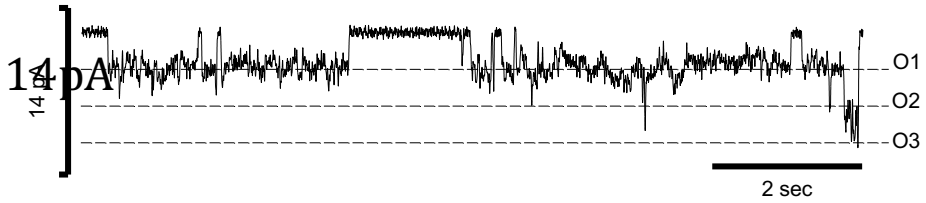

Figure 1.18. Ten second recordings of LS3 channels in 1M KCl pH 7. The channels open downward and the holding potential was at -50mV. Experiments were conducted at room temperature between 21°C-23°C, pH 7 with a filtering frequency of 2.kHz. (O1 = -3.44pA, O2 = -6.69pA O3 = -9.55pA). Conductance of the primary opening was at 68.8pS (conductance is a measurement of permeability of the membrane)

The Lear study showed that a voltage sensitive channel was created and a current of free flowing potassium ions could be measured across the membrane (Lear et al., 1997). Although not as stable as other isolated voltage sensitive ion channels, it showed that there was a potential to create synthetic ion channels by designing peptides that are sensitive to specific membranes, ions and potential differences across a membrane.

This particular study was focused on creating voltage sensitive ion channels, by understanding ion channel pore openings and closings of dynamics of synthetic systems. This allowed another potential use for these synthetic channels, which was initially not considered by the particular researchers.

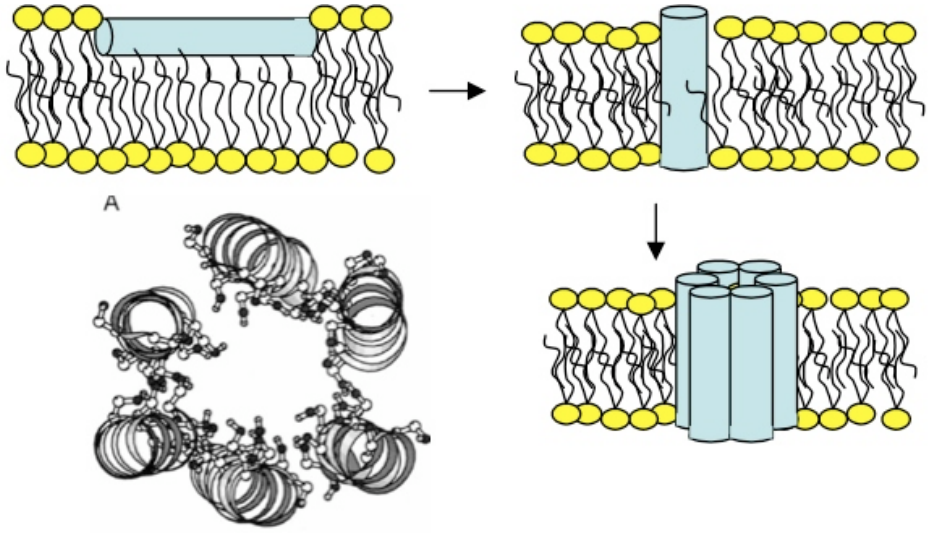

Figure 1.19: Proposed action of LS3 peptide by voltage gating. Initial parallel orientation of peptide with zero potential difference (top left). Peptide 'flips' trans-membrane under a potential difference (top right). Peptide aggregates in a hexamer structure to form a ion channel like structure with the hydrophilic region of the helices lining the channel pore (bottom right and left) (image kindly supplied by Arwel Hughes, ISIS, 2007)

Project Premise and Aims

My project was based on a simple premise: if these small, simple, synthetic peptides can be synthesised easily, form a channel when aggregated, and literally put holes in a membrane for ions to freely flow, then why not take the extra leap and consider these peptides as a potential antimicrobial?

On that principle, I wanted to mimic a simple bacterial membrane. With prokaryotic membranes, they contain a relatively high percentage of phosphatidylethanolamine (PE) lipids compared to an average eukaryotic membrane (**Table 1.2**) (Hickel et al., 2008) and (Epand et al., 1995).

Membrane		% Total Phospholipid			
	PE	PG	CL	PC	SM
E.coli inner membrane	80	15	-	-	-
B.subtilis cell membrane	12	70	4	-	-
Human erythrocyte	29	(13)	-	30	27

Table 1.2: Showing the type and percentage of phospholipid constituents in different cell membranes (data from table obtained from Epand et al., 2006).

These type of lipids are referred to as "non lamellar" lipids. In plain terms, these particular lipids alone do not form biologically stable lamellar membranes. These "non lamellar" forming lipids are required for many functions of the cell including cell division. It has been hypothesised that the fusion and fission of lipid bilayers require "non-bilayer" structures to form during these processes, hence the relative high PE composition in the membrane (Lindblom & Rilfors., 1992). These

lipids give flexibility to the bacterial membrane to bend and curve depending on the environment they are surrounded in. By that rationale, I wanted to create a (PE) membrane system and study the interaction of the synthetic peptide on our model membrane. To do this, I would be using biophysical tools and processes to try and understand the structure and interaction between the peptide on the membrane using, differential scanning calorimetry (DSC) to understand the thermodynamics between the interaction of the peptide and lipid membrane.

X-Ray diffraction and Neutron Scattering:

Mathematically, the collected scattered intensity for X-ray diffraction and Neutron scattering are the same:

$$I(Q) = (\rho_p - \rho_s)^2 \phi_p V_p P(Q)$$

Equation: 1.1: Scattering intensity equation of an elastic signal for X-ray diffraction and Neutron scattering

$I(Q)$ = scattered intensity of the measured elastic signal ρ_p = scattering length density of a particle

ρ_s = scattering length density of a solvent ϕ_p = volume fraction of particles

V_p = volume of the particle

But one variable that is different between the two techniques is the scattering length density:

$$\rho = \frac{\rho_m N_A}{M} \sum_i n_i b_i$$

ρ = scattering length density (of molecular volume) ρ_m = mass density

M = molecular weight b_i = scattering length of atom i

n_i = number of atoms of type $_i$ N_A = Avogadro's Number

X-ray diffraction is due to the photons interacting with the electrons of an atom. The diffraction strength of X-rays is proportional to the atomic weight of an atom, as a result the heavier the atoms the stronger the diffraction. Electrons are diffracted from both atomic electrons and nuclei, and the functions are derived from the electron diffraction patterns from both the atomic electrons and nuclei. The resolution is not necessarily connected to atoms weight; it is connected to the low mosaicity of the lipid system (lower mosaicity is an angular measure of the degree of long-range order and indicates more ordered lipid arrangement and therefore stronger diffraction). The long-ranged order of the lipid lattice is key in having a high-resolution structure achieving a resolution of up to 1Å. The high resolution achieved using X-ray diffraction comes at a price, the consequence of such a technique is that lighter atoms, like hydrogen are essentially considered invisible under X-ray diffraction., even though over protein crystals 80,000 structures have been elucidated using X-ray diffraction (Langan & Chen., 2013). The location and orientation of the hydrogen atoms in those structures are not completely known. Understanding the positioning of the hydrogen atoms in the structure is essential, especially when it comes to looking at enzyme binding sites and general hydrogen bonding.

Neutron diffraction follows the same principles of other particle/wavicle diffraction. Following the same diffraction effects that correspond to the de Broglie wavelength = Plank's constant/neutron momentum ($\lambda = h/mv$). Neutrons are created from a nuclear fission reaction (involving the interaction of a thermal neutron to a ^{235}U), which produces neutrons of high energies. With neutron

diffraction experiments, a liquid nitrogen cooled moderator slows the neutrons. When leaving the reactor, the neutrons have a lower energy state (below 1 keV), the wavelengths of the resultant slowed neutrons are in the 4nm range. The cooled beam is then collimated and monochromatised by a crystal, and the neutrons chosen for the neutron diffraction experiments have been selected by being diffracted from a selected angle at a specified wavelength. The downside is that the neutron flux of the beam from the monochromator is several orders lower in comparison to the X-ray flux. The non-ionising nature of the neutron beam gives an advantage when studying biological materials. The beam causes no damage to the sample and experiments can be conducted over several days without the sample deteriorating unlike X-ray diffraction, where the beam is strongly ionising, and can damage the sample within minutes to exposure to the beam. With Neutron Diffraction, the diffraction occurs from the nuclei of the atoms within the lipid membrane. The consequence of diffraction coming from the nucleus, is that neutron diffraction is sensitive to changes in isotopic nucleus. Exchanging hydrogen for deuterium, increases the neutron scattering on the lipid system. This allows neutron diffraction the advantage over X-ray diffraction by being able to localise specifically labelled hydrogen atoms that are unseen using X-rays. For membrane structure analysis, 8% heavy water is added to the exterior water bath. This is done in order to eliminate the non-coherent scattering of the undeuterated hydrogen atoms in the water. In essence, this is removing the background water scattering and the only coherent scattering comes from the lipid membrane multilayers. The structural models derived from the neutron diffraction are calibrated in units of neutron scattering length density.

With regards to neutron scattering, the neutrons directly interact with the nuclei of the atoms, how much an atom scatters, is defined by the scattering length density, compared to the X-ray definition of form factor. With neutron scattering, the scattering length of hydrogen and deuterium are strong. Hydrogen has a negative scattering length of -3.74fm and deuterium has a scattering length density of +6.67fm. Hydrogen scattering has a large incoherent scattering resulting in the scattering background, which reduces the diffracted intensities. Using deuterated water (^2H_2O) solutions with the prepared samples, this is done to replace any exchangeable hydrogen with deuterium. The result would be a reduced background scattering and a clearer coherent scattering that would provide higher resolution models. The combination of X-ray diffraction and neutron scattering can refine and make more accurate structural models.

Chapter 2: Measuring the Phase Transition Temperatures and Enthalpies of LS3/Liposome System using Differential Scanning Calorimetry

Aims of the chapter

Design a mixture of *cis*/*trans* DOPE lipid that has a phase transition temperature in the region of hyperpyrexia of 40°C-42°C.

Record any differences in the phase transition temperature and change in enthalpy with the introduction of LS3 peptide.

To study the effect of the interaction that LS3 peptide has on the thermodynamic properties of the lipid MLV mixtures.

Introduction

Differential Scanning Calorimetry (DSC):

Understanding the dynamic properties of the membrane mobility is temperature dependent. The use of DSC is to understand the different forms of thermal transitions that are dependent on measuring the phase transitions formed.

DSC is used to measure the heat of transition. It allows the study of the dynamic properties of lipids during their various phase morphological changes. Lipid mobility and structural changes is temperature dependent and by using DSC we can analyse the thermal properties during the phase transitions.

Principles of DSC:

Specifically, it measures the change in enthalpy. The observed heating curves are measured and the area under the curve measures the total amount of energy required (an endothermic event). If the sample were cooled, the resultant cooling curve would measure the exothermic energy released. The heating or cooling of a substance will maintain a constant temperature during a phase transition as the energy absorbed by the in breaking Van der Waals forces (VdWs) or energy is released during the formation of VdWs during atom aggregation. To accurately measure the thermotrophic profile of a sample, a control reference is also heated and cooled at the same rate as the sealed sample. The heat flow between the two samples is maintained constant until a change of phase occurs within the sample. The temperature of the sample remains the same until it has melted whilst the

reference temperature continues to rise in temperature and energy difference between the two samples is directly measured.

Objectives:

One of the main objectives early on in this study was to formulate a lipid mixture that would have a phase transition temperature within the region of (40°C -42°C). This localised increase in temperature is created as a result of an infection from bacteria and viruses in a host cells. In order to determine the phase transition temperature and thermodynamics of our lipids mixtures, I used a differential scanning calorimeter to measure these values. DSC allows us to indirectly measure the stability of my membrane system by measuring the thermotropic behaviour of PE multilamellar vesicles (MLVs) with and without the addition of LS3 peptide at various concentrations.

Since I wanted to obtain a phase transition temperature between 40°C -42°C, I used non-lamellar forming lipids that have two clear distinct phase transition temperatures (L_α – H_{II}). Specifically, I focused on using a mixture of *cis* and *trans* DOPE as it was found that both isomers of the lipid have a wide range of phase transition temperatures.

Cis DOPE	*Trans* DOPE
T_m: -16°`C	T_m: 38°`C
H_{II}: 10°`C	H_{II}: 64°`C

Experimental Materials and Methods

Synthetic 1,2-dioleoyl-*sn*-glycero-3-phosphatidylethanolamine (*cis* DOPE) and 1,2-dielaidoyl-*sn*-glycero-3-phosphatidylethanolamine (*trans* DOPE) were purchased from Avanti Polar Lipids (Alabaster, AL) and used without further purification. Synthetic peptide (LS3) was synthesised by ALMAC Sciences (Edinburgh, UK) to the sequence NH_2LSSLLSLLSSLLSLLSSLLSL-COOH.

Multilamellar vesicles (MLVs) were prepared by dissolving appropriate PE mixtures in chloroform. Thin lipid films were created by evaporating the chloroform, using a gentle stream of nitrogen gas. For the peptide-containing samples, LS3 peptide was dissolved in methanol and appropriate amounts were added to the DOPE mixtures to produce a range of peptide: lipid molar ratios. Thin lipid films were desiccated under vacuum for 6 hours to remove any residual solvent. An appropriate amount of PIPES buffer (1mM EDTA, 150mM NaCl and 0.3 NaN_3 pH 7.4) was added to obtain an equivalent of 50mg/ml of lipid. Lipid dispersions were sonicated for a period of five to ten minutes, vortexed thoroughly and freeze thawed with liquid nitrogen. The cycle of sonication, vortexing and freeze thaw was repeated six times. Throughout the procedure the temperature of the lipid dispersions was kept above the melting temperature of the lipids.

Differential Scanning Calorimetry

Differential scanning calorimetry measurements were performed using a Perkin Elmer Pyris1 calorimeter. 20μl of 50mg/ml liposome dispersion was dispensed into a sealed aluminium can and placed inside the sample cell. All samples were run in conjunction with a 20μl PIPES buffer reference sample. Samples were equilibrated at 2°C for two minutes and then heated at 20°C per minute from 2°C to 80°C (The scans were performed at 20°C per minute because the model of the calorimeter that was used is more sensitive and accurate during a high heating rate). Each cycle was repeated five times. DSC data were recorded using the Perkin Elmer data software package and were analysed and plotted using the Microsoft Office Excel package.

Results

Calculation of phase transition temperatures of *cis*/*trans* DOPE mixtures

I calculated the phase transition temperatures of various mixtures of *cis*/*trans* DOPE (**Figure 2.1**) to find out which ratio of *cis*/*trans* DOPE had a phase transition temperature within the zone of pyrexia.

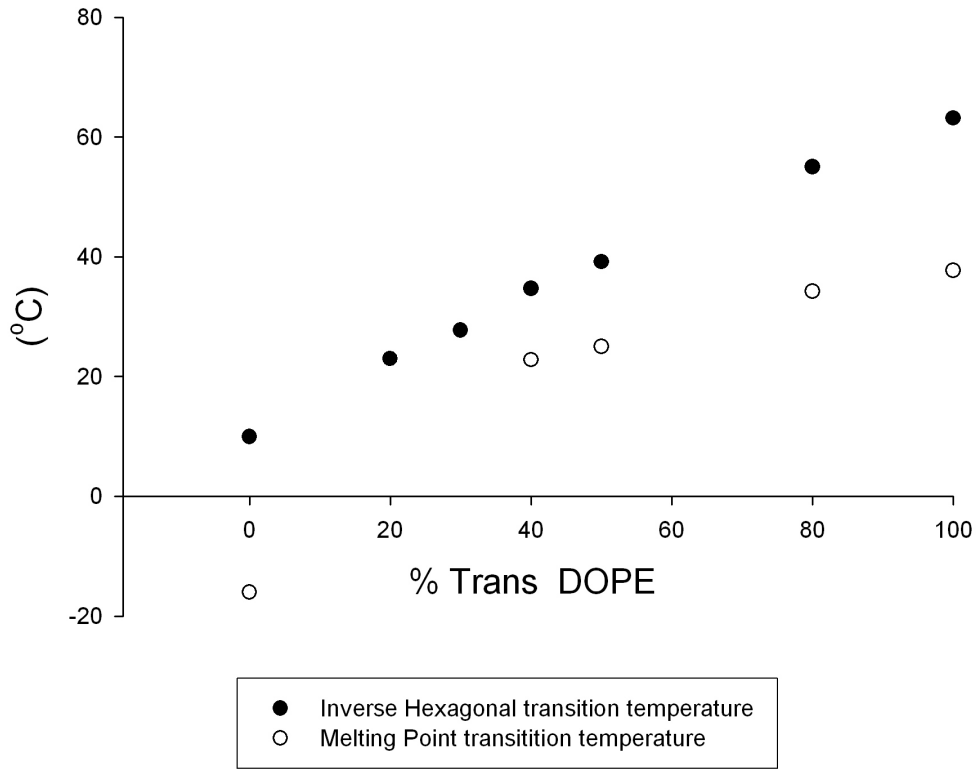

Figure 2.1: Inverse hexagonal and melting temperatures of the different compositions of *cis* and *trans* DOPE.

I found that the 60% *cis* and 50% *cis* DOPE mixtures had a phase transition temperature of 35.7˚C and 40.3˚C respectively.

Introduction of LS3 on lipid system and effect on phase transition temperature

I used peptide to lipid molar ratios 1 to 200, 1 to 100, 1 to 75, 1 to 50, 1 to 33 and 1 to 25.

Although the local concentration of the peptide to lipid could vary due to independent interaction with each layer of the MLV, DSC measures the relative change in enthalpy over the entire sample and reports from the average peptide: lipid value for the whole sample. Each sample contains hundreds of multilayers stacks, so the method provides a relatively accurate enthalpy for each peptide/lipid concentration. For the majority of scans, depending on composition of PE and peptide ratio, two endothermic peaks were identified. A relatively sharp melting point transition and a smaller, broader $L_\alpha - H_{II}$ phase transition. In this study I focused on the data obtained from the $L_\alpha - H_{II}$ phase transition.

My original hypothesis stated that the introduction of LS3 into the lipid system would stabilise the lamellar phase by increasing the phase transition temperature of the lipid system (Polozov et al. 1997).

However, when introducing LS3 into our mixed DOPE MLV system I noticed that the phase transition temperature decreased (**Figure 2.2**). At 50% *cis,* the phase transition temperature decreased by 2.76˚C whereas at 60% *cis,* the temperature decrease was only 1.27˚C over the same LS3 concentration range (**Figure 2.2**). During this phase transition, the enthalpy of the 50% and 60% *cis* varies considerably during the peptide range of 1 to 4 mol%. At 2 mol% LS3, the enthalpy divergence is at its greatest. At 50% *cis* PE, the enthalpy is 82.2 J/mol compared

to 60% *cis* PE where the enthalpy is at 154.2 J/mol (**Figure 2.3**). During these enthalpy changes, the width of the transition peak was measured as it relates to sample uniformity of the LS3/PE system, (**Figure 2.4**)

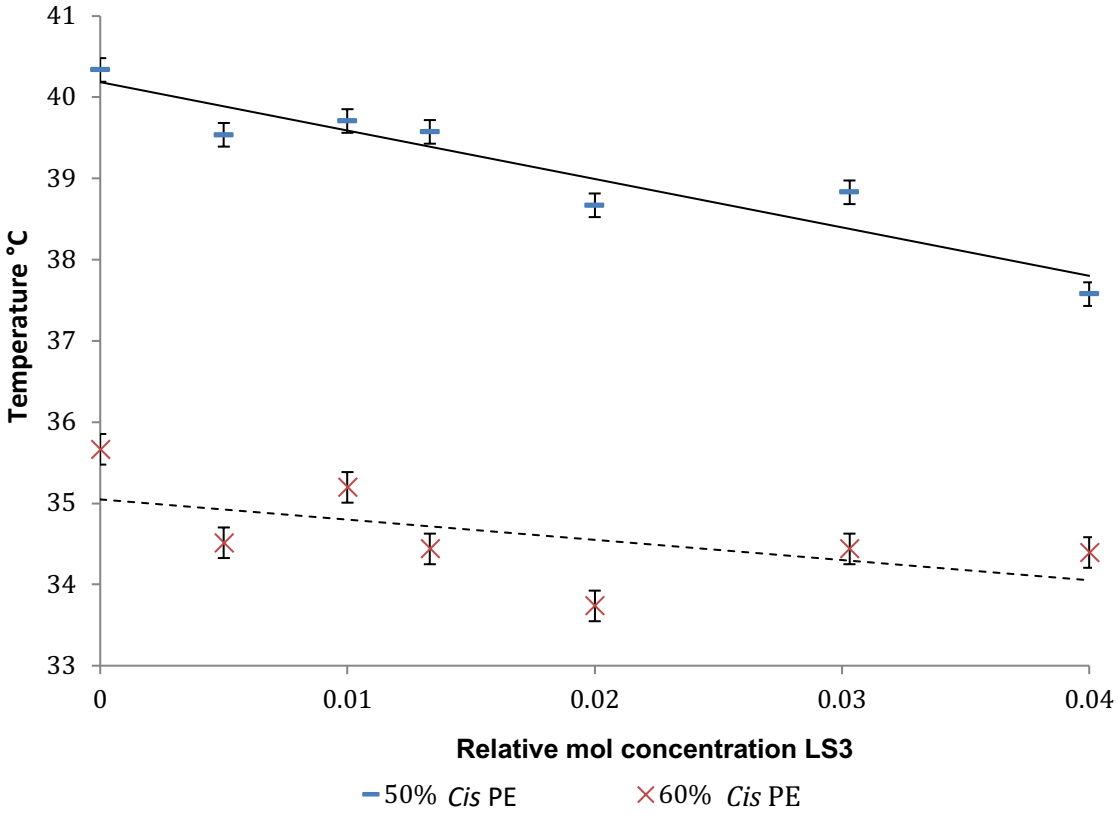

Figure 2.2: The effect of LS3 concentration on T_h of PE bilayers containing 50% and 60% *Cis* PE. The T_h of 50% and 60% *cis* PE mixtures decreased from 40.3°C and 35.7°C (without LS3) to 37.6°C and 34.4°C (0.04 relative mol concentration LS3) The rate of change in T_h 50% *cis* PE, the gradient of the line is -60°C/mol whereas at 60% *cis* it is -25°C/mol. Error bars represent the standard deviation of the mean calculated form each lipid mixture data set. Standard deviation of the mean is calculated by first calculating the standard deviation: $\sigma = \sqrt{\frac{1}{\mathrm{N}}\sum_{i=1}^{N}(x_i - \mu)^2}$. The standard deviation of the mean is then calculated using $\sigma_{mean} = \frac{\sigma}{\sqrt{N}}$ N in this case being the calculated mean from the data obtained via DSC.

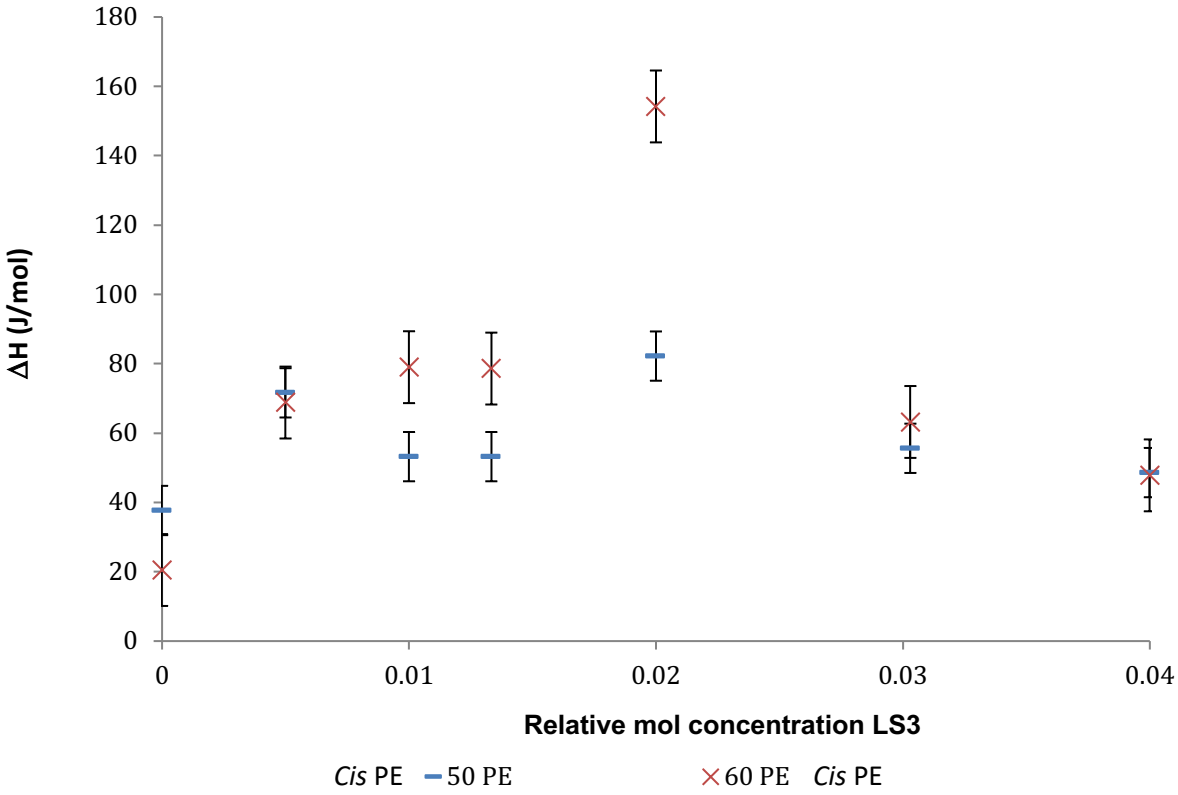

Figure 2.3: Enthalpy of the L_{α} – H_{II} phase transition containing 50% and 60% *cis* PE as a function of LS3 concentration.

The ΔH for 50% *cis* PE increases by 54.5% from 53.2 J/mol (0.013 relative mol concentration LS3) to 82.2 J/mol (0.02 relative mol concentration LS3). With 60% *cis* PE, the ΔH increases by 96.2% from 78.6 J/mol (0.013 relative mol concentration LS3) to 154.2 J/mol (0.02 relative mol concentration LS3). Increasing the concentration of LS3 in the lipid mixtures to 0.03 relative mol concentration LS3 decreased the ΔH of 50% and 60% *cis* PE by 32.4% and 59% respectively (**Figure 2.3**).

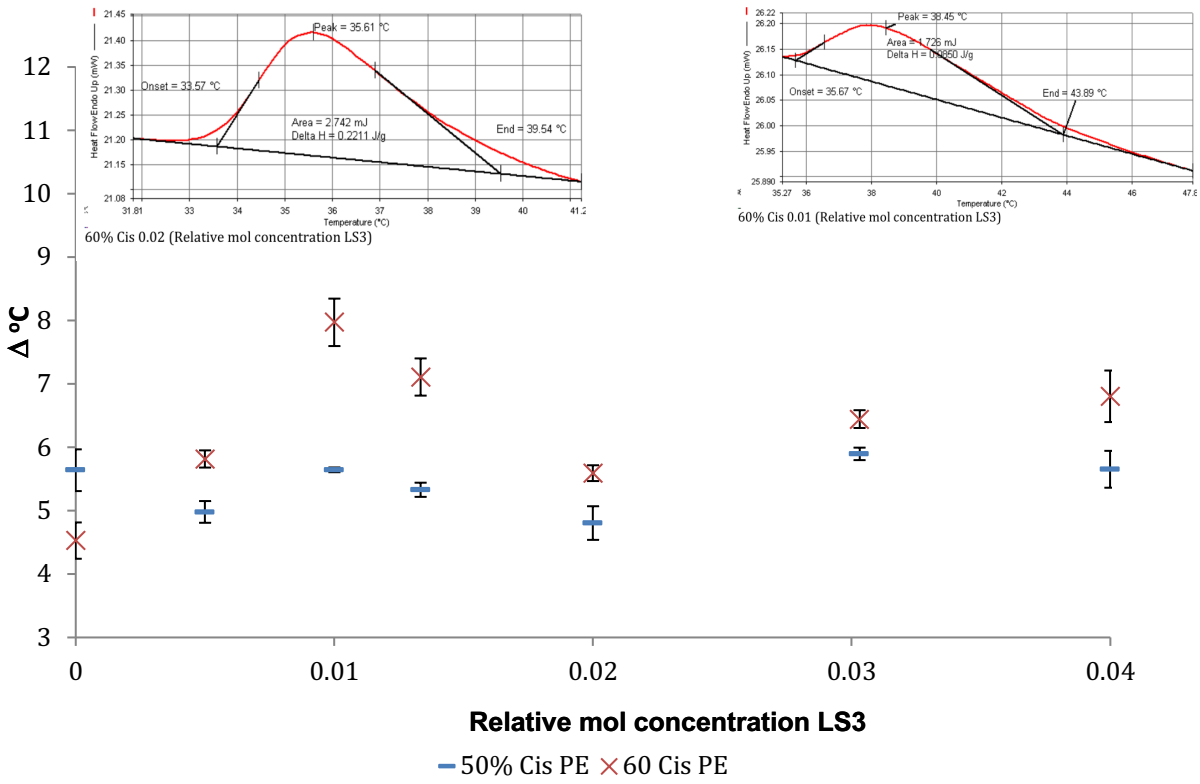

Figure 2.4: Temperature range of L_α – H_{II} transition (width of transition peak) of PE bilayers containing 50% and 60% *cis* PE as a function of LS3 concentration.

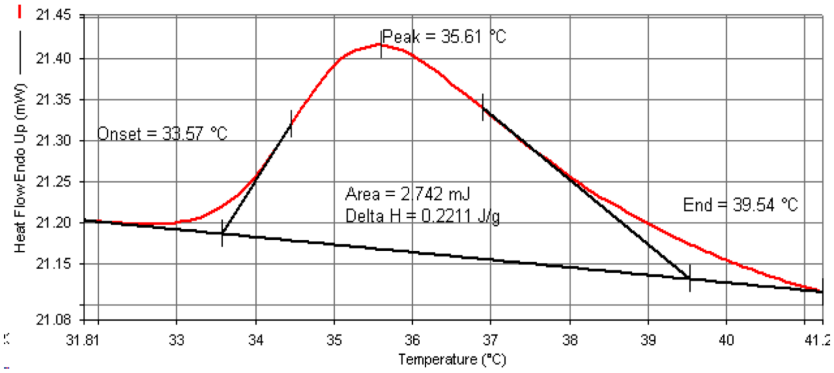

60% Cis 0.02 (Relative mol concentration LS3)

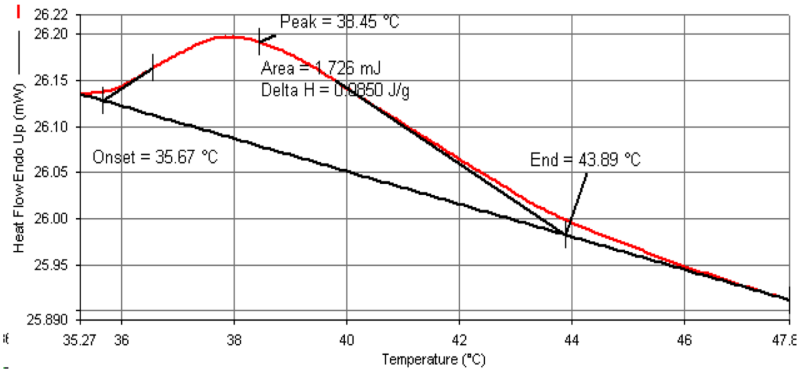

60% Cis 0.01 (Relative mol concentration LS3)

Figure 2.5: Width of the L_α – H_{II} transition peaks are calculated by using linear regression at the start and end points of the phase transition curve, using the Perkin and Elmer software.

When LS3 is introduced to the lipid systems, the temperature range during the L_α – H_{II} transition increases and then decreases to a minimum (4.8°C and 5.6 °C) at 0.02 relative mol concentration LS3 in both lipid concentrations 50% and 60% *cis* PE respectively (**Figure 2.4**). The range in temperature covered by a phase transition relates to the uniformity of the sample. At 0% the sample only contains lipid and water and is likely to be uniform. Sample uniformity is restored at 0.02 relative mol concentration LS3, which therefore must represent the optimal peptide/lipid ratio. Points that are to left of 0.02 relative mol concentration LS3 have an excess lipid and points to the right of 0.02 relative mol concentration LS3 have an excess of peptide, leading to non-uniformity of sample composition. Insets are example DSC traces.

Discussion

The effect of concentration of LS3 on T_h

Before I tested the effects that LS3 had on the mixed *cis*/*trans* PE bilayers, I first determined the T_h of different compositions of *cis*/*trans* PE lipids (**Figure 2.1**). I decided to focus on PE mixtures within a mid-range T_h (heating was from 2°C - 80°C) and found that the T_h of 50% and 60% *cis* PE lipids were 40.3°C and 35.7°C respectively.

The literature does not contain any reports of the effect of transition temperature of phospholipids by LS3. Since LS3 has been designed to lie parallel on the membrane surface (Regan, Degrado., 1988), it was anticipated that the peptide would tend to stabilise the bilayer (increase T_h), rather like the apolipoprotein (Class A) type of lipid-associating amphipathic helices (Segrest et al., 1990). Class A peptides are believed to stabilise the membrane promoting positive curvature by countering the minor negative curvature which is inherent within a dynamic bilayer system as they reside on the surface of the bilayer (Matsuzaki et al. 1998). In the case of phospholipid bilayer nanodiscs, they are surrounded by apoA-I to maintain bilayer stability (Nath, Atkins, & Sligar., 2007). There are other classes of amphipathic helices; lytic polypeptides (Class L) act by disrupting membrane stability because of the orientation of the peptide to the membrane. Peptides that reside within the bilayer (obliquely or transversely) are known to disrupt membrane order, specifically by increasing the negative curvature strain on the bilayer forming pores/channels in the membrane and as a result, these peptides have antimicrobial properties and cause cell lysis.

Figure 2.2 shows that the addition of LS3 to the PE mixtures lowers T_h. This decrease in T_h continues with increased molar concentration of LS3 in the 50% and 60% *cis* PE mixture from 40.3°C and 35.7°C (without LS3) to 37.6°C and 34.4°C (4 mol % LS3). This contradicts what I hypothesised originally about actually stabilising lamellar phase and increasing the T_h of the system. The decrease in T_h implies that LS3 increases disorder and destabilises the lipid system by increasing the negative curvature on the bilayer. Rather than acting as a class A lipid-associating amphipathic helix, the LS3 peptide decreases the T_h by destabilising the lamellar phase. In this manner, the peptide behaves more like the class L peptides, which are characterised by a "wide and bulky" hydrophobic face and a narrow hydrophilic area containing several positively charged residues (Polozov et al. 1997) by creating negative curvature on a system and decreasing the T_h value of a lipid system (Matsuzaki et al. 1998).

The mechanism of action of this model peptide is closer to the mechanism of action of alamethicin and magainin as LS3 also forms a pore in a bilayer (Lear et al. 1997). Matsuzaki (Matsuzaki et al. 1998) showed that magainin 2 embedded in the headgroup region of the membrane induces positive curvature. Incorporating the peptide into *cis*/*trans* PE LUVs inhibited the magainin-induced membrane permeabilisation (Matsuzaki et al. 1998). This is because the negative curvature of the PE lipids cancelled the pore forming ability of the peptide by neutralising the positive curvature strain on the membrane. They also found that this correlated with an increase of T_h of DPoPE when magainin 2 and other magainin homogeneous compounds (Wieprecht et al. 1997) were incorporated into the membrane. Alamethicin is a membrane thinning, barrel-stave pore forming

peptide (Huang., 2000), it has been shown to insert fully in the bilayer in a PC lipid system (Heller et al. 1997). However the addition of 10% PE lipids to the PC mixture showed that alamethicin total insertion was inhibited as the negative curvature of the lipid counteracted the membrane-thinning action of alamethicin (Heller et al. 1997).

From the data shown in (**Figure 2.2**), it is possible to quantify the relationship between the change in T_h and the peptide concentration. For mixtures containing 50% *cis* PE, the gradient of the temperature change is -60°C/mol whereas with 60% *cis* it is -25°C/mol. It is surprising that a 10% difference in *cis* content has such a large effect (2.4x) on the gradient. The destabilising effect of the peptide is greater in 60% *cis* than in 50% *cis*, due to the increased amounts of *cis* PE in the former. At 60% *cis*, the system is inherently under greater negative curvature strain and the effect of the peptide on the bilayer is minimised because the system is already relatively unstable. Whereas at 50% *cis* PE, there is an extra 10% *trans* PE in the membrane composition. The effect of the *trans* bond on the shape of the tail allows closer packing between the acyl chains, so the lipids are more regularly packed, closer together, providing greater stability and less inherent negative curvature on the system. Since the peptide has been shown to destabilise lamellar cohesion and reduce the T_h, the result is a relatively sharp, sudden increase in negative curvature on the system (**Figure 2.5**). The rate of decline of T_h is much steeper, because the change in negative curvature is more pronounced than in the 60% *cis* system. This is an intriguing observation, because it suggests that the peptide has a greater influence on more "stable" fluid, lamellar systems.

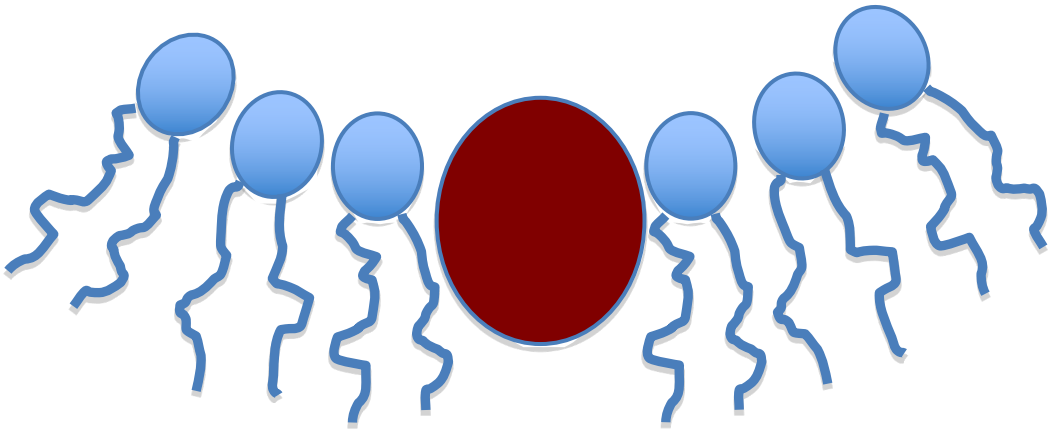

Figure 2.6: Cartoon representation of LS3 residing on the membrane at the critical peptide insertion concentration. (Note the increase of negative curvature on the system).

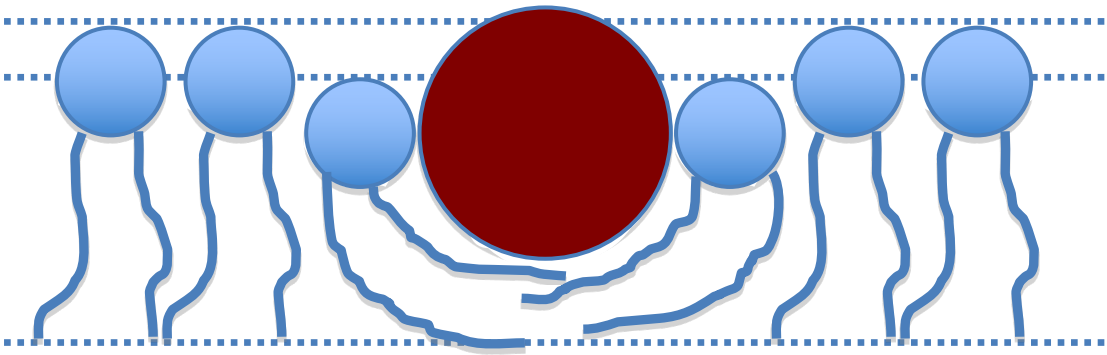

Figure 2.7: Cartoon representation of proposed mechanism of membrane thinning of LS3 on the membrane pre-critical peptide insertion concentration

The effect of LS3 on the thermodynamics of phase transition

Addition of LS3 to the lipid mixtures has a clear effect on T_h. However, the effect on the thermodynamic profiles is not as obvious. The change in enthalpy of the lipid system was measured. This shows the change in energy that is required to rearrange the lipid molecules, in order to undergo the structural rearrangement process that occurs during a phase transition.

It was observed that when LS3 is introduced to the lipid systems, the temperature range during the L_α – H_{II} increases and then decreases to a minimum at 0.02 relative molar concentration LS3 (4.83°C and 5.60°C) at 50% and 60% *cis* PE respectively. The range in temperature covered by a phase transition relates to the uniformity of the sample; if a sample possesses multiple orientations/lipid-peptide interactions, each orientation will have a subtle different phase transition temperature, which will merge together to form a single broad peak.

Figure 2.3 shows that the enthalpy of transition for both lipid concentrations are similar and often overlap (especially at 0.5, 3 and 4 mol% LS3). This is understandable, as the samples are almost identical in composition and the energy required for the phase transition will also be similar. However, there is a significant increase in energy at 2 mol% LS3 at both PE concentrations. The ΔH for 50% *cis* PE increases by 54.5% from 53.2 J/mol (1.3 mol% LS3) to 82.2 J/mol (2 mol% LS3). With 60% *cis* PE, the ΔH increases by 96.2% from 78.6 J/mol (1.3 mol% LS3) to 154.2 J/mol (2 mol% LS3). Increasing the concentration of LS3 in the lipid mixtures to 3 mol% LS3 decreased the ΔH of 50% and 60% *cis* PE by

32.4% and 59% respectively. It is also observed that an increase of enthalpy occurs at 0.01 (79.0 J/mol), 0.013 (78.6 J/mol) and 3 mol% of LS3 (63.2 J/mol) at 60% *cis* PE compared to the enthalpy change of 50% *cis* PE which remains relatively constant at 1 (53.2 J/mol), 1.3 (53.2 J/mol) and 3 mol% LS3 (55.6 J/mol). This can be interpreted in two ways: 1) That the increase and subsequent decrease in enthalpy between 1 to 2 and 3 mol% LS3 indicates a change in membrane orientation and stability which could represent intermediary structures being formed. 2) The more likely option is that the increase in enthalpy is a result of the increased amounts of *cis* PE in the lipid system. The *cis* configuration of PE double bonds is kinked in comparison to the *trans* PE where the double bonds are in a linear configuration. The endothermic energy absorbed for molecular rearrangement is an enthalpic reaction. As a result, the extra *cis* PE molecules present in the lipid mixture increases the disorder within the lipid system and more energy is required to rearrange the lipids into a more ordered (inverse hexagonal) arrangement.

The data suggests that there is a significant rearrangement between LS3 and the lipid bilayers occurring at 2 mol% LS3 because the enthalpy increases to 82.2 J/mol and 154.2 J/mol at each respective *cis* lipid concentration. One possible explanation is that, at this concentration, LS3 may be completely saturating the bilayer surface and as a result requires greater energy to undergo the L_{α} – H_{II} phase transition. If this occurs, it would have the effect of compressing the bilayer making the membrane thinner and increasing the negative curvature on the system (**Figure 2.7**). At higher LS3 concentrations, the membrane surface is saturated, and the peptide may have flipped trans-bilayer. Since the peptide has

been shown to destabilise lamellar phase, the flipping of the peptide may separate the lipid molecules from each other and as a result increase disorder within the bilayer system, (**Figure 2.6**), and so brings down the energy required for the transition phase.

The results observed in this study correlate to the observations of Chen and co-workers with regards to membrane thinning (F.-Y. Chen et al, 2003). They hypothesised that the peptide has two binding states in a lipid bilayer; the surface state (S) and a pore forming state (I). They predicted that the membrane thinning would terminate when the peptide concentration initiates the peptide reorientation from S-I in the membrane (Chen et al. 2003). Using the elastic energy of membrane thinning, the energy difference between the surface adsorbed state of the peptide and the pore state of the peptide would equal each other when the peptide is at the intermediate S-I state. This would correlate to an increased enthalpy at the critical concentration, as increased energy would be required for LS3 to be in both S and I intermediate state. From **Figure 2.3,** the enthalpies at 2 mol% LS3 for both lipid concentrations increase dramatically. So, we can postulate that at 2 mol% LS3, the peptide is at the S-I intermediate state and the membrane thickness is near its minimum.

Conclusion

Using DSC to study the effects of LS3 incorporation on a neutrally charged, negatively curved membrane, I hypothsised that it would stabilise the lamellar phase of the PE system. Surprisingly the data clearly showed that the opposite occurs; the T_h of the lipid mixtures decreased compared to what was reported in Matsuzaki and Wieprect (Matsuzaki et al., 1998 and Wieprecht et al. 1997). The data also suggests that the relative amounts of ratio of *cis* and *trans* PE lipids changes the potency of LS3 destabilisation on the bilayer. It seems that the effectiveness of LS3 interacting on the bilayer is more pronounced on more "stable" lamellar lipid systems as the change in membrane curvature is more pronounced. With regards to the thermodynamics of LS3 on our lipid system, the data shows that at 2 mol % LS3 at both lipid mixtures, the enthalpy increases significantly which suggests a reorientation of LS3 on the bilayer. Whether this is due to LS3 saturation on the bilayer or flipping of LS3 requires further structural study using neutron scattering techniques. Finally, it was observed that the range in temperature covered during the phase transition relates to the uniformity of the lipid/peptide system. I observed the most uniform orientation occurred at 2 mol % LS3 for both lipid PE mixtures. This observation could be because at 2 mol % LS3 the peptide concentration is at the surface state (S) and pore forming (I) interface of the membrane. The consequence of this is that membrane thinning would stop to allow the re-orientation of the peptide in the new position within the membrane. As a result, the system would be in relative order for this reorientation to occur.

Note:

The methods, results and conclusions for this chapter have been taken from my paper (Sa'adedin & Bradshaw 2010).

Chapter 3: The Lipid Phases Formed with the Interaction of LS3 Revealed by X-ray Diffraction

Aims of the chapter

The aim of the work described in this chapter was to:

Follow on from the DSC experiments to determine any permanent or transient lipid structures formed during the different phase transitions of the *cis*/*trans* DOPE lipid mixture with and without LS3 peptide.

Determine phase transitions using temperature ramping and a temperature gradient cell experiments on the small angle X-ray (SAXS) diffractometer.

Determine the size, shape, and *d*-repeat of structures that are formed with increasing concentrations of LS3 peptides.

Record the differences of structures formed with the introduction of the LS3 peptide into the *cis*/*trans* PE mixture.

Introduction

In the previous chapter I discussed the use of differential scanning calorimetry on the PE mixture and on the LS3 peptide/PE samples. I was able to show a clear phase transition occurring between the L_α and the H_{II} phase. The introduction of the peptide on the lipid system showed a decrease in phase transition temperature of the lipid system.

As previously mentioned, non-lamellar forming lipids like DOPE, can form inverse hexagonal and cubic phases. Cubic phases are known to contain bicontinuous regions of water and hydrocarbon (Erbes et al. 1994). These non-lamellar phases have been shown to play a role in membrane fusion (Ellens et al., 1989), fat digestion (Tenchov et al., 1998), rod cells (Albert et al., 1984) and a very important role in bacterial fatty acid synthesis (Dowhan and Bogdanov., 2002). It has been postulated that bacteria uses the relatively high level of non-lamellar forming lipids in the membrane to maintain a "constant curvature at growth temperature" (Erbes et al. 1994).

To understand more about the structural changes the peptide has on the lipid system I will use small angle X-ray diffraction (SAXS) to further understand the molecular rearrangement of the lipid system and the interaction of the peptide on the lipid.

X-Ray diffraction theory:

X-ray diffraction is an analytical technique used to determine the phase composition, crystal lattice structure of a solid or liquid sample.

The chemical compositions and structure of the sample can have multiple phases that have either crystalline and non-crystalline components. For lipid samples multiple phases can be observed depending on temperature and composition of the lipid sample.

X-Ray diffraction is the result of constructive interference between X-rays and the phospholipid lamellar bilayers, the wavelength used is of similar magnitude of the distance between the lipid atoms in the multilamellar lattice. The resultant constructive wave interference of the phospholipid bilayers produces a diffraction pattern that is recorded on detector as reflections. The diffraction pattern comes from the reflection of the X-ray waves of the Bragg planes within the phospholipid system. These planes are regularly arranged (in this case a multilamellar lipid plane) where the structure is aligned with the X-ray beam.

Bragg's law is defined by **Equation 3.1:**

$$n\lambda = 2d\ hkl\ sin\ \theta$$

Equation 3.1: Bragg's Law where n = is the diffraction order (n = 1 is first order, n =2 is the second order and so on.) λ = wavelength of the incident X-ray beam, d = spacing between the lipid bilayers in the lattice, θ = angle between the incident ray and scattering planes.

During wave reflection off the Bragg planes, if the path difference between the waves is a multiple of λ of the initial X-ray wave, then the diffracted waves combined constructively and follows Bragg's Law on the constructive interference between reflected waves (**Figure 3.1**).

This version of Braggs Law shows which crystal place satisfies the Bragg condition.

The effect of constructive and destructive interference is intensified due to the accumulative effect of reflection of consecutive planes (h, k, l) of the crystalline lattice.

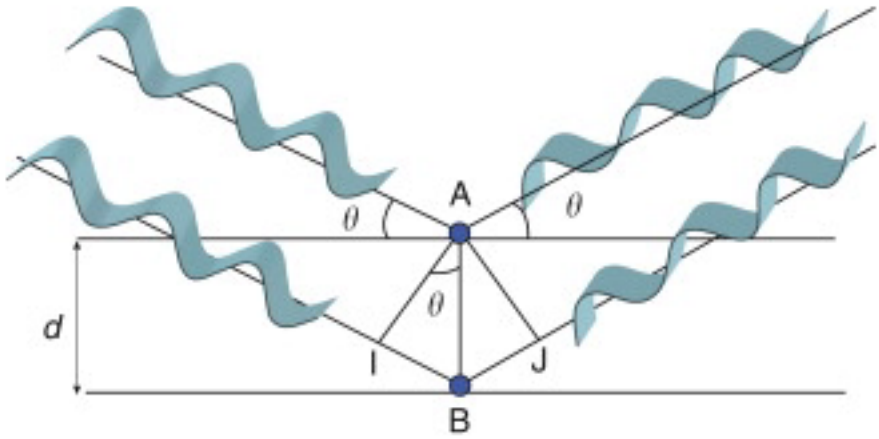

Figure 3.1: Cartoon representation of Bragg's Law and its derivation, X-ray beams interacting with a parallel lattice planes Miller indicies *hkl* with a spacing of *d* with an angle of incidence θ. Each lattice plane *hkl* in the figure acts as a mirror in the different lattice structures. Distance IB = *d* sin θ and when measuring the path difference between the scattered waves at A and B, this is equal to IB + BJ = 2*d* sin θ. (Image taken from Le Pevelen., 2010)

X-ray diffraction shows the electron density, which is the time-averaged distribution of the electrons in the sample. In order to obtain a detailed structure

of the diffracted sample, the electron density of the diffracted sample requires high resolution data. In order to obtain such data, an ordered crystal structure is required. This is because an ordered crystal structure amplifies the effects of X-ray diffraction by using Bragg's Law to add up the waves that are constructively or destructively interfering with each other, and are observed as Bragg Peaks on the detector.

The observed X-ray diffraction pattern can be transformed using a Fourier transformation (**Equation 3.2**) which is a mathematical function which acts like a lens to determine the structure of the lipid/LS3 system.

$$F(x) = \sum_{hkl} F_{hkl}\ e^{2\pi i(hx+ky+lz)}$$

Equation 3.2 : Condensed version of Fourier transformation used in X-ray and Neutron diffraction. In this case F_{hkl} represents the electron density function in real space and $F(x)$ is the form factor which depicts the shape of the lipid system. The Fourier transformation is a function that describes the spation distribution of each atoms in the system diffracted by the incident X-ray beam.

While the equation above looks complex (Aubert, E. and Lecomte, C., 2007), the Fourier transformation can simplistically be explained as the sum of all of the electron densities along each plane and axis. The Fourier transform of the diffraction pattern provides the structure of the phospholipid system.

X-rays diffraction produces a scattered X-ray pattern of a diffracted sample; the resultant pattern produced is linked to the electron density distribution of the lipid sample. And as a consequence, the following scattered intensity is of a result of a Fourier transformation of the electron density distribution of the lipid sample (Yeagle., 2004).

X-ray diffraction patterns give 2 types of information:

1) Reflections relate to the lattice structure of the sample, including the different phases that are formed and the thickness of the repeating unit (*d*-repeat) (**Figure 3.2**).

2) Intensity of the reflections gives the Fourier transformation of the electron density distribution of a repeating cell (Yeagle., 2004).

In static diffraction, X-rays are superior to neutrons due to the higher intensities that allow a greater reduction of the incident beam with respect to wavelength $(\Delta\lambda/\lambda)$. The scattered intensity is the total amount of radiation scattered at any given angle. Scattering intensity is given by $I(q)$ where q is a vector in reciprocal space.

The detector measures the scattering intensity, but further analysis requires that the scattering intensity is converted to Form factor and Structural factor (**Equation 3.3**).

$$I(q) = P(q)S(q)$$

Equation 3.3: The Scattering Intensity I formulae where Form Factor = P depicts the shape of the lipid, Momentum transfer = q is a vector in reciprocal space and Structural Factor = S represents the arrangement of the lipid sample.

The result is, X-ray data collection that can be done in a matter of minutes compared to a matter of hours with respect to neutron scattering, especially at a Synchrotron facility like ELETTRA that has high levels of X-ray flux passing

through the different instruments. With prolonged exposure to the beam, the sample would be easily damaged and become deteriorated.

The preparation of the MLV liposomes allows the orientation of the lipid bilayers to be scattered isotropically into concentric diffraction rings (also known as Debye-Scherrer rings) (Rappolt & Pabst., 2008). The resultant profile shows regular, equal Bragg reflections representing the lamellar structure within the MLV (Rappolt & Pabst., 2008).

With small angle X-ray diffraction (SAXD), the MLV liposome preparations are exposed to X-rays and the resultant scattering intensities are recorded as a function of the scattering vector (the intensities can be seen on the y-axis **Figures 3.7**, **3.8**, **3.9** and **3.10**). The resultant diffraction pattern gives rise to the structural information via the electron density profiles.

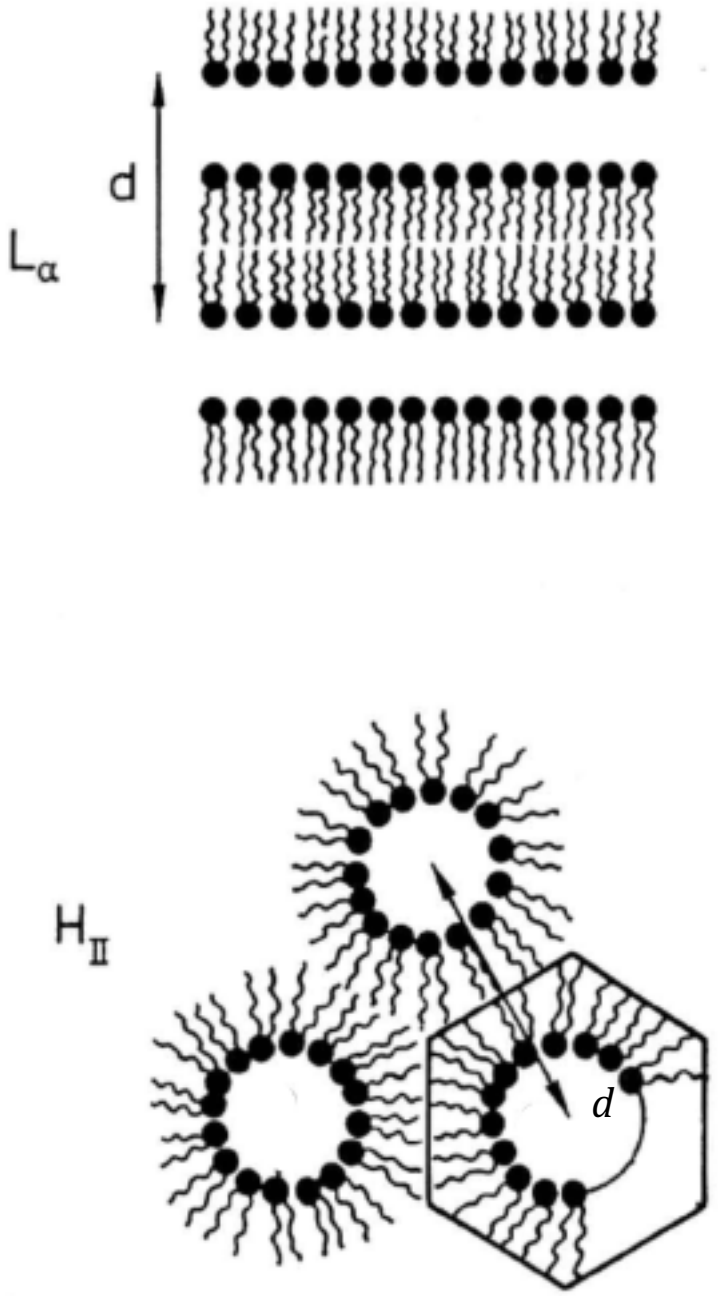

Figure 3.2: Modified cartoon of the unit cell and cross sectional segments of the $L\alpha$ and the H_{II} phases. Bilayer and water thickness is a measure of the repeating cell-unit (d-repeat distance) (Erbes *et al*. 1994)

X-Ray Diffraction

SAXS Methodology

MLVs were prepared by dissolving appropriate amounts of DOPE *cis*/*trans* mixtures in chloroform, thin lipid films were created by evaporating the chloroform by using a gentle stream of nitrogen gas. In creating the MLV peptide mixtures, the LS3 peptide was dissolved in methanol and was added to the DOPE *cis*/*trans* mixtures to produce a range of peptide to lipid molar ratios (1 to 200, 1 to 100, 1 to 75, 1 to 50, 1 to 33 and 1 to 25.). Thin lipid films were desiccated under a vacuum for 6 hours to remove any residual solvent. An appropriate amount of PIPES buffer (1mM EDTA, 150mM NaCl and 0.3 NaN_3 pH 7.4) was added to obtain an equivalent of 40 mg/ml of lipid for the DOPE *cis*/*trans* mixtures. Lipid dispersions were sonicated for a period of five to ten minutes, vortexed thoroughly and freeze thawed with liquid nitrogen. Each cycle of sonication, vortexing and freeze thaw was repeated six times. Throughout the procedure the temperature of the lipid dispersions was kept above the melting temperature of the lipids. The resultant lipid dispersions were placed into an aluminium cell and covered with a mica layers.

The sample preparation for the SAXS experiment was similar to the sample preparation of differential scanning calorimetry. (This is because I was essentially doing a DSC-like experiment but with the inclusion of X-rays to find out about the structures formed and interaction of the peptide on the lipid structures.) One of

the differences between the methodologies was the concentration of lipid used. Instead of using a concentration of 50mg/ml of MLVs the lipid concentration for DSC, the lipid concentration was increased to 200mg/ml. This was done in order to maximise the amount of diffraction on the sample, as DOPE is known to be a poor diffractor. I also used a temperature gradient cell; this is where a sample is in a metal cell that is cooled on one side and heated on the other side (5°C and 75°C). The theoretical advantage of using such a system is that any transient structures formed during the phase transition of my sample are stable, compared to temperature ramping where any transient structures observed are unstable, and their structures cannot be analysed. I only used the temperature gradient cell for two of my samples DOPE *cis/trans* and 1:75 peptide: lipid molar ratio as I wanted to compare the diffraction data from the temperature gradient to diffraction data collected using the temperature ramping experiments.

Temperature scanning SAXS

X-ray diffraction was conducted on the SAXS instrument at ELLETRA synchrotron light source Trieste, Italy (Amenitsch et al., 1998 and Rappolt, et al., 2003). Diffraction patterns of 50:50 mixture of *cis* and *trans* isomers DOPE, LS3 MLVs were monitored on a one-dimensional position sensitive detector (Petrascu, et al., 1998) over the *s*-range 1/450 $Å^{-1}$ to 1/12 $Å^{-1}$ (**Equation 3.4**).

$$s = 2\pi \, sin\theta/\lambda$$

Equation 3.4: Calculation of *s* range on the SAXS instrument at ELETTRA.

Silver behenate ($CH_3(CH_2)_{20}$-COOAg) was used for angular calibration of the 1024 detector channels detector at λ=1.54Å (**Figure 3.5**). Silver behenate (AgBH) is used as calibration in SAXS because it is a long chain fatty acid that forms lamellar structures with a regular *d*-spacing of 5.838nm (Huang et al. 1993). As a result, it produces a defined diffraction rings where the *q*-positions are well-defined (**Figure 3.5**). Calculation of *s* range (**Equation 3.4**) was extrapolated linearly with *s* as a function of the detector channels (**Figure 3.6**), using a sample detector distance of 1.00m. Background water and sample holder diffraction were subtracted from the raw data in order to maximise the detector efficiency. An aluminium sample holder (80mm x 40mm), with an aperture (5mm x 2mm) was used for the X-ray diffraction. MLVs samples were placed in the aperture and covered using a mica film on both sides. The sample cell was connected to an electronic water thermal heater (Unistat CC, Huber, Offenburg, Germany) that heated the sample at 1.0˚C per minute. The temperature was monitored with a thermocouple at a linear heating rate of 60 K/h. Each data frame collected

represents 0.5˚C change and data collection for each temperature frame was allocated to 30s. Sample convection and thermal radiation from the X-ray beam had negligible impact on the sample. Raw data was normalised for the incident beam intensity and no further corrections were made. Each data frame was analysed by manually measuring the width, position and peak intensity of the diffraction pattern of each observed phase in the sample using Igor Pro (Wavemetrics). Transition temperatures was calculated by the starting point of the different phases. The phases were determined using the square root peak intensity of the form factor for each reflection.

Lamellar X-ray diffraction (LXD) (performed by Ming Tao Lee)

Lamellar X-ray diffraction was used to investigate the structural phases of *cis*/*trans* DOPE at two LS3 peptide concentrations: 1 to 100 (0.01 mol%) and 1 to 10 (0.1 mol%). The measurements were carried out at the National Synchrotron Radiation Research Center in HsinChu, Taiwan on beam line 13A1 SW6. The diffractometer is comprised of a two-circle goniometer (designed for a vertical θ-2θ scan). The distance between the sample and the detector was 906.6 mm. The X-ray beam dimensions were: 1 mm in width, 300 μm in height and the wavelength set to λ=1.03Å. Attenuation of the beam using two aluminium pieces were installed to give a total attenuation of 1120 times, attenuation was conducted to stop the first order Bragg peak from saturating the detector.

For each diffraction sample, sample preparation was conducted by myself. 10mg DOPE was dissolved in 200μl chloroform to make a 50mg/ml lipid solution and dried under nitrogen. The samples were re-dissolved in methanol. The samples

were vortexed and sonicated, 10µl of the peptide/lipid sample mixture was spread on a silica slide and was vacuumed between one to two hours. The sample was placed horizontally in the sample chamber at 32°C, sample humidity was increased incrementally by producing a temperature differential between the sample plates and water baths. Humidity levels between 93% rh and 64% rh were created in order to stimulate the formation of multiple lipid phases. X-ray exposure time was varied between 5 seconds and 180 seconds in order to obtain a visible diffraction pattern.

Temperature Gradient SAXS

As detailed previously in the temperature scanning SAXS, all previous stated variables remain constant. The aluminium sample holder was replaced with an aluminium temperature gradient cell (**Figure 3.3**) (60mm in length) in which one end was held at 5°C and the other end at 75°C (**Figure 3.3)**, thereby producing a temperature gradient across the sample between 23°C and 49°C. Each data frame collected represents an increment of 0.3°C.

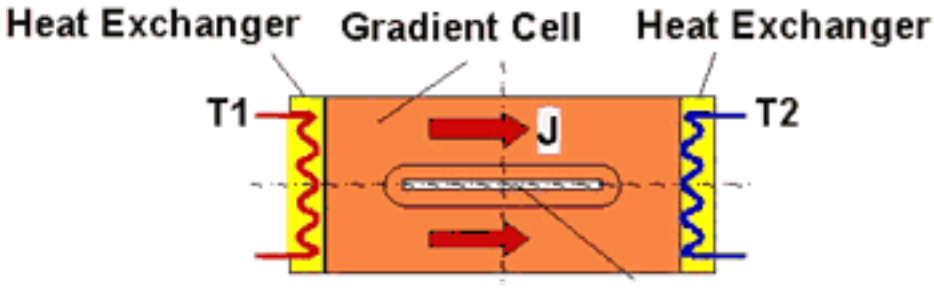

Figure 3.3: Cartoon representation of the gradient cell used on the SAXS beamline at ELETTRA. The cell is heated at a constant rate in order to obtain stable transient structures that would not be traditionally observed via traditional temperature ramping methods. A sealed capillary tube would be placed along gradient cell and equilibrated for 1 hour between 23°C and 49°C prior to experimentation in order to form stable transient states. Available from: https://www.elettra.trieste.it/lightsources/elettra/elettra-beamlines/saxs/beamline/page-2.html?showall= [Last accessed 20th April 2014]

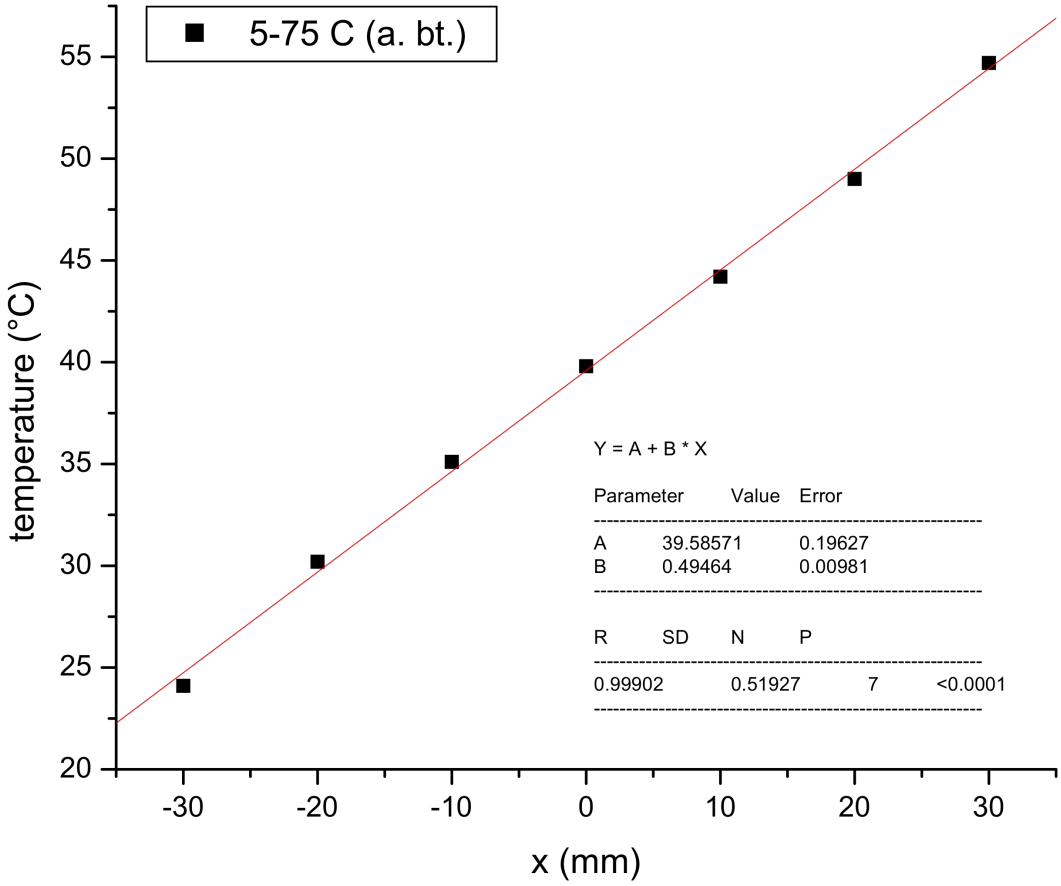

Figure 3.4: Temperatures measured at different positions along the temperature gradient cell (mm) the temperature was monitored with a thermocouple at a linear heating rate of 60 K/h.

X-ray diffraction analysis

Calibration and alignment of the SAXS instrument on the detector was done by scanning AgBH (**Figure 3.5**). AgBH is used because it has a saturated hydrocarbon tail of 20 carbon atoms in length and forms a clearly defined lamellar like structure. The resultant diffraction pattern was analysed to calibrate the *d*-repeat at 58.4Å (**Table 3.1**).

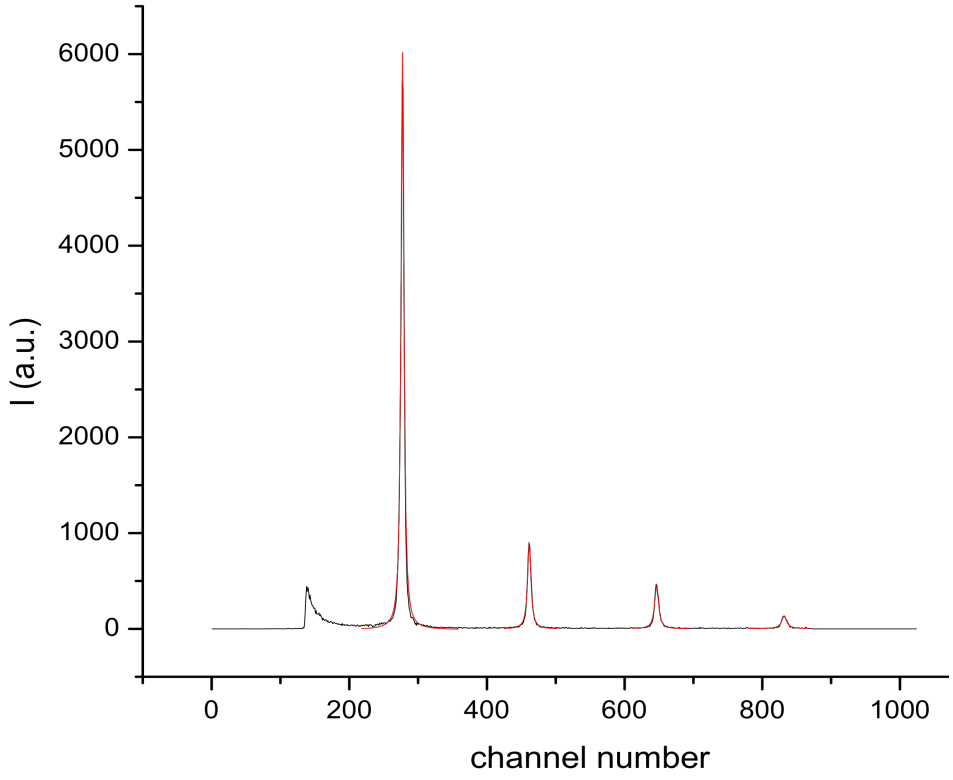

Figure 3.5*:* Diffraction pattern of Silver Behenate $CH_3(CH_2)_{20}$-COOAg with a known *d*-spacing of 58.4 Å.

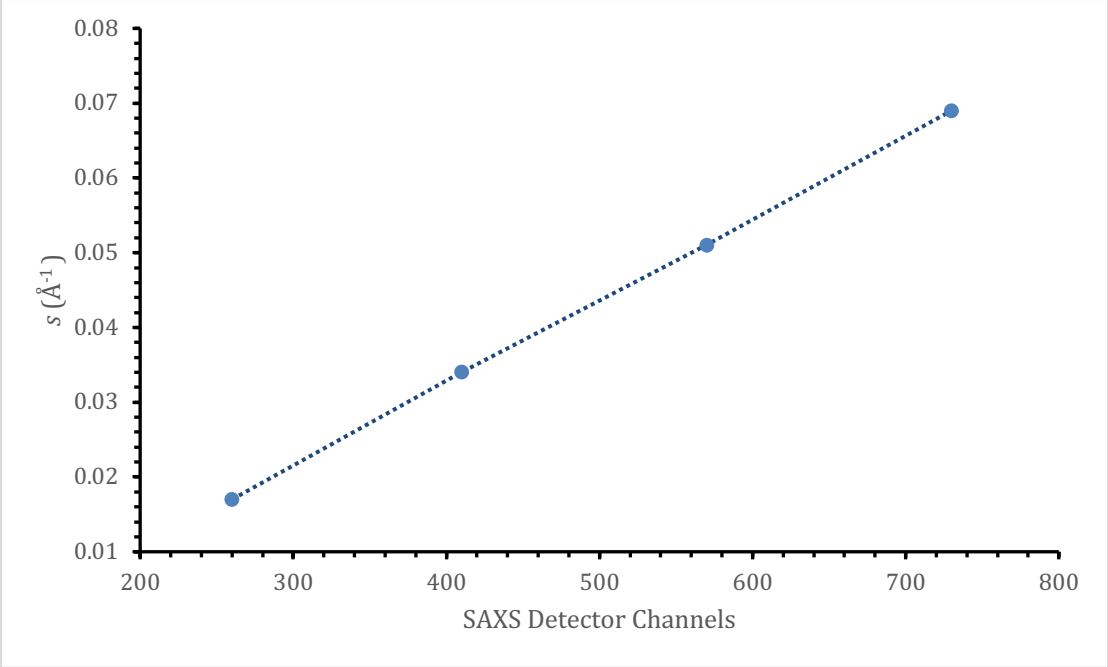

Figure 3.6: Calculation of the *s*-range curve using equation S ($Å^{-1}$) = 0.0001× channel - 0.008, R^2=1.000

Each X-ray data channel number of AgBH (pixel numbers on the detector) is converted to 1/*d*-repeat (**Table 3.1**).

Orders	Centre	s Å^{-1} = 1/d	d-repeat Å
1	277.27049	0.017123288	58.4
2	461.531533	0.034246575	29.2
3	646.590586	0.051361068	19.47
4	831.913802	0.068493151	14.6

Table 3.1: Calculation of *s* value peaks of Silver Behenate at each Bragg peak.

For **Figures 3.7** to **3.11** the location, width and amplitude of each Bragg peak are fitted by Gaussian distribution (Igor Pro, Wavemetrics). Indexing of non-lamellar phases was used in order to calculate the *d*-repeat and structures observed. This involves analysing the diffraction pattern using the relative position of the Bragg peaks, lipid phases are identified depending on their Bragg peak position ratios detailed in the results section.

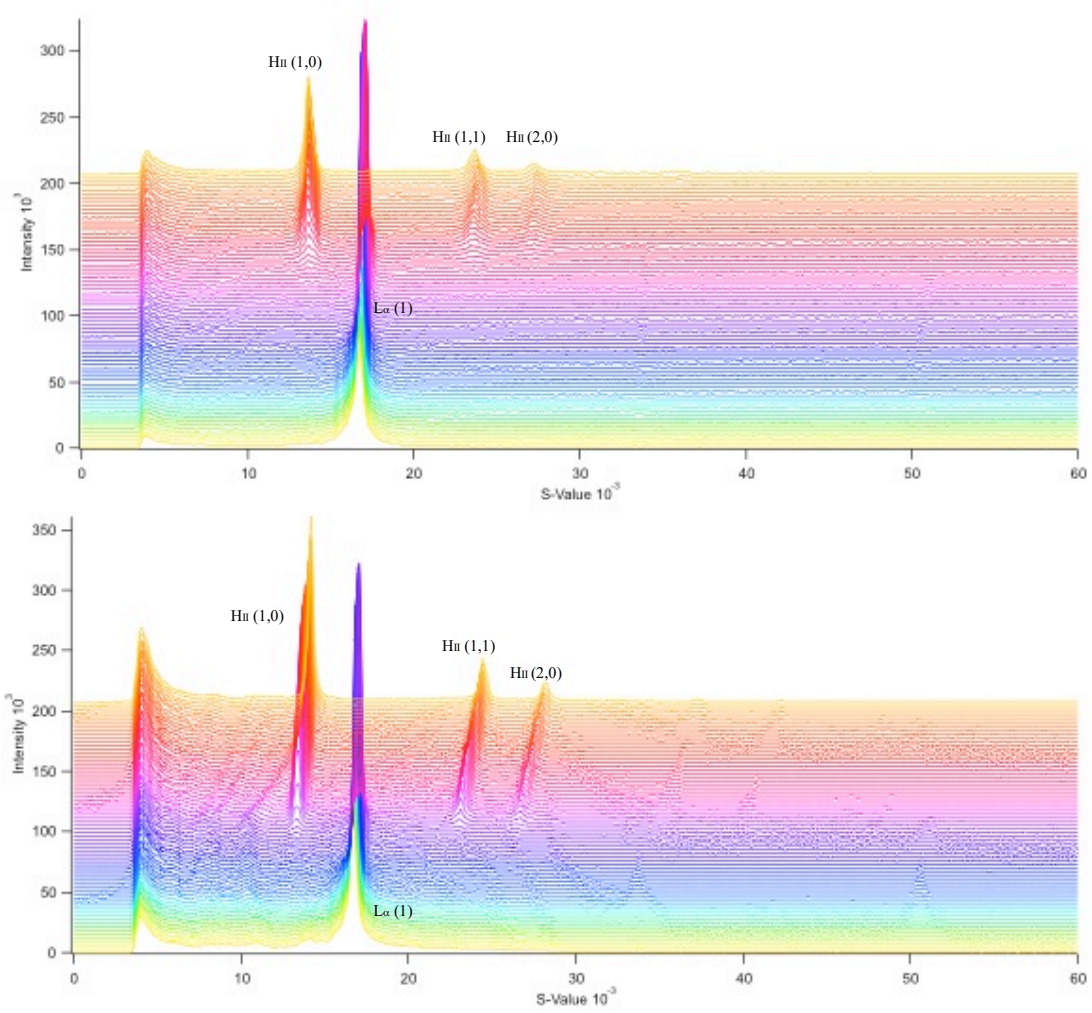

Figure 3.7: Diffraction pattern of *cis/trans* PE (top) and 1 to 200 (LS3:PE) (below). *Cis/trans* PE Seventy frames of data (represented as a coloured line) were collected. Each line represents an increase of temperature of 0.5°C. Start temperature of experiment was at 20°C (bottom yellow), the end of the experiment was at 55°C (top yellow). 1 to 200: Seventy frames of data were collected. Each line represents an increase of temperature of 0.5°C. Start temperature of experiment was at 20°C (bottom yellow), the end of the experiment was at 55°C (top yellow).

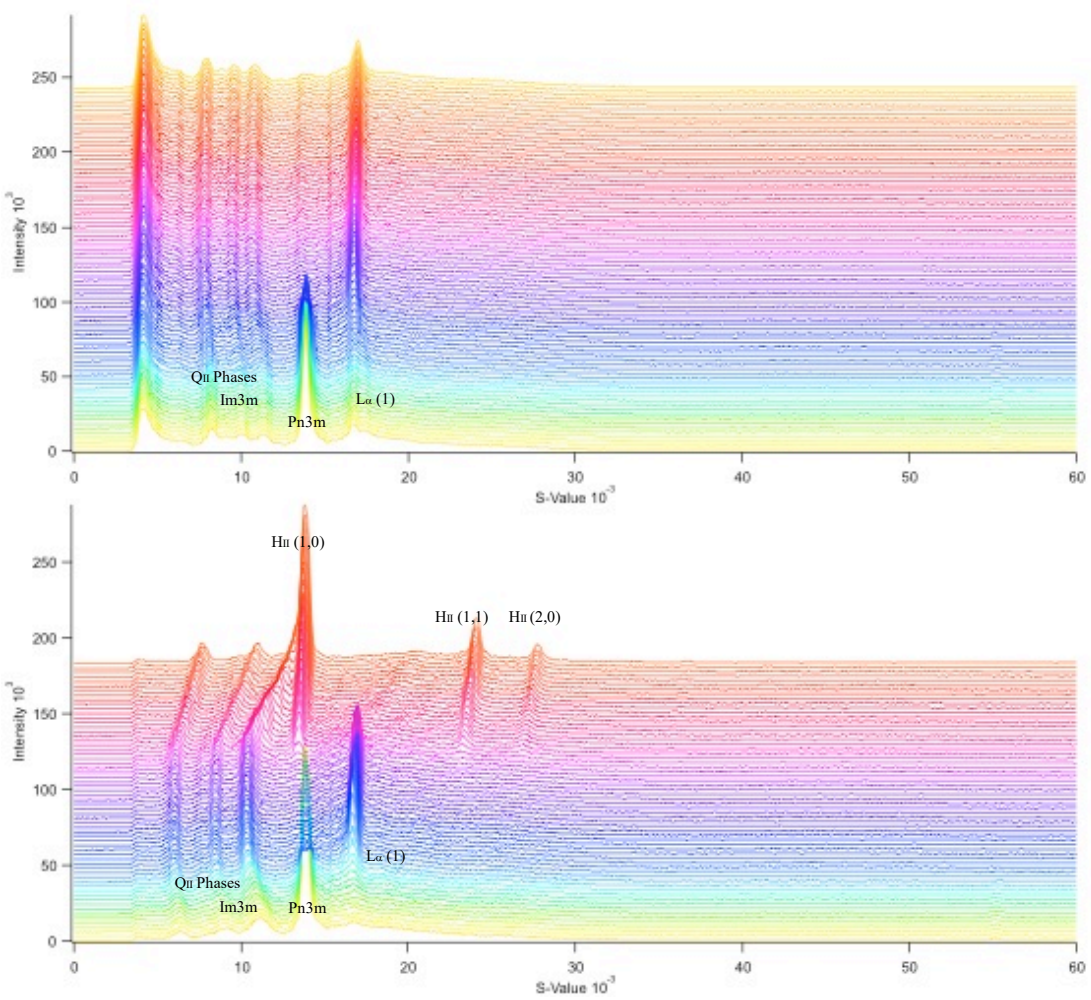

Figure 3.8: Diffraction pattern of 1 to 100 (LS3:PE) (top) and 1 to 75 (LS3:PE) (below). 1 to 100: Eighty frames of data (represented as a coloured line) were collected. Each line represents an increase of temperature of 0.5°C. Start temperature of experiment was at 20°C (bottom yellow), the end of the experiment was at 60°C (top yellow). 1 to 75: Sixty frames of data were collected. Each line represents an increase of temperature of 0.5°C. Start temperature of experiment was at 20°C (bottom yellow), the end of the experiment was at 50°C (top red).

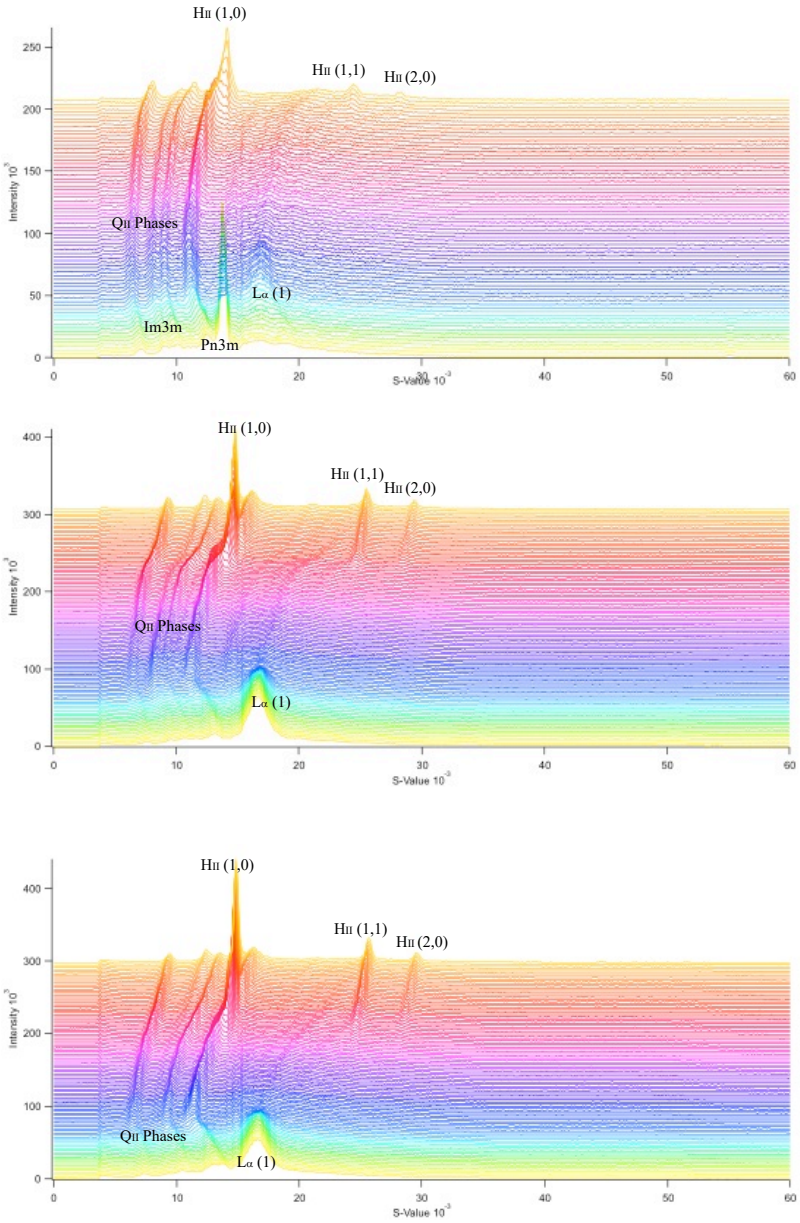

Figure 3.9: Diffraction pattern of 1 to 50 (LS3:PE) (top), 1 to 33 (LS3:PE) (middle) and 1 to 25 (LS3:PE) (bottom) 1 to 50: Seventy frames of data (represented as a coloured line) were collected. Each line represents an increase of temperature of 0.5°C. Start temperature of experiment was at 20°C (bottom yellow), the end of the experiment was at 60°C (top yellow). 1 to 33: One hundred frames of data were collected. Each line represents an increase of temperature of 0.5°C. Start temperature of experiment was at 20°C (bottom yellow), the end of the experiment was at 70°C (top yellow). 1 to 25: One hundred frames of data were collected. Each line represents an increase of temperature of 0.5°C. Start temperature of experiment was at 20°C (bottom yellow), the end of the experiment was at 70°C (top yellow)

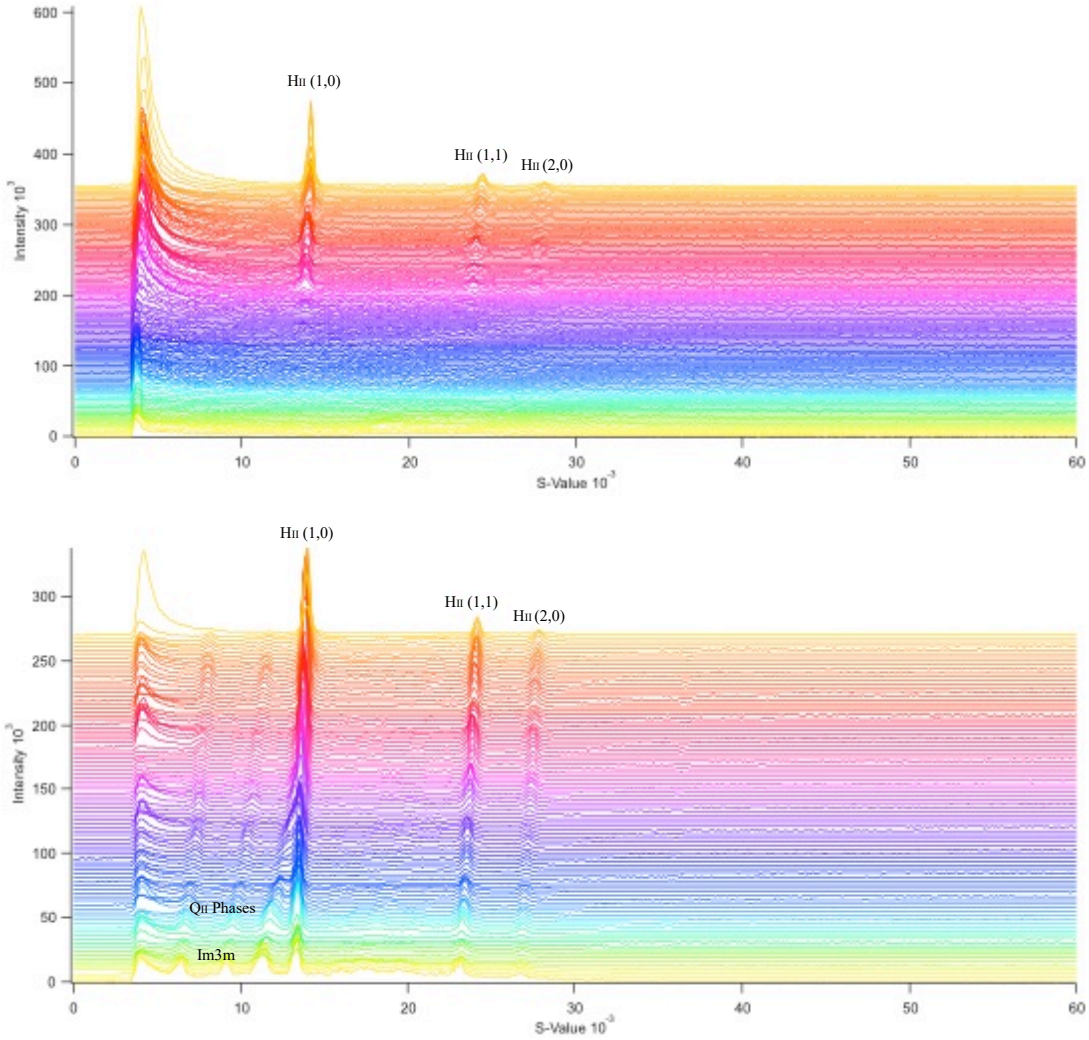

Figure 3.10: Diffraction pattern observed of *cis/trans* PE (top) and 1 to 75 (LS3:PE) (below) using a temperature gradient cell heating the sample from 23°C (bottom yellow) to 49°C (top yellow). Fifty-two frames of data were collected, each line represents an increase of temperature of 0.5°C.

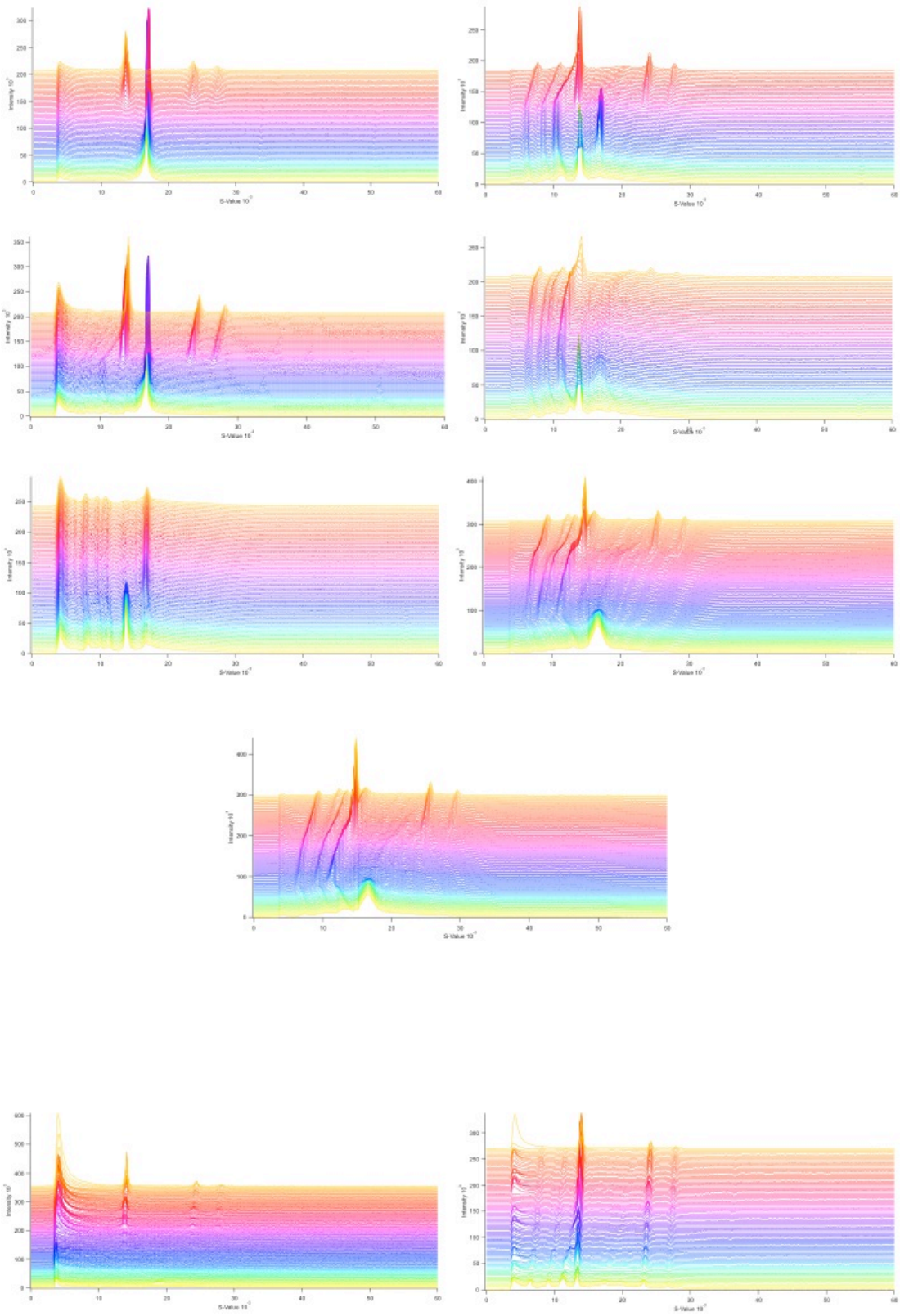

Figure 3.11: Minimised representation of the diffraction patterns observed on samples PE (top left), 1 to 200 (second left), 1 to 100 (third left), 1 to 75 (top right), 1 to 50 (second right), 1 to 33 (third right) and 1 to 25 (fourth middle) and PE temperature gradient cell (bottom left), and 1 to 75 temperature gradient cell (bottom right).

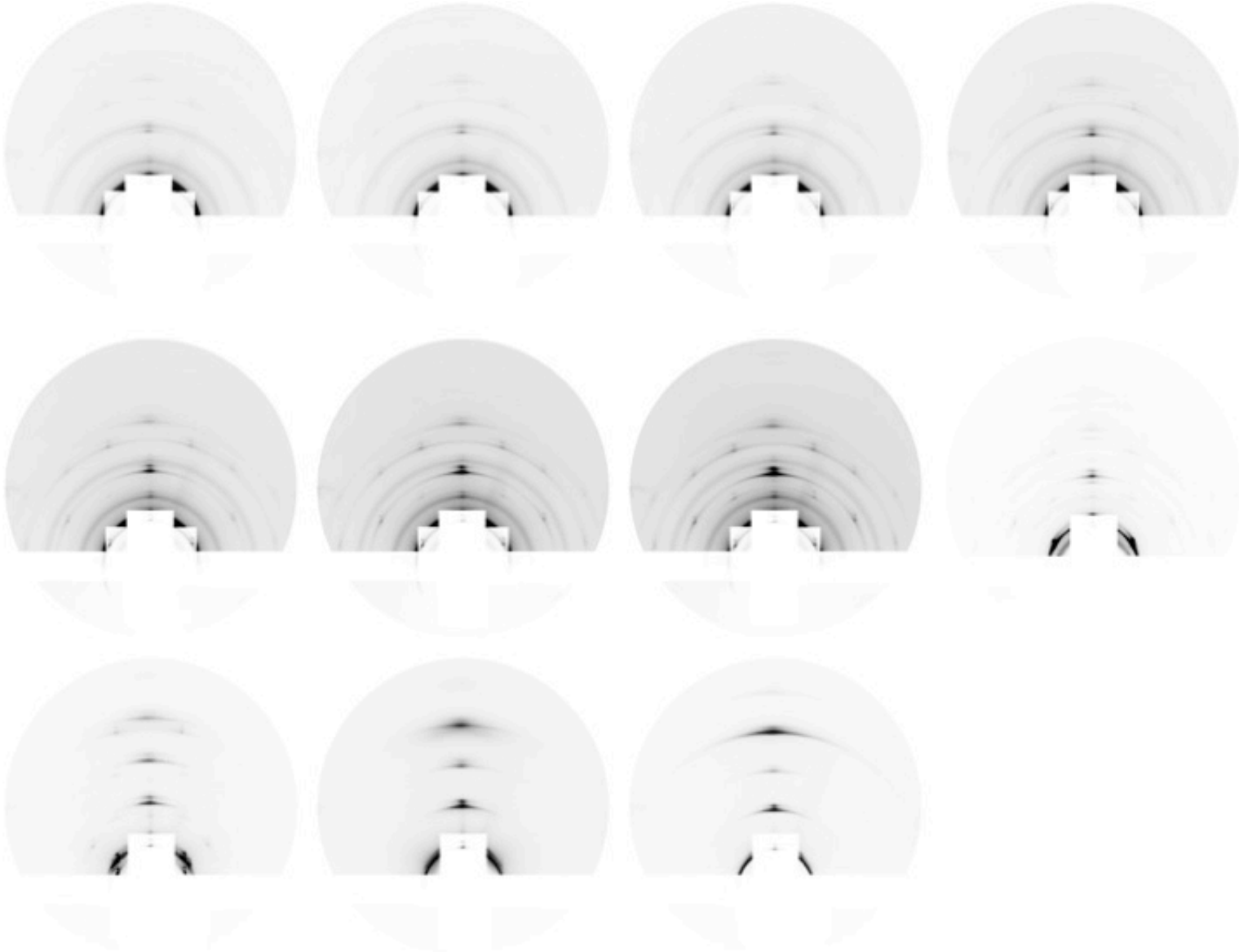

Figure 3.12: Lamellar X-ray diffraction patterns of *cis*/*trans* PE samples at different relative humidities (rh). Starting from the top row, 32 °C at 64rh, 66rh, 69rh, 72rh (left to right top row), (middle row) 75rh, 78rh, 81rh, 84rh, (bottom row) 87rh, 90rh, 93rh.

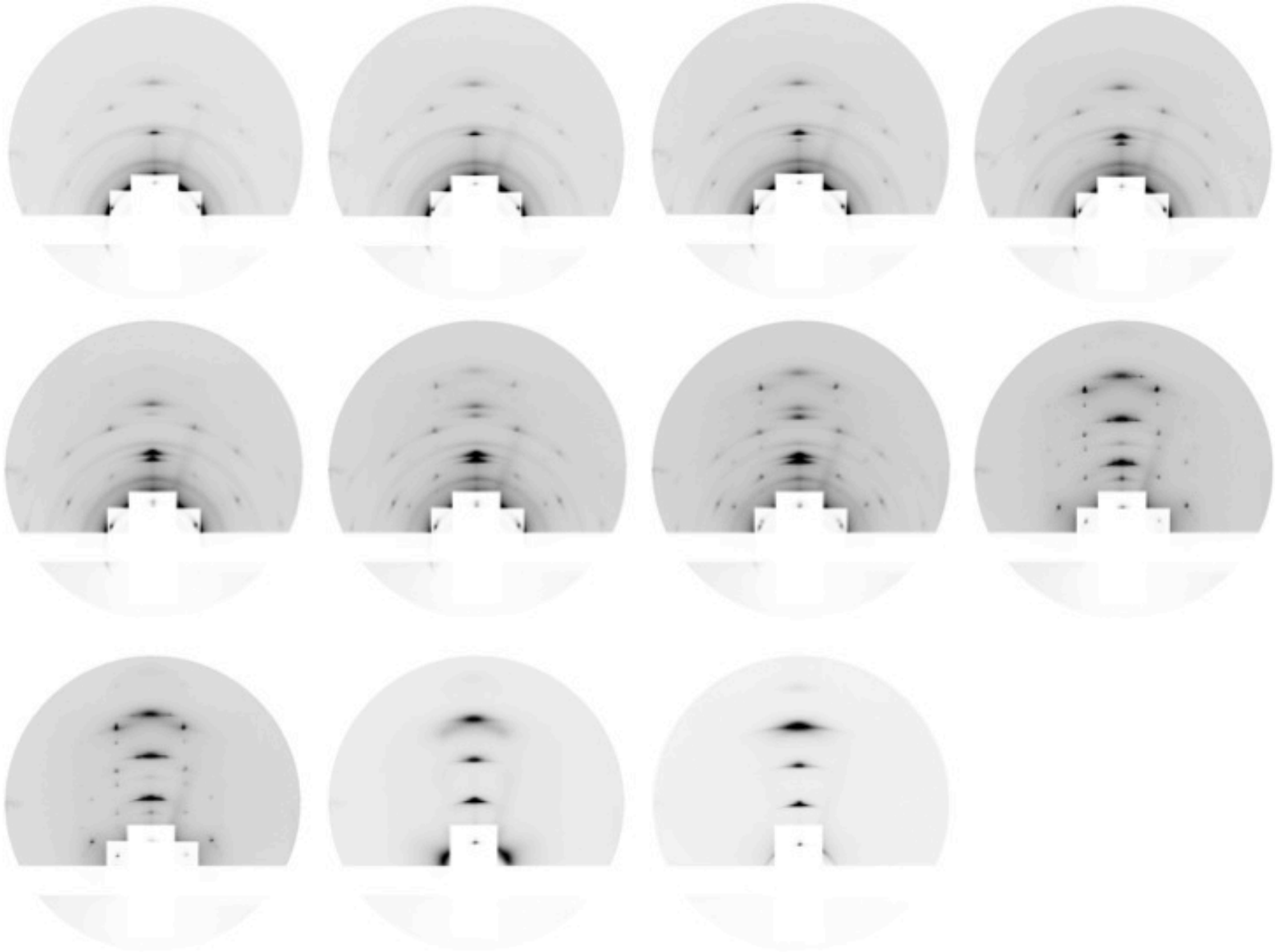

Figure 3.13: Lamellar X-ray diffraction patterns of LS3/DOPE 1 to 100 samples at different relative humidities (rh). Starting from the top row, 32 °C at 64%rh, 66%rh, 69%rh, 72%rh (left to right top row), (middle row) 75%rh, 78%rh, 81%rh, 84%rh, (bottom row) 87%rh, 90%rh, 93%rh.

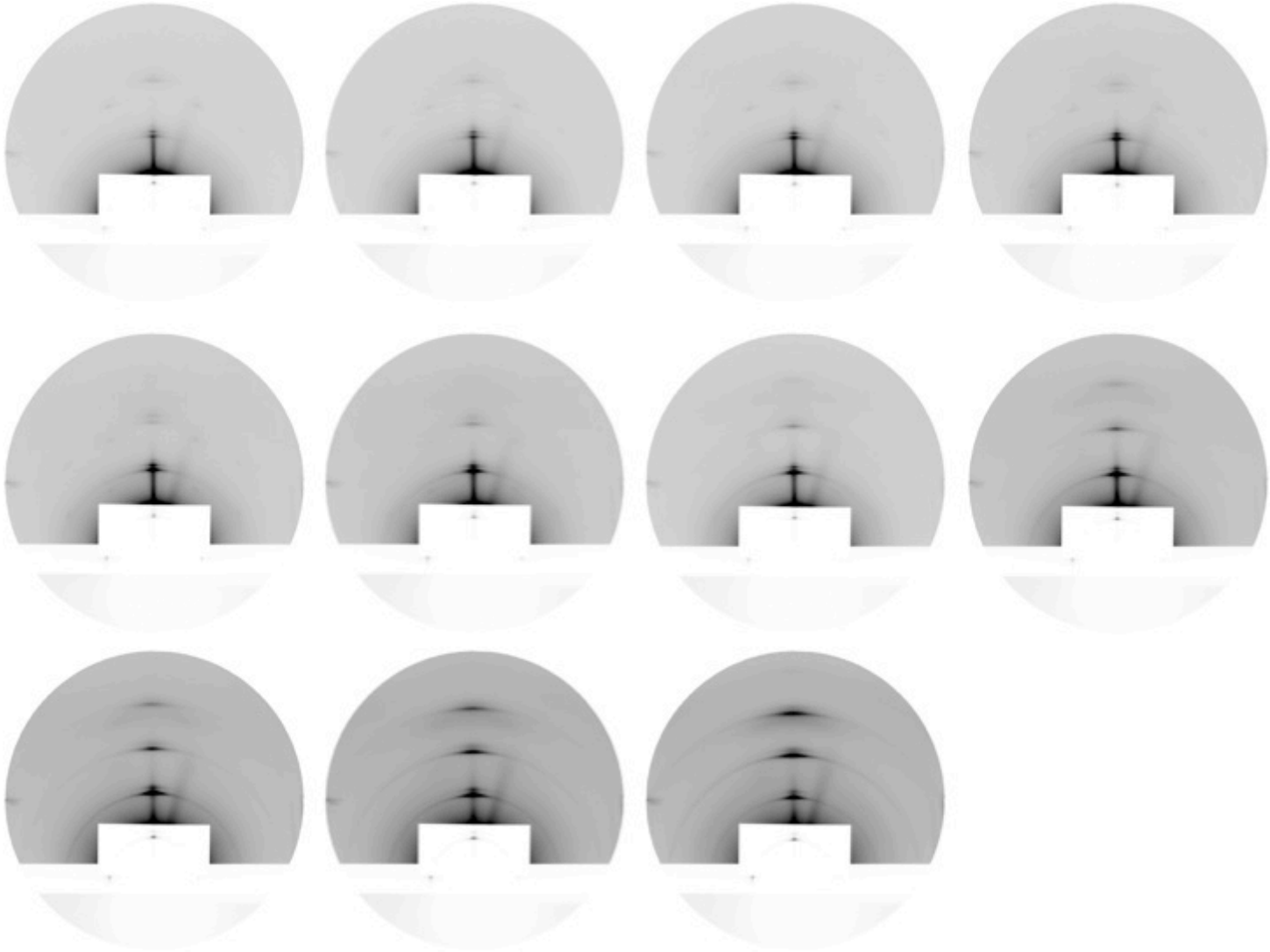

Figure 3.14: Lamellar X-ray diffraction patterns of LS3/DOPE 1 to 10 samples at different relative humidities (rh). Starting from the top row, 32 °C at 64%rh, 66%rh, 69%rh, 72%rh (left to right top row), (middle row) 75%rh, 78%rh, 81%rh, 84%rh, (bottom row) 87%rh, 90%rh, 93%rh.

Results

Bragg peaks from the temperature ramping experiments were indexed to determine the phases observed in the samples (**Figure 3.15**).

Identifying the different phases using Phase Indexing

Lipid phases can be identified by the relative position of the Bragg peaks using phase indexing. Phase indexing uses the Bragg peak position ratios to determine the structure of lipid phases formed (Koynova, Caffrey., 2002).

Inverse Hexagonal:

1, √3, 2, √7, 3, √12 (Turner, Gruner., 1992)

Cubic phases:

Primitive Cubic (*Pn3m*)

√2, √3, √6, √8, √9

Body Centered Cubic (*Im3m*)

√2, √4, √6, √8, √10,

Inverse Body Centered Cubic (*Ia3d*)

√6, √8, √14, √16, √20

Indexing the phases requires the s-values of the observed diffraction peaks. To index the inverse hexagonal phase I will be using data from **Figure 3.7** (1:200 LS3) as an example:

When indexing the Bragg peaks for the inverse hexagonal phase, the Bragg reflections must correspond to these index values at each Bragg reflection:

1, √3, 2, √7, 3, √12 (Turner, Gruner., 1992)

The first diffraction peak was observed at s-value 13.35^{-3}.

Using 13.35^{-3} as the first index, then the locations of the 2nd and 3rd Bragg peaks can be located.

To determine if the 2nd and 3rd diffraction peaks fit the H_{II} phase, the first diffraction peak must be multiplied by √3 and by 2 respectively to determine the s-values of the 2nd and 3rd diffraction peaks.

2nd diffraction peak s-value location = $13.35 \times \sqrt{3} = 23.12^{-3}$

Observed s-value location of the H_{II} 2nd diffraction peak was 23.15^{-3} for sample 1:200 LS3 (**Figure 3.7**).

3rd diffraction peak s-value location = $13.35 \times 2 = 26.7^{-3}$

Observed s-value location of the H_{II} 3rd diffraction peak was 26.78^{-3} for sample 1:200 LS3 (**Figure 3.7**).

Indexing of the lamellar and *Im3m* phases were performed using the methodology mentioned previously.

Phases observed after indexing samples

Cis/Trans PE: Lamellar and inverse hexagonal phase transition observed at 41.7°C.

1 to 200 (LS3:PE): Main phases observed are lamellar and inverse hexagonal phase. Small cubic phase is observed, but due to the peak being small and no other measurable reflections being observed, no indexing of phase can take place to identify the type of cubic phase formed. (Lamellar to Inverse Hexagonal 35.9°C.) (Lamellar phase ends at 41.4°C) (Cubic phase ends at 41.7°C).

1 to 100 (LS3:PE): Lamellar, and body centred cubic (*Im3m*) (Lamellar phase ends at 59.9°C).

1 to 75 (LS3:PE): Lamellar, inverse hexagonal and body centred cubic (*Im3m*) (Lamellar phase ends at 40.7 °C).

1 to 50 (LS3:PE): Lamellar, inverse hexagonal and body centred cubic (*Im3m*) (Lamellar phase ends at 36°C) (Lamellar to Inverse Hexagonal phase transition at 38.8°C).

1 to 33 (LS3:PE): Lamellar, inverse hexagonal and body centred cubic (*Im3m*) (Lamellar ends at 33.7°C) Inverse hexagonal phase transition at 51.6°C).

1 to 25 (LS3:PE): Lamellar, inverse hexagonal and body centred cubic (*Im3m*) (Lamellar phase ends at 31.1°C, inverse hexagonal phase starts at 53°C. Cubic phase starts at 25.1°C).

There seems to be an outlier in results with regards to 1 to 100 (LS3:PE), the lamellar phase transition ends significantly higher (59.9°C) which is 19.2°C higher than 1 to 75 (LS3:PE). The lamellar phases transition temperatures (if you omit 1:100 result) of the other samples showed a clear decline with increasing concentration LS3.

It is difficult to compare the lamellar and inverse hexagonal phase transition temperatures from the previous DSC chapter to the phase transition temperatures observed using the temperature ramping X-ray experiments. Firstly, there are differences due to the different temperature scan rates, the DSC scan temperature scan rate is at 20°C/min compared to X-ray which was at 1°C/min. The lower heating rate may encourage the formation of more stable lipid phases that is observed compared to the higher rate of DSC of 20°C/min. As a result of the lower heating rate, I was able to detect the formation of cubic phases within the samples using X-ray diffraction compared to DSC where no cubic phase was observed due to the high heating rate. Another reason is that there are only three peptide concentration samples that have clear lamellar to inverse hexagonal phase transition between each other. This is compared to the clear lamellar to inverse hexagonal phase transition observed for all peptide concentrations using DSC. (All sample diffraction patterns can be seen on **Figure 3.11**).

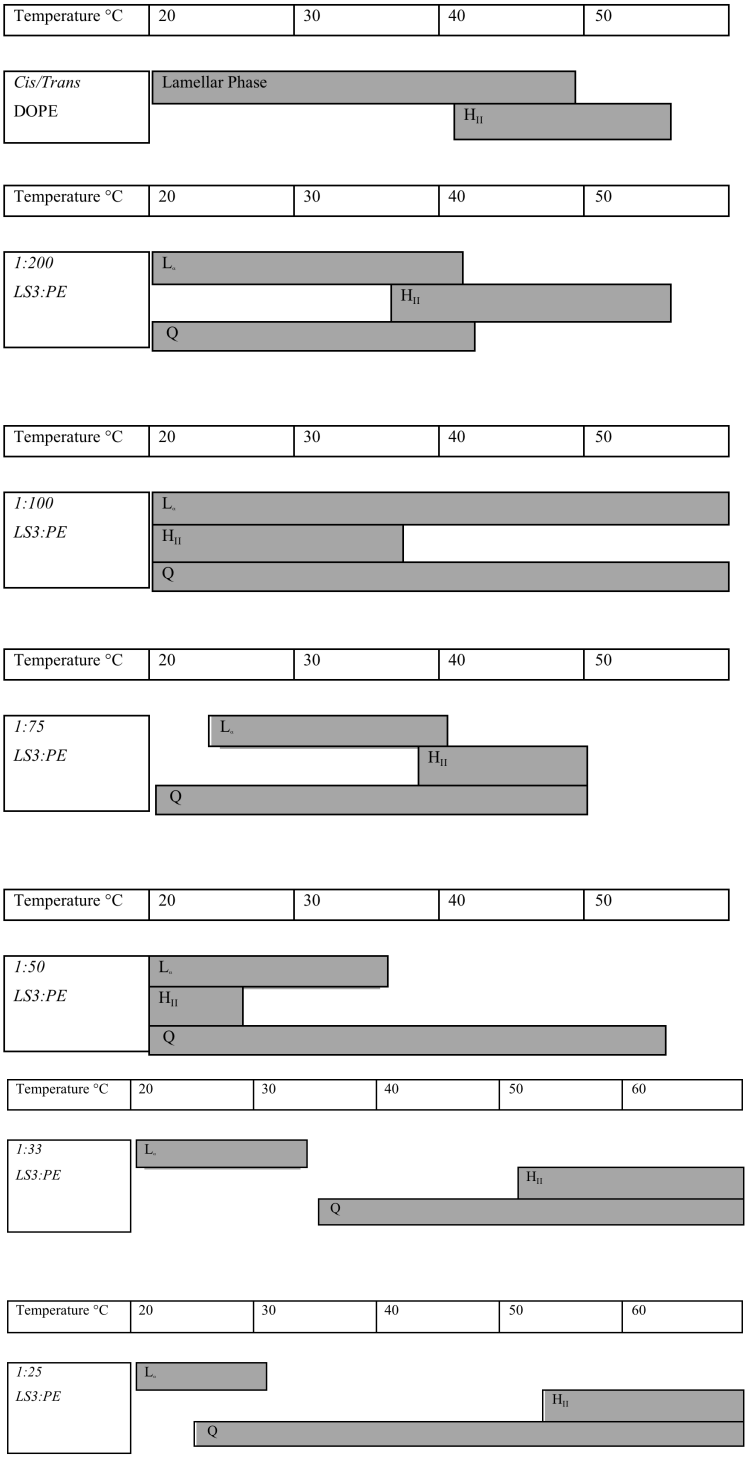

Figure 3.15: Cartoon representation of the different phase transitions temperatures that are observed at for the samples (cis/trans PE, 1 to 200, 1 to 100, 1 to 75, 1 to 50, 1 to 33 and 1 to 25 LS3:PE)

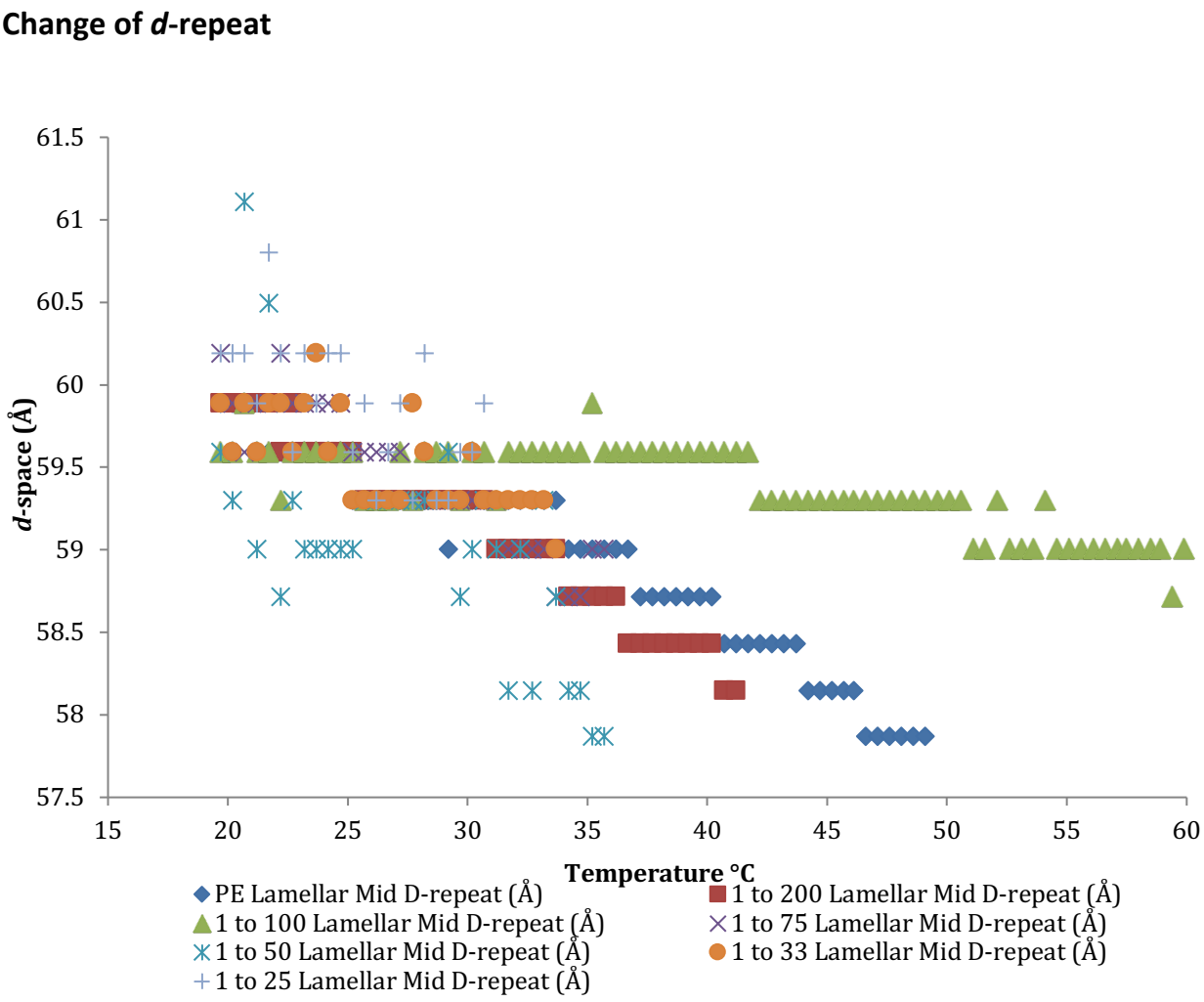

Figure 3.16: Results of temperature ramping experiments showing the lamellar phase Mid-D repeat length of *cis*/*trans* PE with increasing concentrations of LS3 peptide over a temperature range. (Mid-D repeat is defined as the calculated *d*-repeat from the middle of each diffraction peak observed in **Figures 3.5**, **3.6**, **3.7** and **3.8** for each observed phase.)

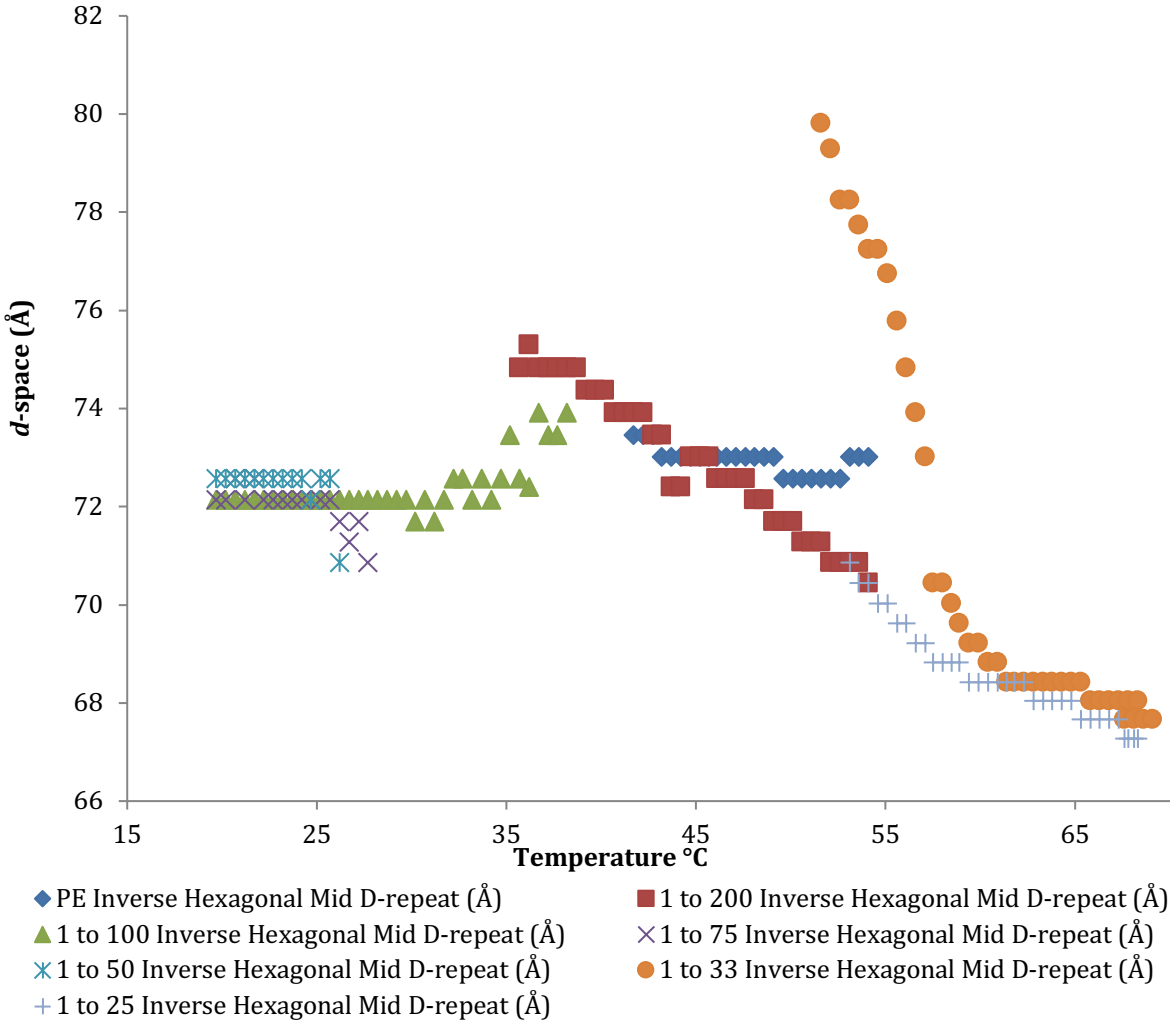

Figure 3.17: Results of temperature ramping experiments showing the inverse hexagonal phase Mid-D repeat length of *cis*/*trans* PE with increasing concentrations of LS3 peptide over a temperature range. (Mid-D repeat is defined as the calculated *d*-repeat from the middle of each diffraction peak observed in **Figures 3.5**, **3.6**, **3.7** and **3.8** for each observed phase.)

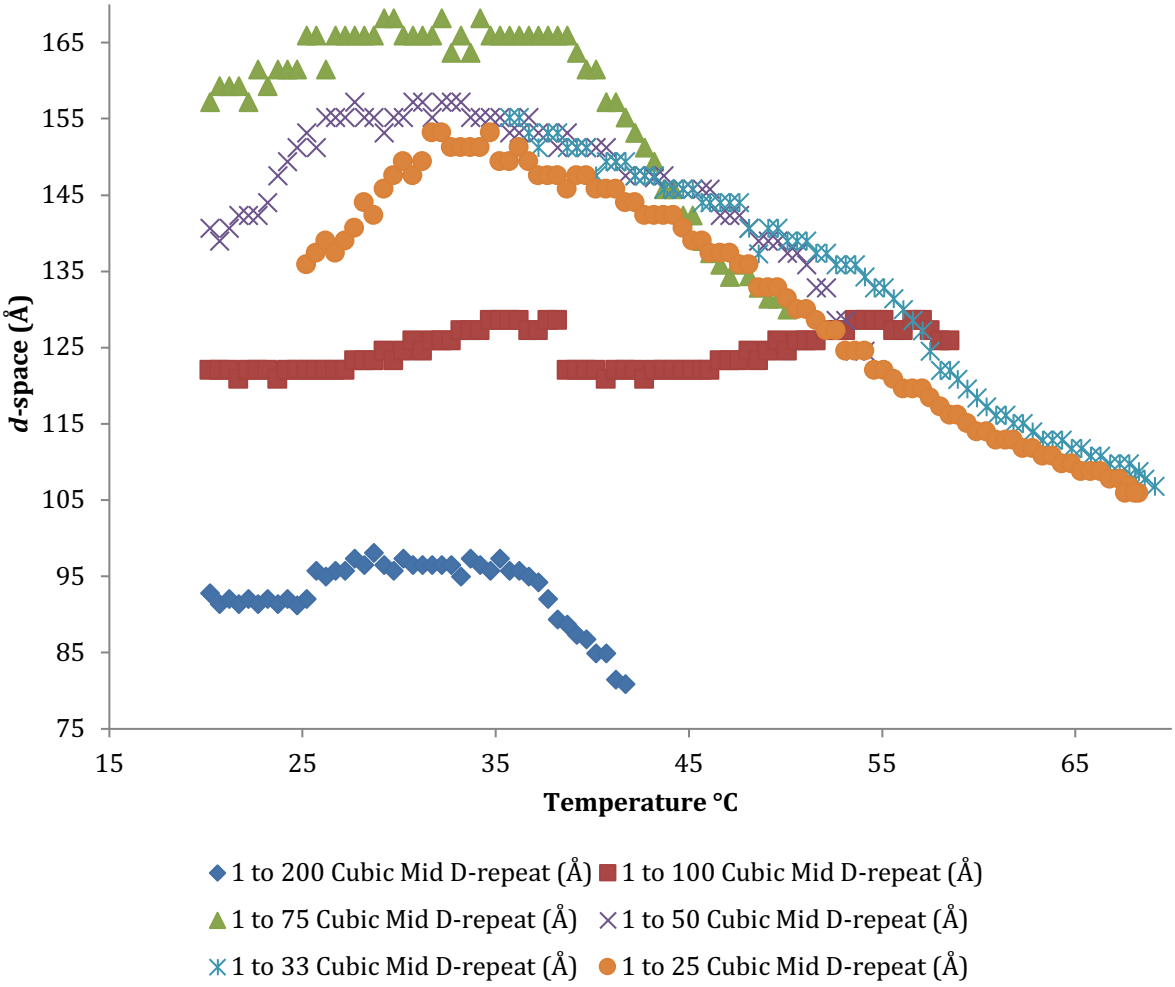

Figure 3.18: Results of temperature ramping experiments showing the cubic phase Mid-D repeat length of *cis*/*trans* PE with increasing concentrations of LS3 peptide over a temperature range. (Mid-D repeat is defined as the calculated *d*-repeat from the middle of each diffraction peak observed in **Figures 3.5**, **3.6**, **3.7** and **3.8** for each observed phase.)

SAXS results:

The changes of *d*-repeat at different temperatures are measured for the different samples at each phase observed.

Lamellar:

Increasing the temperature causes the *d*-repeat of the lamellar samples to decrease in a broadly linear manner (**Figure 3.16**). The difference in *d*-repeat is extremely low 3.2Å (61.1Å to 57.9Å), as a result the change lamellar *d*-repeat distance is minimal with increasing LS3 concentrations. The data shows that the introduction of LS3 at higher concentrations the *d*-repeat is larger than *cis*/*trans* PE alone, the higher *d*-repeat is observed at lower temperatures compared to pure *cis*/*trans* PE.

Inverse Hexagonal:

The relationship between LS3 concentration and *d*-repeat is difficult to initially comprehend. With regards to samples 1 to 200, 1 to 33 and 1 to 25, it is clear that there is a decrease in *d*-repeat in relation to increasing temperatures. With two of the samples, (1 to 33 and 1 to 25), the *d*-repeat clearly reaches the same *d*-repeat of around 68Å. It seems clear that at high concentrations of LS3, the decrease in inverse hexagonal phase *d*-repeat is more pronounced. This can also be described at the lowest LS3 concentration (1 to 200), where there is an obvious decrease in *d*-repeat with regards to temperature. The other samples' *d*-repeat seems to remain constant in size regardless of the temperature. Although this may be explained by the fact that increasing the temperature, the inverse hexagonal phase is eliminated in some of the samples and then transformed into cubic phase. From these results it seems that there is no clear correlation with regards to the LS3

concentration and *d*-repeat. But what does seem to be clear is that at high concentrations of LS3, stabilises the inverse hexagonal phase (**Figure 3.17**).

Cubic:

The increase in LS3 concentration shows a dramatic increase in *d*-repeat when compared to inverse hexagonal and lamellar phase. Although the LS3 concentration that has the highest *d*-repeat is 1 to 75. LS3 concentrations higher than 1 to 75 had a similar *d*-repeat range from 31°C to 53°C. This may be because that LS3 concentrations higher than 1 to 75, the phosphate group of the bilayer is saturated with LS3 lying horizontally, potentially increasing the *d*-repeat. Any further increase in LS3 concentration may cause the LS3 peptide to flip perpendicularly into the bilayer that may explain the *d*-repeat decreasing at higher LS3 concentrations. With all the samples tested, it can be observed that there is a general decline in cubic *d*-repeat with increasing temperatures. The only sample that does not follow the trend is the 1 to 100 (LS3/PE), where the *d*-repeat increases by 3.8Å with temperature (122Å at 19.7°C, 125.9Å at 59.7°C). Upon further investigation of the *d*-repeat on the remaining samples, it can be seen that increasing the temperature to around 35-36°C the *d*-spacing increases in length from its original *d*-repeat at 20°C. The increase in *d*-repeat length ranges from 92-98Å (1 to 200) to 135-153Å (1 to 25) before the d-spacing decreases in length from 6.04% (128.56Å to 120.79Å) to 31.17% (155.17Å to 106.81Å) from its maximum *d*-repeat length. The increase in LS3 concentration shows a larger decrease in *d*-repeat length at higher temperatures (**Figure 3.18**).

Phase Peak Intensities and Peak Width

Peak intensities can be used as a proxy of DOPE/LS3 phase packing order in the sample. The higher the peak, the greater number of ordered DOPE/LS3 is in its respective phase. The width of the *d*-repeat can be used as a proxy of lipid packing order and stability. The wider the *d*-repeat peak, this indicates that the lipids in a particular phase have a wider variation of *d*-repeat at a specific temperature, which would suggest a lower packing order and stability. The higher the diffraction peak intensity and the smaller the width of the *d*-repeat would therefore correlate to a high number of DOPE/LS3 molecules that are ordered in a particular phase with minimal *d*-repeat variation.

Lamellar phase:

Lamellar peak intensity decreases with increasing LS3 concentration, this would correspond to a reduced number of DOPE/LS3 in the lamellar phase. If you omit the 1:100 sample as an outlier, then increasing the concentration of LS3 showed a general decrease in the peak intensity temperatures from 42.1°C to 23.6°C. This decline in temperature and decline in peak intensity, seems to indicate that the lamellar phase is less stable/ordered at higher temperatures. The *d*-repeat distances tend to increase with increasing concentration of LS3 from between 59Å to 60Å. However, the width of the *d*-repeat peaks at high LS3 concentrations (1 to 50, 1 to 33 and 1 to 25) increase from 4.97Å to 16.05Å, which shows that the range of *d*-repeats in the lamellar phase has widened. Which indicates that the increase in LS3 causes greater disorder on the lamellar phase as the diffraction peak is broader and peak intensity has reduced. The data suggests that increasing the concentration of LS3 reduces the amount of lamellar phase observed in the DOPE

lipid system, because the stability and order of the lamellar phase has been reduced.

Inverse Hexagonal Phase:

Identifying a pattern with the inverse hexagonal phases observed across the range of concentrations for the DOPE/LS3 system was more difficult to ascertain. The peak intensities show no obvious decrease or increase with LS3 concentration and this uncertainty is reflected in the temperatures that are observed with the peak intensities. With peak intensity being used as a proxy of the number of ordered lipid packing, increasing concentrations of LS3 showed no obvious correlation with the amount of lipid in the inverse hexagonal phase. However, with regards to the *d*-repeat distance, the distances generally decrease in length with increasing LS3 concentration. The increase in LS3 concentration also showed a general decrease in the width of the *d*-repeat. The width of the *d*-repeat is an indirect measurement of order and stability. The smaller the width, the more ordered/stable the lipid structure is. Therefore, increasing the concentration of LS3 on the PE lipid system seems to stabilise the inverse hexagonal phase; this could be done by eliminating water from the lipid and as a consequence, the lipid tubes are packed more tightly together.

Cubic phase:

No cubic phase was identified in the *cis*/*trans* DOPE lipid sample. Cubic phase was only identified with the introduction of LS3 into the lipid system and there appeared to be a correlation with increasing cubic peak intensity and an increase in LS3 concentration; this also correlated with an increase in temperature that the

peak intensity was observed (**Table 3.2**). Previously studies have reported that increasing the temperature of a DOPE system, the formation of inverted bicontinuous phases (*Im3m*, *Pn3m* and *Ia3d*) are observed (Seddon., 1990). There was a significant increase in *d*-repeat when the concentration of LS3 was greater than 1:200, increasing from 96.5Å to a *d*-repeat range between (127.2Å – 137.4Å). The data also suggests that cubic order increases with increasing temperatures and peptide concentration as the peak intensity generally increased with increasing LS3 concentration. This suggests that the peptide initiates the formation of cubic phases in the sample.

	Temperature (°C)	Peak Intensity	Mid *d*-repeat (Å)	Start rep - Mid (Å)	Mid rep - End (Å)	Width of Peak (Å)
PE (Lα)	32.7	221624	59.30	4.07	3.58	7.65
1 to 200 (Lα)	33.4	238306	59.00	2.74	2.23	4.97
1 to 100 (Lα)	42.1	42446	59.30	3.08	2.52	5.61
1 to 75 (Lα)	30.3	72703	59.59	2.79	1.72	4.51
1 to 50 (Lα)	27.5	27259	59.29	6.50	4.60	11.10
1 to 33 (Lα)	20.2	66290	59.59	9.23	6.82	16.05
1 to 25 (Lα)	23.6	56363	60.19	5.25	4.99	10.24
	Temperature (°C)	Peak Intensity	Mid *d*-repeat (Å)	Start rep - Mid (Å)	Mid rep - End (Å)	Width of Peak (Å)
PE (H_{II})	54.2	73653	73.01	4.73	3.79	8.52
1 to 200 (H_{II})	54.4	153751	70.44	3.47	3.16	6.63
1 to 100 (H_{II})	20.2	80486	72.13	4.13	5.60	9.73
1 to 75 (H_{II})	20.6	123673	72.57	3.21	3.75	6.95
1 to 50 (H_{II})	20.4	122752	72.57	3.21	3.35	6.56
1 to 33 (H_{II})	69.1	104647	67.66	1.96	2.21	4.17
1 to 25 (H_{II})	69.7	142952	67.28	1.94	2.54	4.48
	Temperature (°C)	Peak Intensity	Mid *d*-repeat (Å)	Start rep - Mid (Å)	Mid rep - End (Å)	Width of Peak (Å)
1 to 200 (Q_{II})	34.4	11360	96.51	4.11	5.23	9.34

1 to 100 (Q/Q_{II})	44.1	19306	128.56	12.06	7.77	19.82
1 to 75 (Q/Q_{II})	49.2	15469	132.83	11.16	9.55	20.72
1 to 50 (Q/Q_{II})	50.5	17433	137.40	13.86	10.20	24.05
1 to 33 (Q/Q_{II})	55.1	22598	132.83	12.91	12.04	24.95
1 to 25 (Q/Q_{II})	52	22219	127.20	10.20	11.08	21.28

Table 3.2: SAXS peak diffraction intensities of the different phases observed of all lipid + LS3 concentrations. Start rep to Mid is the distance in Å from when the diffraction peak starts and till it reaches peak intensity (peak intensity = Mid-*d* repeat). Mid rep to End is the distance in Å from the peak intensity to the end of the diffraction peak.

Temperature Gradient Cell Samples

***Cis*/*Trans* PE:** Inverse hexagonal phase was the only structure observed (from 36°C to 49°C). It was unusual that only the inverse hexagonal phase was observed without any lamellar phase in the sample. The cell covered a suitable temperature range that would show both phases with a clear transition between phases (**Figure 3.10**). The absence of the lamellar phase in the temperature gradient sample was unexpected, but it has been shown previously that the coexistence of lamellar and inverse hexagonal phases does not necessarily follow each other (Laggner et al., 1991).

1 to 75 (LS3:PE): Inverse hexagonal phase is clearly observed. Evidence of primitive cubic phases is observed, but confirmation of the type of cubic phase (either *Pn3m* or *Im3m*) cannot be made without appropriate peaks to index (**Figure 3.10**). The cubic phase diffraction peaks decease in size across the temperature gradient cell and one can observe the cubic peak (initially observed at s-value 0.0115) moving towards the inverse hexagonal peak (positioned at *s*-value 0.014) and merging with the inverse hexagonal diffraction peak around 36°C. The introduction of LS3 to the DOPE system, provides evidence to suggest that it initiates the formation of the cubic phase. The weak diffraction signal may indicate that the formation of the cubic phases, may be transitory process in the formation of the inverse hexagonal phase.

Lamellar X-ray Diffraction: Taiwan X-ray scans analysis

Three samples (*cis*/*trans* PE, 1 to 100 LS3/PE and 1 to 10 LS3/PE) were tested at 32°C varying the relative humidity (rh) of the samples from 64rh to 93rh (**Figures 3.12, 3.13** and **3.14**).

Cis/*Trans* PE:

The diffraction peaks at all relative humidities were relatively strong (**Figure 3.12**). At low humidity 69rh, lamellar diffraction is extremely weak, the initial formation of the inverse hexagonal phase is just visible to the naked eye. The inverse hexagonal phase diffraction peaks increase in intensity to a maximum of 81rh. With regards to the lamellar phase, a double peak is observed at the first Bragg reflection. This indicates the formation of two separate bilayers of different *d*-repeat distances, which can be explained by the difference in the packing of the *cis* and *trans* PE in the bilayer. From 84rh onwards, inverse hexagonal diffraction has been eliminated, whereas the lamellar diffraction reflections increase in intensity as the humidity increases to three Bragg reflections at 93rh.

1 to 100 (LS3:PE)**:**

Weak dual lamellar and inverse hexagonal diffraction reflections observed from 64rh (**Figure 3.13**). Diffraction for both phases increase in strength until 84rh where the inverse hexagonal phase reflections are at their peak. At 90rh, the inverse hexagonal phase has been eliminated from the sample. The lamellar phase reflections become narrower and sharper, showing a higher order of lamellar phase in the sample. This would indicate that the hydration level is high enough

for the DOPE lipids to reorient from inverse hexagonal phase to the lamellar phase. No cubic phases observed in the sample across the different hydration levels.

1 to 10 (LS3:PE):

At all humidities, the Bragg reflections observed are weaker in intensity compared to the intensities observed with PE and the 1:100 reflections (**Figure 3.14**). Weak inverse hexagonal phase Bragg reflections are observed at humidities 64rh% to 78%rh, by 81%rh the inverse hexagonal phase has been eliminated. This result would seem to corroborate the previously conducted 1:25 SAXS experiment, where no inverse hexagonal phase was observed in a fully hydrated sample at 32°C, and was only detected at around 53°C. Lamellar diffraction increases in intensity as the relative humidity increases. At 84rh, three orders of lamellar diffraction peaks are observed and increase in intensity with increasing humidity. There is also a noticeable small angle scattering diffraction peak observed from the main diffraction patterns.

Unfortunately, due to time and resources constraints, further LXD experiments could not be conducted on the range of DOPE/LS3 concentrations that were conducted on SAXS experiments.

Further electron density analysis is required on the LXD data in order to understand the effect of hydration levels on the change in membrane thickness and the change of area per DOPE molecule as a function LS3 concentration.

T (°C)	*d* (Å)	*w* (Å)	(*l*) (Å)	*v* (Å^3)	*A* (Å^3)
Cis DOPE -4	53.1	13.1	20.1	1190	59.3
0	52.9	13.0	20.0	1190	59.7
4	52.6	13.0	19.9	1190	60.3
Trans DOPE 50	53.3	13.0	20.2	1210	60.4
55	52.7	12.9	20.0	1220	61.2
60	52.2	12.7	19.8	1220	62.0

Table 3.3: Data in the table shows the *d* (*d*-spacing), *w* (water layer thickness), *l* (lipid length), *v* (lipid volume), *A* (headgroup area at the lipid-water interface) for *cis* and *trans* DOPE in the Lα phase (modified table data taken from Harper et al., 2001).

T (°C)	*d* (Å)	*r* (Å)	*(l)* (Å)	*v* ($Å^3$)	*A* ($Å^2$)
4	79.8	23.8	18.3	1190	47.8
8	78.5	23.2	18.2	1200	47.8
12	77.3	22.6	18.2	1200	47.8
20	75.3	21.6	18.1	1210	47.6
30	72.9	20.4	18.0	1220	47.4
40	70.8	19.4	17.9	1230	47.2
50	68.9	18.5	17.8	1230	47.2
60	67.2	17.9	17.5	1240	47.8
70	65.7	17.2	17.4	1250	48.3

Table 3.4: Data in the table shows the *d* (*d*-spacing), *r* (average water radius), *l* (lipid length), *v* (lipid volume), *A* (headgroup area at the lipid-water interface) for *cis* and *trans* DOPE in the H_{II} phase (modified table data taken from Harper et al., 2001).

Diacyl-PE		
	d-spacing	
Chain Structure	L_α (Å)	H_{II} (Å)
Cis DOPE	52.1	77.9
Trans DOPE	51.6	75

Table 3.5 : *Cis* and *Trans* DOPE *d*-spacings of the lamellar phase and inverse hexagonal phase at the L_α/H_{II} phase transition (data from table was taken from Harper et al.,2001)

Discussion and Conclusion

Only the inverse hexagonal phase was observed during the *cis*/*trans* PE temperature gradient experiment, the lack of the lamellar phase being observed was unexpected, especially as prior DSC and X-ray temperature ramping experiments have clearly shown the presence of lamellar phase between 20°C – 36°C. Previous research has shown that the coexistence of lamellar and inverse hexagonal phases does not necessarily follow each other (Laggner et al., 1991), so this may explain why only the inverse hexagonal phase is observed in the *cis*/*trans* PE sample. With the introduction of LS3, (1:75), the diffraction pattern indicates a strong inverse hexagonal phase observed in the sample from 23°C to 49°C. As the temperature rises through the temperature gradient cell, smaller cubic phases increase in s-value towards the first inverse hexagonal peak at a *S* value of 0.014. As previously stated, the introduction of LS3 to the DOPE system, suggests that it triggers the formation of the cubic phase. The weak diffraction signal may indicate that the formation of the cubic phases, may be transitory/precursor process in the formation of the inverse hexagonal phase.

Previous studies have shown that cubic phases of DOPE do not form instantaneously and usually requires several days of equilibration for the formation of a cubic phase to occur (So et al., 1993). The literature has also shown examples of the formation of the cubic phases in PE lipids systems being accelerated with the introduction of sodium salts, disaccharides sucrose and trehalose during multiple lamellar to inverse hexagonal phase cycling (Tenchov et al., 1998). The introduction of LS3 to both the temperature gradient cell and the

temperature scanning DOPE samples showed the formation of cubic phases, previous literature has shown that viral fusion peptides can promote the formation of bilayer cubic phases in lipid samples (Tenchov et al., 2013). While the wild type influenza virus fusion peptide disordered the lamellar phase like LS3. LS3 did not abolish the inverse hexagonal phase, but rather stabilised the inverse hexagonal phase at higher temperatures.

With regards to the temperature ramping experiments, increasing temperatures increased the disorder of the lamellar bilayer from the head group towards the end of the hydrocarbon chains. This resulted in a tendency to form cone shaped lipid molecules, leading to a temperature-induced lamellar to inverted hexagonal H_{II} phase transition. The curved interface of a H_{II} phase allows the chains to splay apart more while allowing the interfacial area to be kept minimal. With the formation of various cubic phases, they consist of a bicontinuous area of water and hydrocarbon tails. Inverted cubic phases also exist and they have their periodic minimal surfaces reside along the middle of the bilayer. Inverted cubic phases also the follow the same space group as a normal *Pn3m* (primitive cubic phase) (Erbes et al. 1994). With my results, it cannot be confirmed if my cubic phase is inverted or not. Identification via indexing alone cannot differentiate between the two cubic structures. The scattered intensities obtained from my results only showed at most, two Bragg reflections for each phase. It is unfortunate that this is not enough detail to calculate the electron density profiles of the lipid system. If this information was available, I would have been able to calculate the size, area and volume of the headgroup, acyl chains and water layer of my bilayer systems at different temperatures and peptide concentrations, which would have provided

greater insight to the effect that the peptide and temperature has on my bilayer system during different phases.

Comparing the *d*-repeats from my *cis*/*trans* DOPE temperature ramping experiment to the results observed from Harper et al., 2001 (**Table 3.3** and **Table 3.4**). The results obtained for the *d*-repeats observed using SAXS are not directly comparable for both the lamellar phase and inverse hexagonal phase. This may be explained by the fact that Harper et al., 2001 was testing *cis* DOPE and *trans* DOPE separately which may explain the discrepancy in *d*-repeats. In the lamellar phase, I observed a *d*-repeat of 57.8Å at 49°C compared to 53.3Å at 50°C for Harper (Harper et al., 2001). For the inverse hexagonal phase I observed *d*-repeat of 73.5Å at 42°C, whilst Harper (Harper et al., 2001) observed 70.8 Å at 40°C. When it came to the *d*-repeat observed at the lamellar to inverse hexagonal phase transition, the *d*-repeat that I observed in the inverse hexagonal phase of 73.5Å was more comparable to the Harper results of 75Å (**Table 3.5**). With more detailed analysis of the data, I would focus on determining the water layer thickness, average headgroup area and lipid length at the different phase transitions. Understanding the change in these variables would provide more insight into how the introduction of LS3 in the DOPE system encourages the formation of cubic phases in the lipid system.

With the introduction of LS3, increasing the concentration of the peptide in the lipid also showed a decreased *d*-repeat during the inverse hexagonal phase. This is an interesting observation, as this would suggest a loss of water from the core of the inverse hexagonal phase, resulting in a more tightly packed inverse hexagonal phase. With regards to the lamellar phase, the *d*-repeat at 50°C

observed in *trans* DOPE is 53.3Å; in my studies, my mixed *cis*/*trans* DOPE bilayer without peptide showed that at 50°C my *d*-repeat was at 57.9Å. The difference between the two *d*-repeats can be explained by the fact that the composition of my membrane included the cone shaped *cis* DOPE. The consequence is, that there is an increase in disorder in the bilayer that decreases the ability of the lipid molecules to pack closer together, resulting in a thicker *d*-repeat.

The *d*-repeat for the cubic phase after 40°C decreased in value almost linearly (the exception, peptide/lipid 1 to 100 concentration which showed gave anomalous results in all observed phases). This is an interesting observation as the majority of the cubic phases *d*-repeat decreased by 35-50Å above 40°C. It could be hypothesised that the drastic decline in size of the cubic phase is a result of the lipid being destabilised by the presence of the LS3. It is completely bypassing the traditional cubic/lamellar phase transition and undergoing a phase transition directly to the inverse hexagonal phase (**Figure 3.15**).

It has been reported that WALP peptide (an alanine-leucine repeat peptide anchored with tryptophan at either end) has been shown to stabilise inverted cubic phases of N-monomethylated dioleoylphosphatidylethanolamine (DOPE-Me) (stabilisation of the cubic phase is dependent on peptide length and the study focus on peptide length between 19-31 amino acids in length) (Siegel et al., 2006). This study is easily comparable to research conducted in this study; peptide/lipid concentrations that were tested are comparable, the composition of LS3 is similar (in my case leucine/serine repeat and with Siegel an alanine/leucine repeat). The results in the WALP study are comparable to this study, as upon heating, the

lamellar phase forms either primitive cubic or inverted primitive cubic phase being formed (in Siegel's case, inverse cubic phase).

Further heating showed the formation of inverted hexagonal phase from the relative cubic phase, but the major difference with my findings and the Siegel study (Siegel et al., 2006) is that with increased peptide concentration (particularly at 1 to 33 and 1 to 25 concentrations) the lamellar/cubic phase temperatures shows a general increase in temperature (compared to Siegel where the lamellar/cubic phase transition decreases in linearly). Admittedly in my results, the 1 to 33 concentration has a higher phase transition temperature 35.7°C than at 1 to 25 peptide/lipid concentration which has a phase transition temperature of 25.2°C). But it is clearly observed that at the lower peptide concentrations, the formation of cubic phases was already present in the sample during the start of the temperature ramping experiments at 20°C.

Mentioned earlier, the maximum intensities for each phase were observed for each of the samples as it indirectly represents the order and regularity of the lipids. In order to make a comparison of peak intensity, it is only comparable with sample concentration. In this case lipid concentration was comparable in all the samples, the only difference in concentration was the change in LS3 across the *cis*/*trans* DOPE samples. The higher the peak intensity, the greater number of ordered DOPE/LS3 is in its respective phase. The width of the *d*-repeat can be used as a proxy of lipid packing order and stability. The wider the *d*-repeat peak, this indicates that the lipids in a particular phase have a wider variation of *d*-repeat at a specific temperature, which would suggest a lower packing order and stability. As concluded, the inverse hexagonal phase was stabilised in the presence of LS3,

at the highest peptide concentration (1 to 25) the intensity was 142952 compared to 73653 without LS3, which is approximately a 100% increase of the intensity of the sample without the peptide. For the corresponding concentrations the lamellar phase, the intensity also decreased from 221624 (with no LS3) to 56363 (1 to 25), a reduction in intensity by almost 75%. The cubic phase intensity at 1 to 200 LS3/lipid concentration was 11360 compared to 22219 (1 to 25), which is approximately a 100% increase in intensity at the highest peptide concentration. When put into context, the maximum cubic intensity at 1 to 25 is still around 15.5% of the maximum intensity of the inverse hexagonal phase and around 40% of the maximum intensity of the lamellar phase. The introduction of the LS3 clearly initiates the formation of cubic phases in my lipid system, and the formation of the cubic phases seem to be an intermediary phase in the formation of the inverse hexagonal phase. Hypothetically, the destabilisation caused by LS3 may be as a consequence of increasing the curvature and thinning of the lamellar phase, where the lamellar phase may be undergoing stalk fusion formation (Siegel, 1993) during this intermediate cubic phase that is formed. This indicates that the most energetically favourable orientation of the peptide on the bilayer in descending order of phases are:

Inverse hexagonal > Lamellar > Cubic

Chapter 4: Positioning of LS3 in the *Cis*/*Trans* DOPE Bilayer using Neutron Scattering

Aims of the chapter

The aim of the work described in this chapter was to:

Follow on from the X-ray experiments to determine the position and orientation of the peptide on my *cis*/*trans* DOPE bilayer.

Test two peptide/lipid concentrations on my lipid bilayer system to determine if there is any change in orientation and position of the peptide on the bilayer.

Calculate the water profiles of the peptide/lipid systems to determine the distribution of water along the bilayer.

In previous chapters, I have discussed about the introduction of LS3 into the lipid bilayer system and how it has changed the phase transition and phases observed in the lipid system. In this chapter I shall be focusing on the positioning of the LS3 peptide in the bilayer using neutron scattering.

Neutron Scattering Summary:

Neutron scattering is a non-invasive technique used to study biological molecules in their native environment. Compared to X-rays, which interact with the electron cloud of the atom, and potentially damage the sample, neutrons interact directly with the nucleus of the atom, this is because the wavelengths of neutrons can be configured to match the distance between atoms. This means that the strength of neutron scattering by an atom is not simply a function of the atomic number. Different isotopes of the same element can scatter neutrons either positively or negatively, the difference in scattering between isotopes is known as the neutron scattering length. Neutrons can scatter elastically or inelastically either coherently or incoherently. Inelastic scattering is associated with the neutron having a change in kinetic energy after interacting with a sample, so when the scattered waves interact with each other, then you are able to follow the dynamics of a particular atom over a period of time, but as a result, the relative positions of the other atoms in the structure are eliminated. With elastic scattering, the energy of the neutrons remains unchanged, but a consequence to that is that the dynamic information of the sample is eliminated and you are left with the static structural information of the sample. When neutrons are scattered coherently, this means that the phase of the incident and scattered wave are the same, and when these

waves interact with each other, the relative positions of the atoms are able to be determined, allowing the collective motion of atoms in the structure to be defined.

The use of 8% heavy water in sample preparation:

The difference in coherent scattering length between ^{1}H and ^{2}H, one can obtain the position of hydrogens within a structure. ^{1}H diffracts negatively whilst ^{2}H diffracts quite strongly positively. The coherent neutron scattering density of water ($^{1}H_2O$) is negative whereas the coherent scattering of heavy water ($^{2}H_2O$) is positive and, conveniently for structural biologists, the neutron scattering densities of all classes of biological macromolecule (protein, nucleic acid, carbohydrate, lipid) fall within the range between the densities of water and heavy water. This means it is possible to "contrast match" the neutron scattering density of any biological macromolecule by a particular mixture of water and heavy water. So, by using an 8% $^{2}H_2O$ solution, the net neutron scattering length density of the water in the sample is zero, and in this case, the only scattering comes from the LS3 DOPE samples and not from the surrounding water.

Neutron scattering data was collected from phospholipid samples at three different relative humidities (rh) (100%, 97% and 95%rh) and $^{2}H_2O$ concentration (8% and 25% $^{2}H_2O$). The samples contained either un-deuterated LS3 peptide, or an analogue in which one of the leucine residues had been replaced with a deuterated leucine. The isotope replacement of leucine, also known as isomorphous replacement, changes the scattering length of the sample without changing the structure of the LS3 peptide. This is one of the strengths of neutron scattering compared to X-ray diffraction as neutron scattering can be used to determine the orientation and interaction of LS3 with the bilayer.

It has been hypothesised that the positioning of LS3 lays perpendicularly on the bilayer surface, and that it is able to "flip" into a trans-membrane orientation, under the influence of the natural membrane potential difference on a living cellular membrane. I aimed to mimic the "flip" across the membrane by using high concentrations of the peptide (1 to 50 and 1 to 10 peptide: lipid ratio) in order to try and force the peptide to flip into a trans-membrane orientation.

Sample Preparation

Three deuterated versions of the LSSLLSLLSSLLSLLSSLLSL peptide were synthesised with a ^{2}H10 deuterated leucine residue at the N terminal (position 1), middle (position 12) or C terminal (position 21) of the peptide. The peptides were synthesized by ALMAC Sciences and purified to 95% as confirmed by HPLC and MALDI-TOF analysis. Leucine residues were chosen for the deuteration sites as it allows a higher level of deuteration (10 deuterons) than serine (only available with 3 or 7 deuterons).

50:50 isomeric mixtures of *cis/trans* DOPE at 20 mg/ml were dissolved in chloroform. The peptide was dissolved in methanol and added to the lipid to form a 1:50 and 1:10 peptide:lipid molar ratio. The mixtures were deposited onto quartz microscope slides, with an artist's airbrush, using an inert gas (either Argon or Nitrogen) at 3 Bar pressure as a propellant. The method has been described previously (Darkes, et al., 2002). All traces of solvent were removed by placing the slides under vacuum in a desiccator for at least two hours.

Figure 4.1: The images show the main components in the D16 set-up. The far left image shows the slide with airbrushed sample held on a goniometer and facing the incident neutron beam; underneath the sample is a reservoir of 8% or 25% $^{2}H_2O$. The upper middle image shows the sample can unattached. The far right image shows the attached sample can to the rotating sample stage, the attached pipes are connected to two water baths that can adjust the temperature of the water flowing in and out of the can which can create a temperature difference between the bottom and top of the can (the temperature change between the top of the can from the bottom of the can creates the difference in humidity in the sample container, so that even with a temperature change of 1°C between the top and bottom of the can, there can be a decrease in the relative humidity by 2%). The final image shows the complete set-up of the sample at D16 at the Institut Laue-Langevin (ILL), Grenoble.

The samples were rehydrated in sealed sample cans for 6 h at 37°C for 1:50 samples and for 6hrs at 32°C for the 1:10 samples (**Figure 4.1**). The relative humidity of the sample was set to 100%, 97% or 95% by controlling the temperature of the water bath in respect to the sample temperature (temperature

range for samples were between 30°C and 37°C). Neutron contrast variation experiments were conducted at 8% (v/v) and 25% (v/v) $^{2}H_2O$ in order to determine the water profile of the sample at the two LS3 concentrations in the bilayer.

Neutron Data Collection

Neutron diffraction data were collected on a Small Momentum Transfer Diffractometer, D16 at the Institute Laue-Langevin (ILL), France with a cold source and a neutron wavelength of λ = 4.754Å with a beam width of 8.02mm collected on a two-dimensional position sensitive ^{3}He detector. The detector has a width (gamma range) of 14° and is able to be moved around the sample in the gamma plane around 160° towards the main neutron beam (**Figure 4.2**). (Gamma is the measurement of the angle between the un-diffracted and diffracted incident neutron beam).

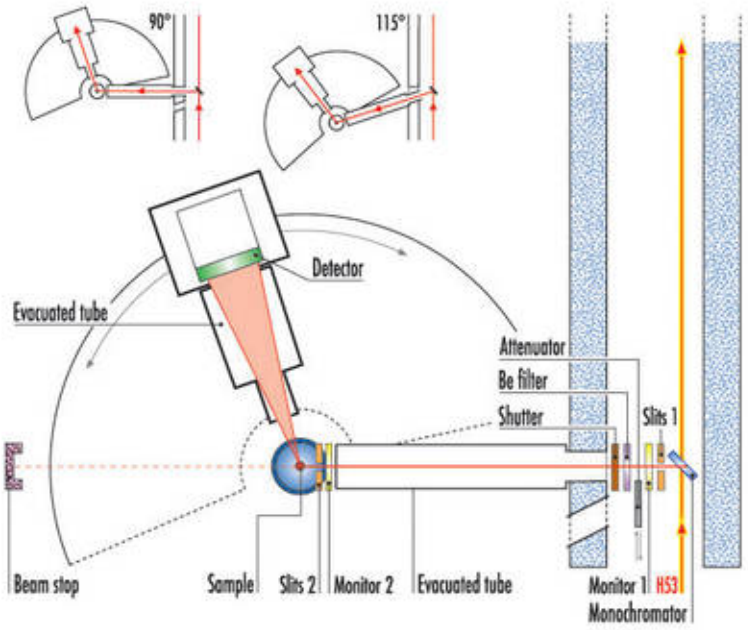

Figure 4.2: Cartoon representation of the layout of D16, showing how the incident neutron beam wavelength of 4.754 Å is selected using the monochromator crystals, the slit system can widen or narrow the width of the beam. The beam is now scattered by the sample and the resultant beam is picked up on the ^{3}He detector. The detector measures the diffracted beam. The sample angle is measured in omega and the detector angle is measured in gamma. The detector works by converting the ^{3}He with the neutron to produce ^{1}H and ^{3}H + Q which has an energy of around 764KeV. (http://web.mit.edu/8.13/www/tgm-neutron-detectors.pdf) (last accessed 9th April 2014). The changes in energy released at different points across the detector are measured and is translated into the appropriate diffraction points on the detector screen. Image from http://www.ill.eu/instruments-support/instruments-groups/instruments/d16/description/instrument-layout/ (last accessed 9th April 2014).

Lamellar diffraction data were collected from up to five orders of diffraction to each of the eight samples tested. The predicted Bragg angle peak was scanned using a range of omega that corresponded to θ - 2θ°. Data collected from each of the detector positions for each run were then summed to produce a single diffraction spectrum. Background was subtracted from the diffraction peaks, and the subsequent Bragg reflections were identified and fitted to the Gaussian distributions, and integrated using *LAMP* software. In order to determine the structure factor amplitudes of the samples, Lorentz and absorption correction calculations and the square-root of the diffraction intensities were used.

Samples Tested on D16 Diffractometer at the ILL

The objective of the neutron diffraction experiments was to determine the orientation of the peptide on the bilayer at the hydrophobic interface at (1:50) LS3:DOPE concentration. The original hypothesis postulated that at high concentrations of LS3 on the bilayer, the peptide would flip into a transmembrane orientation. In order to determine if this hypothesis was correct, I included a sample with a high concentration of LS3 on the DOPE membrane (1:10 concentration), Both concentrations of LS3 were tested at different relative humidities, this was done to measure the change of *d*-repeat of the samples as decreasing the relative humidity of the sample may instigate a change in phase from lamellar to inverse hexagonal phase. Undeuterated samples were also tested at 25% $^{2}H_2O$ and 8% $^{2}H_2O$ in order to determine the water profile against the LS3:DOPE sample.

For each sample, data was collected at three separate humidities (95% rh, 97% rh and 100% rh) at 8% $^{2}H_2O$.

50% *cis/trans* ^{2}H-N terminal LS3 peptide (1 to 50)

50% *cis/trans* ^{2}H-mid LS3 peptide (1 to 50)

50% *cis/trans* ^{2}H-C terminal LS3 peptide (1 to 50)

50% *cis/trans* LS3 peptide (1 to 50) (Conducted at 8% and 25% $^{2}H_2O$)

50% *cis/trans* ^{2}H-N terminal LS3 peptide (1 to 10)

50% *cis/trans* ^{2}H-mid peptide LS3 (1 to 10)

50% *cis/trans* ^{2}H-C terminal LS3 peptide (1 to 10)

50% *cis/trans* LS3 peptide (1 to 10) (Conducted at 8% and 25% $^{2}H_2O$)

Data analysis

For each sample, the diffraction intensity was obtained from the detector counts according to the pixel response, and the diffraction images were folded linearly into a rocking curve. The rocking curves of each scan were visualised by the D16 instrument software *Lamp*. Amplitude, width and position were determined for each Bragg peaks using *Lamp*; peak area values were calculated in *Excel* (Microsoft) (Chen et al., 2013). Corrections made were determined via the scattering vector q (**Equation 4.1**).

$$q = 4\pi \sin(\theta)/\lambda = 2\pi h/d$$

Equation 4.1 = q represents the scattering vector, λ is the wavelength neutron beam and θ is the scattering angle (2θ represents the angle the detector moves across gamma), d represents the unit cell size of the lipid system and h represents the Bragg order reflection number (Harroun et al., 2008).

Using the basis that there is no net coherent neutron scattering from water with an isotopic composition of 8% ^2H_2O, a continuous single transform function can be fitted to all the structure factors collected with water at 8% regardless of the *d*-spacing. Using similar methodology as (Hu et al., 2008) structure factors values at 8% were plotted and the phase angles (+/-) were adjusted so that structure factors from all 3 relative humidities fitted the same continuous transformation. The water profile was calculated by subtracting the 8% ^2H_2O from the profile obtained from the 25% ^2H_2O scan.

Structure factor values (**Table 4.1** and **4.3**) for any given *d*-repeat can then be calculated from the 8% ^2H_2O continuous transform function data using the

swelling series method (Darkes & Bradshaw., 2000). The Fourier summations that have been used to calculate the neutron-scattering density maps gives rise to a one-dimensional bilayer representation that shows the relative position and orientation of the peptide on the bilayer (**Figures 4.3**, **4.4** and **4.5** and **Figures 4.6, 4.7** and **4.8**). The use of one deuterated leucine residue on the peptide has two advantages with regards to data analysis:

1) With one deuterated label, a single Gaussian distribution will be observed. This information will provide structural information on where and how the specific deuterated leucine interacts with the DOPE membrane.
2) The process of model-fitting to difference profiles is simplified, as each deuterated leucine can be represented by a single Gaussian distribution, so there are fewer variables to consider.

In the so-called difference method, data from undeuterated samples are subtracted from the corresponding data from deuterated samples, so that everything disappears in the subtraction apart from the deuterium labels. The subtractions can be carried out in real space (bilayer profiles) or reciprocal space (diffraction patters). The advantage of carrying out the subtraction and subsequent model-fitting in reciprocal space is that it mitigates the effects of termination error. Termination error is the name given to the effect whereby the bilayer profiles are calculated from an incomplete set of diffraction data. In my experiments, I never collected diffraction data from more than 5 Bragg peaks. The bilayer profiles, therefore, were affected by the lack of orders 6, 7, 8 etc. Termination error occurs because the number of Bragg reflections measured is limited. In theory, to avoid termination error completely, an infinite number of

Bragg reflections need to be collected. Termination error in our neutron profiles will be unavoidable, but the effect can be removed by fitting models to the diffraction data, which is a measure of reciprocal space (Schoenborn., 2010).

Results and Discussion

Unfortunately, the raw diffraction data could not be shown in the thesis as the data was visualised using LAMP software which was only situated at the D16 station. Fourier and data analysis was conducted on site the neutron structure factors were directly calculated at the station using a bespoke Microsoft Excel spreadsheet.

Initially, diffraction of the peptide/lipid system was difficult to acquire due to the system diffracting weakly. This was because the peptide/lipid system easily formed non-lamellar structures, which are not suited to measurement using lamellar diffraction techniques. I even observed small non-lamellar inverse hexagonal diffraction occurring, but due to poor diffraction, only two Bragg reflections were observed in this phase.

Once the optimal temperature and humidity ranges had been determined, regular lamellar diffraction peaks were observed for the 1:50 and the 1:10 peptide/lipid systems. The neutron profiles are discussed below. With regards to the different relative humidities (rh) tested in the sample, (95%, 97% and 100% rh) it became clear that the small changes in humidity had little effect on the change in *d*-spacing of the sample and had no effect on peptide orientation across the bilayer.

Peptide System 1 to 50

The *d*-repeat is calculated by the inverse of reciprocal space of the Bragg reflections. The *d*-repeat for 1 to 50 LS3:DOPE bilayers was 45.6Å at 97%rh, which seems small, but this may be explained by a change in the lateral pressure profile.

The lateral pressure of a bilayer describes the lateral forces across the width of a bilayer. Lateral pressure can vary depending on membrane depth, negative at the polar and apolar region between the acyl chains and lipid headgroups and positive due repulsions between acyl chains (Brink-van der Laan., et al 2004). Previous fluorescence and ^{2}H-NMR studies have postulated that conical shaped non-bilayer lipids like DOPE, the lateral pressure would increase in the acyl chain region and be reduced across the headgroup region (Templer et al., 1998 and Gawrisch and Holte., 1996).

With the bilayer being composed using a 50% mixture of *cis* and *trans* DOPE. The *cis* bond at C9, gives the lipid a wide conical profile compared to the *trans* bond at C9 which provides comparably a more cylindrical profile. If you make the hypothesis that LS3 peptide resides parallel to the bilayer at the phosphoethanolamine headgroup, then the DOPE lipids may be compressed due to an increase of lateral pressure at acyl chains region. In the acyl chain region, the PE dielaidoyl and dioleoyl tails may separate further from each other due to the interaction of LS3 on PE headgroup region, which may contribute to a reduction the d-repeat of the bilayer. Previous studies have also suggested that antimicrobial peptide binding parallel to the bilayer surface induces positive

curvature, that increases the surface area of the hydrophilic region of the bilayer, which consequently decreases the thickness of the hydrophobic acyl chain area (Hallock et al., 2003 and Matsuzaki et al 1998).

When LS3 is added to the phospholipid bilayers, it is likely that the *d*-repeat will change. However, the difference in method requires two data sets that have the same *d*-repeat. The swelling series method produces a single continuous transform from which the structure factors for any chosen *d*-repeat can be determined. A *d*-repeat of 45.6Å was chosen for the difference method subtractions because 45.6Å lay within the measured range of *d*-repeats for each of the 1 to 50 samples.

The position of the label peaks confirmed the location of the peptide residing parallel to the hydrophobic/hydrophilic interface of the bilayer (**Figures 4.3, 4.4** and **4.5**). At this peptide concentration, the peptide covers 9% of the bilayer.

Peptide Coverage Calculation

This was calculated as follows:

Marsh (Marsh., 2013 page 452) gives the volume of a DOPE molecule as 1239Å^3. From the bilayer profiles, the width of the lipid bilayer is (approximately) 35Å, so a single DOPE molecule must be 17.5Å long. Dividing 1239Å^3 by 17.5Å gives 70.8Å^2 as the area of each DOPE molecule on the surface of the bilayer.

The volume of the peptide is 2612Å^3 (calculated using Peptide property calculator http://www.basic.northwestern.edu/biotools/proteincalc.html last accessed 24th April 2014). Since the peptide is 21 amino acids long, its length must be approximately 21 x 1.5Å, or 32.25Å. Dividing this into the total volume gives 2612 / 32.25 = 80.4Å^2 as the cross-sectional area of the peptide. Assuming the peptide to approximate to a tube, and noting that the area of a circle is equal to πr^2, the radius of the peptide must therefore be 5.1Å. If the peptide lies parallel to the bilayer surface, its area must therefore be 32.25Å x 5.1Å x 2 = 326.4Å^2.

At a concentration of 1 to 50, the relative areas of total lipid and total peptide are as follows.

Lipid: 50 x 70.8Å^2 = 3540.0Å^2

Peptide: 1 x 326.4Å^2 = 326.4Å^2

Meaning the peptide covers 9% of the bilayer at a concentration of 1 to 50. The corresponding numbers for 1 to 10 is: lipid 708Å^2; peptide 326.4Å^2; total coverage 46%.

1 to 50 Structure Factors

	F (1)	*F* (2)	*F* (3)	*F* (4)	*F* (5)	*Total Error*	*% Error*
1 to 50 LS3	19.7	-0.09	-3.22	-5.05	2.1	N/A	N/A
1 to 50 ^{2}H - Nter	22.6	-1	-5.07	-7	2.1	1.21	3.20
1 to 50 ^{2}H - Mid	16.5	-1.23	-3.55	-3.5	0	1.51	12.93
1 to 50 ^{2}H - Cter	56	1.5	-10	-12.5	0	1.87	2.34

Table 4.1: Neutron structure factors values for the 1 to 50 LS3/DOPE bilayers at 8%$^{2}H_2O$ and 97% rh. Undeuterated LS3 peptide with three separate LS3 peptides with deuterated hydrogens at leucine positions. (1,11 and 21) Total error and % error is the result of the sum of errors of each diffraction order observed.

1 to 50 Bilayer Profiles

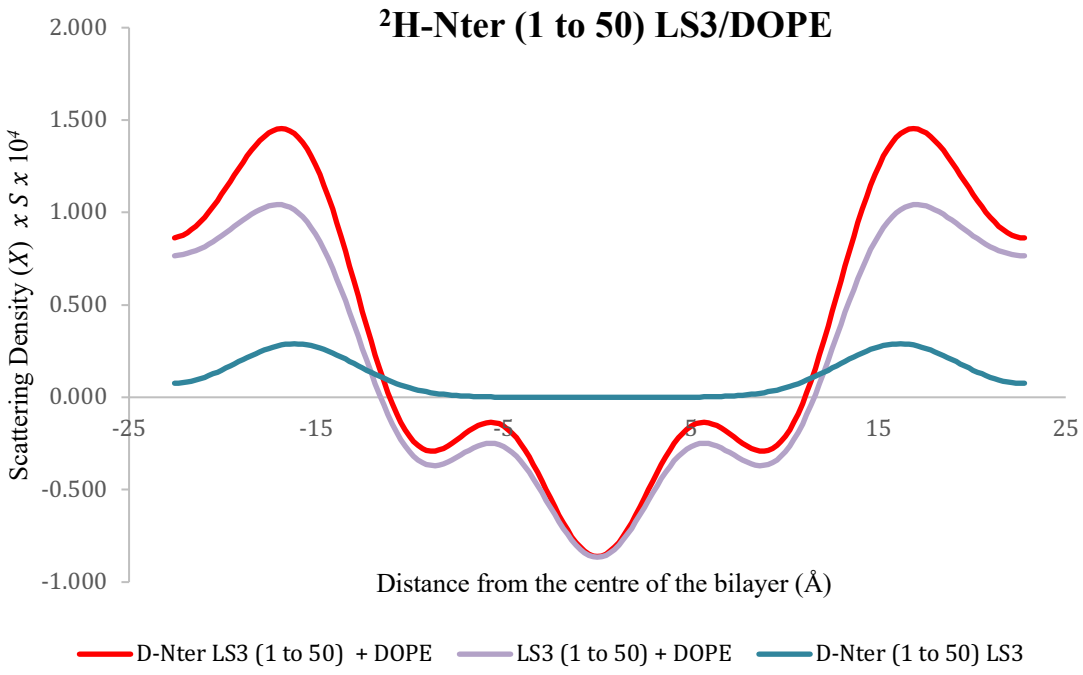

Figure 4.3: Neutron scattering length density profile of 50:50 (mol) mixture of PE lipid with 1 to 50 deuterated LS3 peptide at leucine 1 (start of peptide) in 8% ^2H_2O at 97% relative humidity. Scattering density is expressed in arbitrary units. The red line represents the deuterated peptide + lipid and the lilac line represents the un-deuterated peptide + lipid. The blue line is a representation of the deuterated peptide on the bilayer.

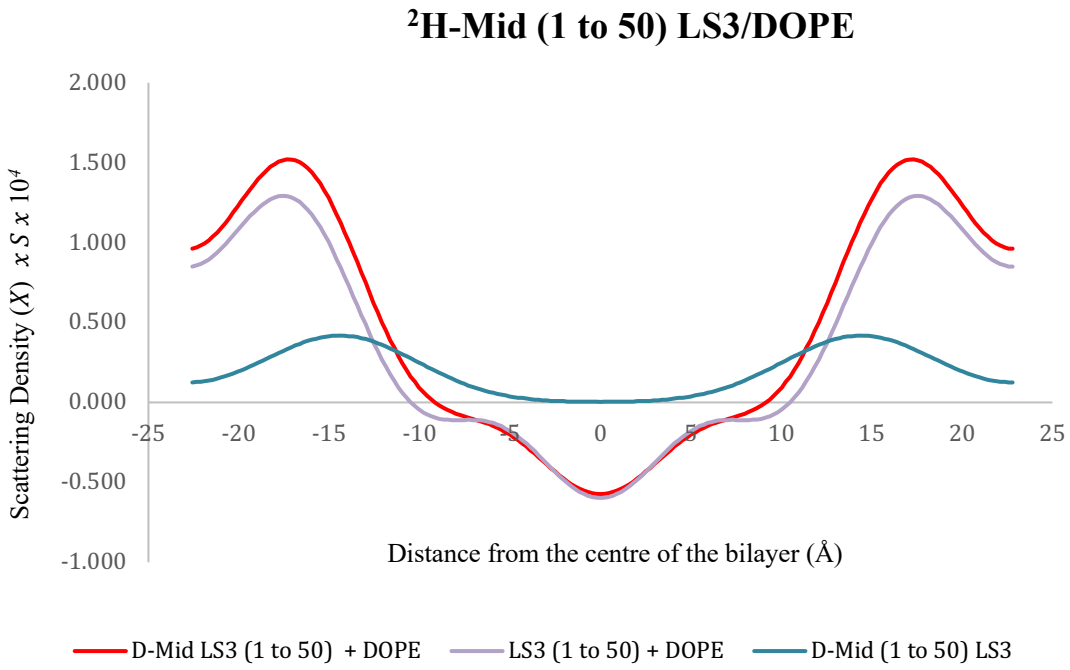

Figure 4.4: Neutron scattering length density profile of 50:50 (mol) mixture of PE lipid with 1 to 50 deuterated LS3 peptide at leucine 11 (middle of peptide) in 8% ^2H_2O. Scattering density is expressed in arbitrary units. The red line represents the deuterated peptide + lipid and the lilac line represents the un-deuterated peptide + lipid. The blue line is a representation of the deuterated peptide on the bilayer.

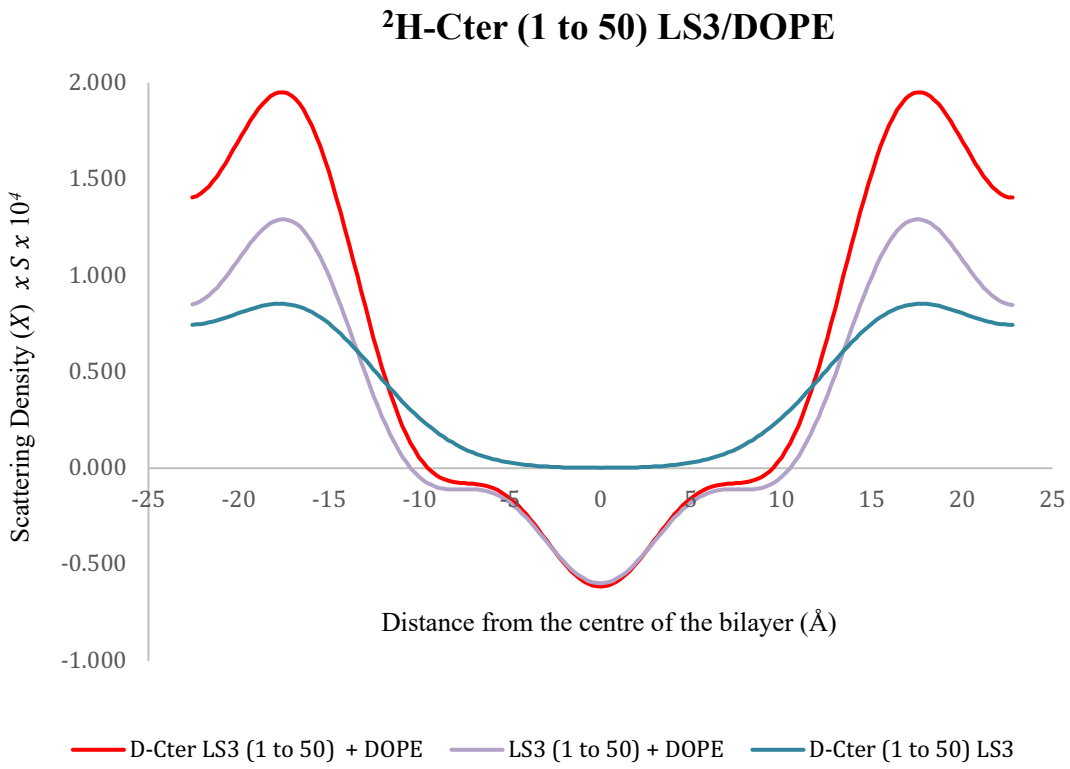

Figure 4.5: Neutron scattering length density profile of 50:50 (mol) mixture of PE lipid with 1 to 50 deuterated LS3 peptide at leucine 21 (C-terminal) in 8% $^{2}H_{2}O$. Scattering density is expressed in arbitrary units. The red line represents the deuterated peptide + lipid and the lilac line represents the un-deuterated peptide + lipid. The blue line is a representation of the deuterated peptide on the bilayer.

LS3 positioning on the bilayer

Peptide system 1 to 50:

Neutron scattering length density profiles (**Figures 4.3, 4.4** and **4.5**) were calculated using the values in **Table 4.1** and **Table 4.3**. Profile differences were determined by subtracting DOPE bilayers from each of the DOPE + LS3 (deuterated and undeuterated samples) profiles. The profiles were fitted in reciprocal space, which consist of Gaussian distributions pairs that were matched to the structure factors using the least-squares refinement method, manual scaling adjustments were made to the model in order to reduce the error observed between the difference between the models (Balali-Mood et al., 2005 and Chen et al., 2013). Using the bilayer profiles of the three deuterated LS3 peptides seen previously (**Figures 4.3, 4.4** and **4.5**) the location of LS3 is shown to be lying on the surface of the DOPE bilayer (**Table 4.2**). If the peptide was trans-membrane, then the Gaussian models which represent the deuterated leucines (shown in blue) would be located between -10Å and +10Å along the Z axis. The leucines at position 1 (^{2}H-Nter) and 21 (^{2}H-Cter) are shown to be level with the positioning of the phosphate headgroup of the lipid bilayer. With regards to the position of leucine 11 (^{2}H-Mid), the results show that the leucine residue is inserted slightly into the bilayer headgroup. As leucine is unipolar and hydrophobic, the orientation with the helical wheel fits with the observed data. This does not mean that deuterated leucines are fixed at that location in the bilayer; the experiment shows the average positions of the deuterated leucines along the bilayer during the experiment.

Deuterated Leucine Positions

	1 to 50 ^{2}H-Nter	1 to 50 ^{2}H-Mid	1 to 50 ^{2}H-Cter
Guassian Position	19.3	17.6	20.1
Guassian Width	4.7	6.1	6.6

Table 4.2: The separate deuterated positions of the 1 to 50 LS3 peptide on the bilayer determined by fitting the Gaussian distributions in reciprocal space. Positions of each deuterated label is calculated from the distance of the centre of the bilayer (Å).

Peptide System 1 to 10

The position of the lamellar Bragg peaks shows the *d*-repeat of the phospholipid bilayers with LS3 peptide at a 1 to 10 molar ratio is 50Å. The position of the label peaks confirmed the location of the peptide residing parallel to the hydrophobic/hydrophilic interface of the bilayer (**Figures 4.6, 4.7 4.8 and Table 4.4**). At this concentration, the peptide covers 46% of the bilayer. The location of the peptide across the bilayer is at a similar orientation and position on the hydrophobic/hydrophilic interface as the previous 1 to 50 peptide system. A high concentration of peptide was used in order to try and flip the peptide perpendicularly in the bilayer. The importance in peptide flipping in the bilayer, is linked to previous electrophysiology experiments conducted on the black membrane experiments showing membrane pore formation (Lear et al. 1997). However, no flipping of the LS3 peptide was observed, even at high peptide concentration.

1 to 10 Structure Factors

	F (1)	*F* (2)	*F* (3)	*F* (4)	*F* (5)	*Total Error*	*% Error*
1 to 10 LS3	14.04	-2.88	-2.77	-2.3	1.98	N/A	N/A
1 to 10 ^{2}H-Nter	23.68	-6.6	-4.51	-2.8	2.7	0.61	1.51
1 to 10 ^{2}H -Mid	20	-6.5	-4.9	-2.4	2.8	0.50	1.37
1 to 10 ^{2}H -Cter	22	-7.7	-4.62	-2.31	2.59	0.25	0.64

Table 4.3: Neutron structure factors values for the 1 to 10 LS3/DOPE bilayers. Undeuterated LS3 peptide with three separate LS3 peptides with deuterated hydrogens at leucine positions. (1,11 and 21) Total error and % error is the result of the sum of errors of each diffraction order observed.

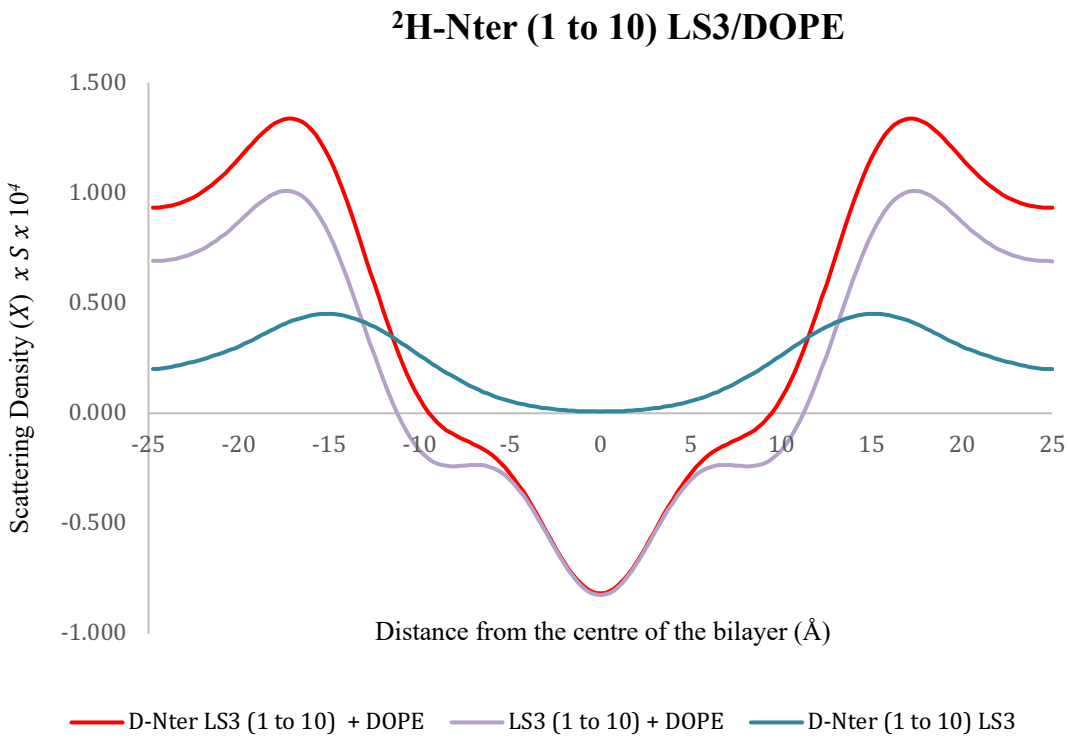

Figure 4.6: Neutron scattering length density profile of 50:50 (mol) mixture of PE lipid with 1 to 10 deuterated LS3 peptide at leucine 1 (start of peptide) in 8% ^2H_2O. Scattering density is expressed in arbitrary units. The red line represents the deuterated peptide + lipid and the lilac line represents the un-deuterated peptide + lipid. The blue line is a representation of the deuterated peptide on the bilayer.

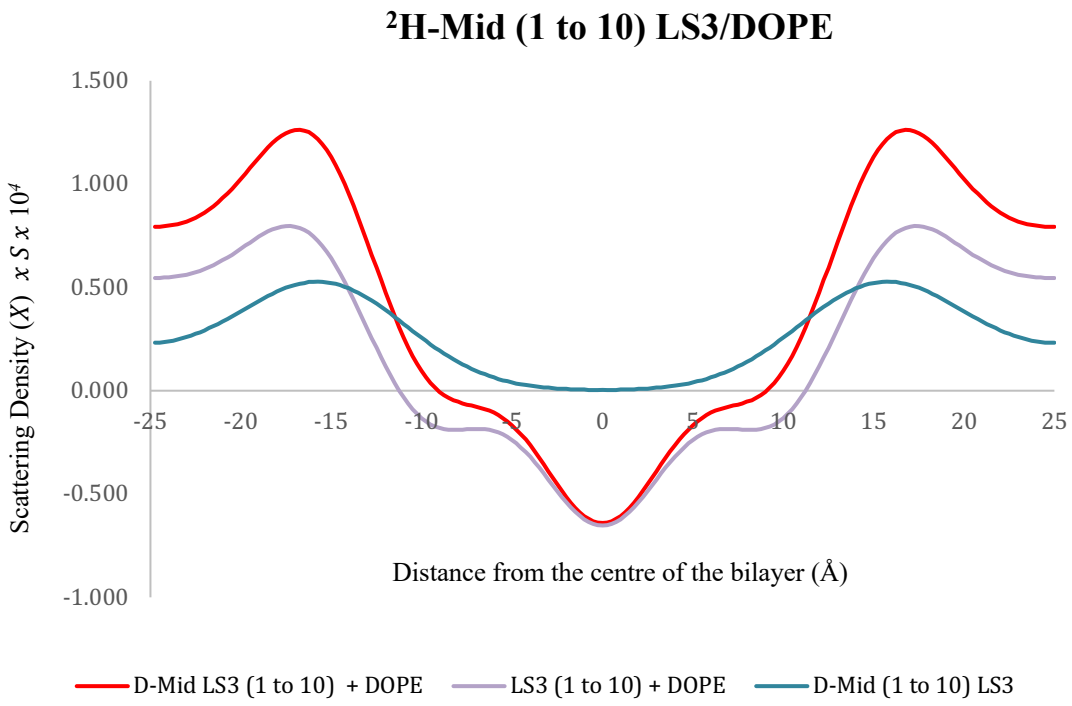

Figure 4.7: Neutron scattering length density profile of 50:50 (mol) mixture of PE lipid with 1 to 10 deuterated LS3 peptide at leucine 11 (middle of peptide) in 8% ^2H_2O. Scattering density is expressed in arbitrary units. The red line represents the deuterated peptide + lipid and the lilac line represents the un-deuterated peptide + lipid. The blue line is a representation of the deuterated peptide on the bilayer.

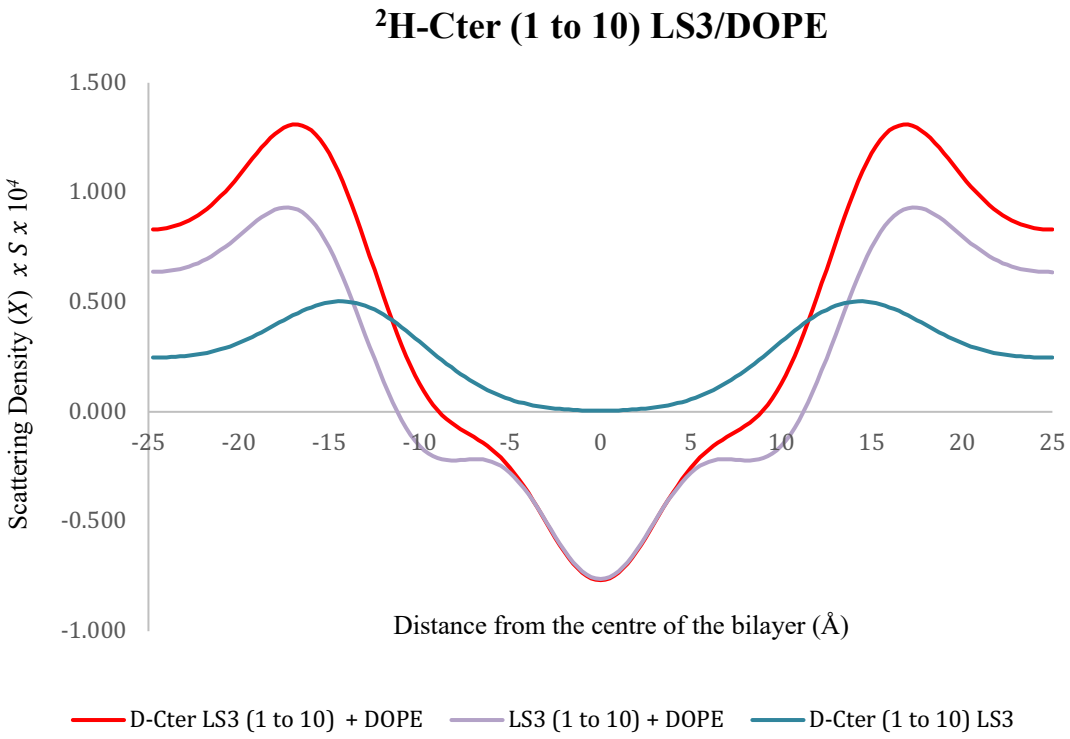

Figure 4.8: Neutron scattering length density profile of 50:50 (mol) mixture of PE lipid with 1 to 10 deuterated LS3 peptide at leucine 21 (C-terminal) in 8% $^{2}H_2O$. Scattering density is expressed in arbitrary units. The red line represents the deuterated peptide + lipid and the lilac line represents the un-deuterated peptide + lipid. The blue line is a representation of the deuterated peptide on the bilayer.

LS3 positioning on the bilayer

	1 to 10 ^{2}H -Nter (1)	1 to 10 ^{2}H-Nter (2)	1 to 10 ^{2}H -Mid (1)	1 to 10 ^{2}H -Mid (2)	1 to 10 ^{2}H -Cter (1)	1 to 10 ^{2}H -Cter (2)
Gaussian Position	16.1	24	16.5	24	15	23.9
Guassian Width	7	3	6.6	6.2	6.2	6.4
Occupancy %	94.1	5.9	89.8	10.2	80.3	19.7

Table 4.4: The separate deuterated positions of the 1 to 10 LS3 peptide on the bilayer determined by fitting the Gaussian distributions in reciprocal space. Positions of each deuterated label is calculated from the distance of the centre of the bilayer (Å).

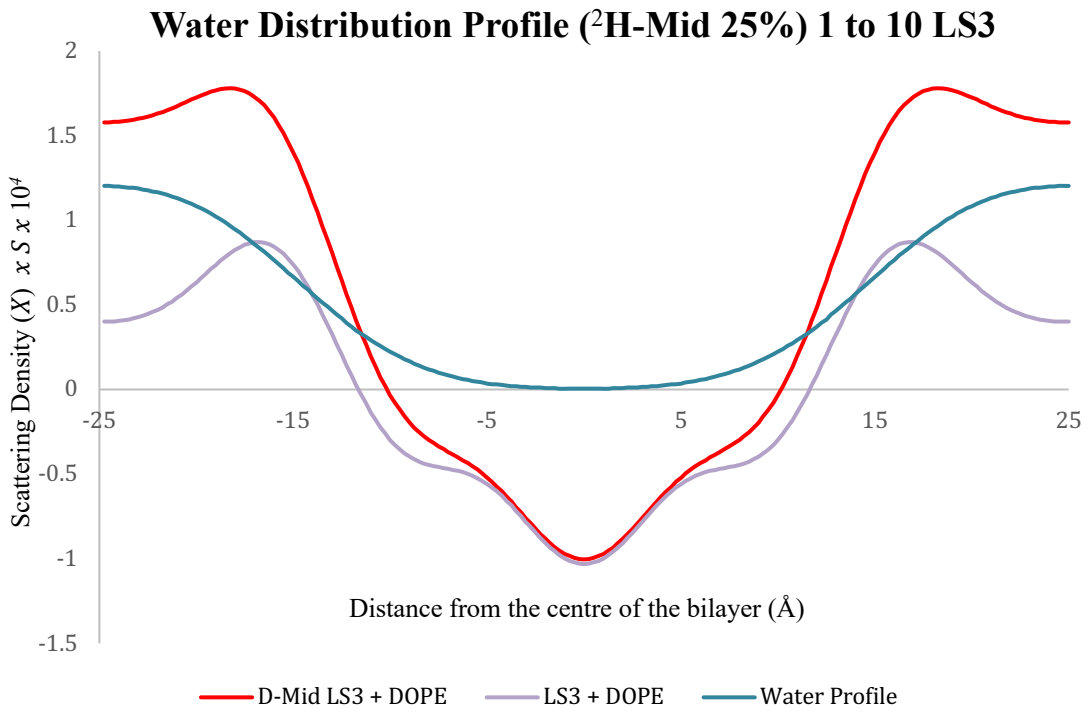

Figure 4.9: Neutron scattering length density profile showing the 25% $^{2}H_2O$ water distribution across the 1 to 10 LS3/DOPE bilayer system. Scattering density is expressed in arbitrary units. The red line represents the water profile of deuterated peptide + lipid and the lilac line represents the water profile of the un-deuterated peptide + lipid. The blue line is a representation of the water profile distribution on the bilayer.

Water Profile Structure Factors

	F (1)	*F* (2)	*F* (3)	*F* (4)	*F* (5)	*Total Error*	*% Error*
25% 1 to 10 LS3	20	-6.5	-4.9	-2.4	2.8		
25% 1 to 10 ^{2}H-Mid	27.31	-3.44	-4.34	-2.05	1.84	0.85	2.18

Table 4.5: 25% $^{2}H_2O$ water profile neutron structure factor values for un-deuterated and deuterated 1 to 10 LS3. Total error and % error is the result of the sum of errors of each diffraction order observed.

Water Distribution at 1 to 10 LS3/DOPE

Water Profile	**1**	**2**
Gaussian Position	21	13.5
Gaussian Width	8	6.1
%	96.3	3.7

Table 4.6: The water profile positions on the bilayer is determined by fitting Gaussian distributions in reciprocal space. Each deuterated label position is calculated from the centre of the bilayer.

The deuterated labels on the LS3 peptide have been located in the bilayer system using the Fourier transformed neutron profiles shown previously (**Figures 4.3 - 4.9**). However, this does not reflect the possible orientations that the peptide can be configured on the membrane. In order to do this the following methodology was used to simulate the position of the peptide on the bilayer using the three deuterated positions of the peptide at both 1 to 50 and 1 to 10 concentrations. To refine the orientation of the peptide further on the membrane, the water profile for the 1 to 10 sample is included. The water profile (**Figure 4.9** and **Table 4.6**), the majority of the water (96.7%) is located ±21Å and above from the middle of the bilayer. There is a 3.7% chance that the water is located 13.5Å from the middle of the bilayer. The phosphate group of our bilayer system shows that it is located at 17.3Å from the middle of the bilayer. Consequently, the results indicate that a small amount of water was able to penetrate the bilayer. No water profile could be submitted for the 1 to 50 sample as performing the experiment at 25% $^{2}H_2O$

resulted in only two diffraction peaks observed, unfortunately not enough diffraction orders to obtain a viable water profile.

Model Fitting (Performed by the Harroun laboratory, Brock University Canada)

An initial helical model with all-atom atomic co-ordinates was created using Avogadro molecule editor and visualiser software to create the LS3 (LSSLLSLLSSLLSLLSSLLSL) peptide, using fixed dihedral angles $\varphi = -60°$ and $\psi = -40°$

With the initial 3D coordinates, the model fitting program first translates the peptide so that the labelled residue with the narrowest distribution is at the z position given by the centre of the neutron distribution for it. The centre of the deuterium label is approximated as the gamma carbon of the leucine residue. The peptide is then pivoted around this point in space until the label with the second narrowest distribution is moved to its z position given by the experimental data. With the two points at the correct location, the peptide is then rotated 360° degrees around the vector connecting the first two label centres until the third label reaches its z position, within 0.001 Å. This process produces 2 possible orientations for the peptide with the correct z positioning for the three- labelled points.

To determine the most probable of the two remaining peptide orientations, an energy penalty is created to measure the hydrophobic mismatch. **Equation 4.2** is adapted from Ducarme, (Ducarme et al., 2000), with a modification to the shape of the energy penalty function.

$$E = -\sum_{i=1}^{N} S_i E_i^{tr} C(z_i)$$

Equation 4.2: Modified equation from Ducarme (Ducarme et al., 2000) to determine the probable peptide orientations.

Where S_i is the solvent accessible surface area for atom i (obtained via the POPS online program (Cavallo, Kleinjung, & Fraternali., 2003), E^{tr} is the transfer energy (***Table* 4.7**) and $C(z_i)$ is the penalty function, all of which are summed over all of the atoms in the molecule.

The shape of the penalty function $C(z)$ is the hydrophobic-hydrophilic transition interface, and can be modelled from the water distribution. Since the centre of the diffraction-determined water distribution is not at $d/2$, that a single Gaussian does not capture the exact shape interface of the hydrophobic-hydrophilic due to the influence of the water distribution mirror-image from the adjacent unit cell.

Thus, a single Gaussian centered at $d/2$ was fit to two Gaussians; one centered at the supplied value of Z and another at $d - Z$, and the values of $Z_0 = d/2$ and fit width were used in **Equation 4.3**. $C(z)$ describes the hydrophobic and hydrophilic range, where -0.5 is the maximum hydrophobic area and +0.5 represents the most hydrophilic area (**Figure 4.10**).

Since we do not have the water distribution for 1 to 50 sample, the value of Z_0 was taken to be $d/2$ for that sample and the width was scaled such that the value of $C(z)$ at the z position of the phosphates was the same in both samples.

$$C(z) = -0.5 + e^{-1/2\frac{(Z-Z_0)^2}{\sigma^2}}$$

Equation 4.3: Calculation of the summed shape of the peptide/lipid penalty function.

Atomic types	Transfer energies per accessible surface (KJ/mol Å^2)
C*sp*3	-0.105
C*sp*2	-0.0134
H (=O)	-0.0397
H (/O)	0.0362
O	0.0403
N	0.112
S	-0.108

Table 4.7: Atomic Surface Transfer Energies for the Seven Atomic Types adapted from (Ducarme et al. 2000)

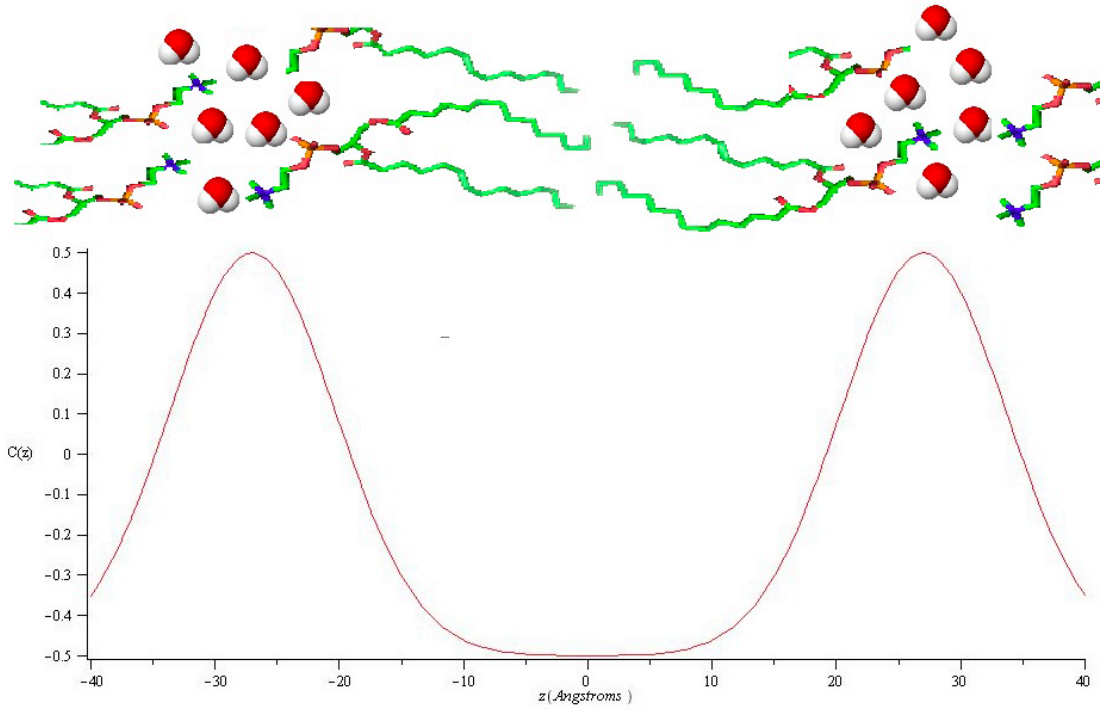

Figure 4.10: The penalty score given to an atom due to its depth in the bilayer (z=0 is the centre of the bilayer). Representative water molecules and lipid molecule are above.

Model Fitting: Possible orientations of LS3 in the bilayer:

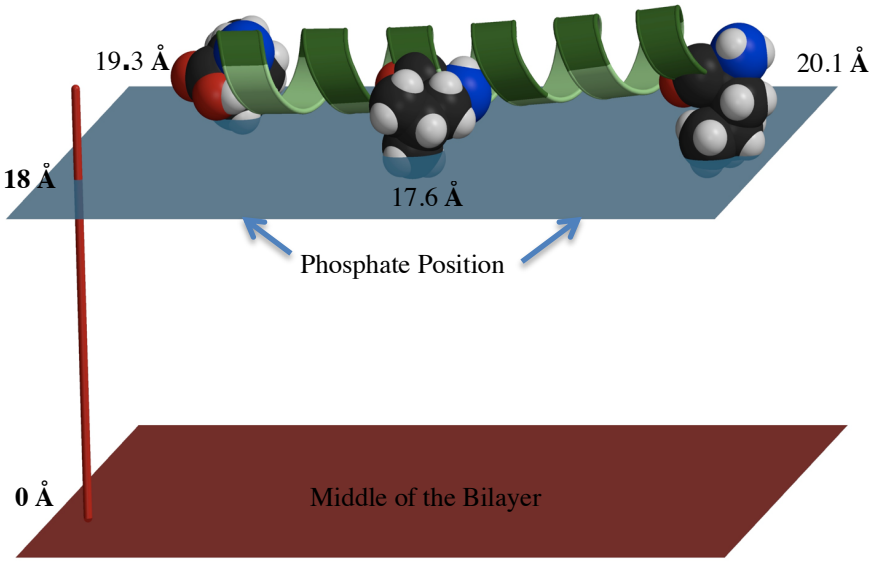

Figure 4.11: 1 to 50 peptide orientation on the bilayer (center of the membrane represented in red, lipid phosphate levels in blue) insertion angle of the peptide 4.0° (insertion angle is calculated from the gradient of a line of best fit through the alpha carbons)

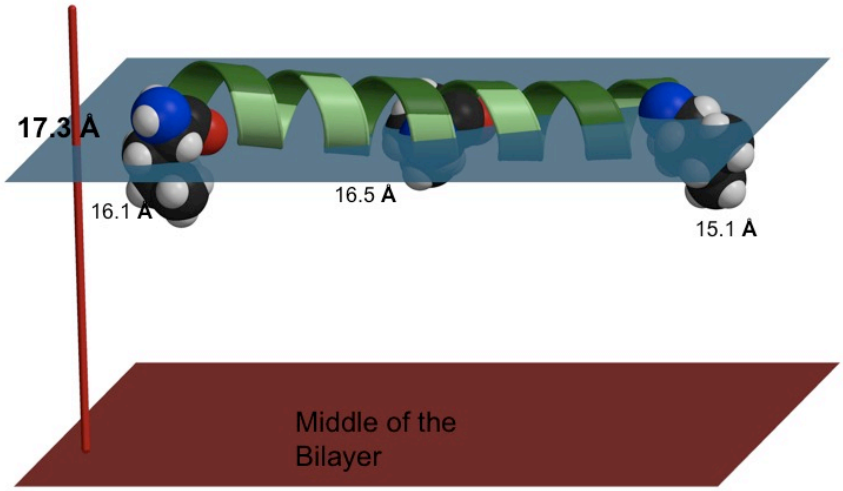

Figure 4.12: 1 to 10 first possible orientations on the bilayer (center of the membrane represented in red, lipid phosphate levels in blue) insertion angle 6.2°.

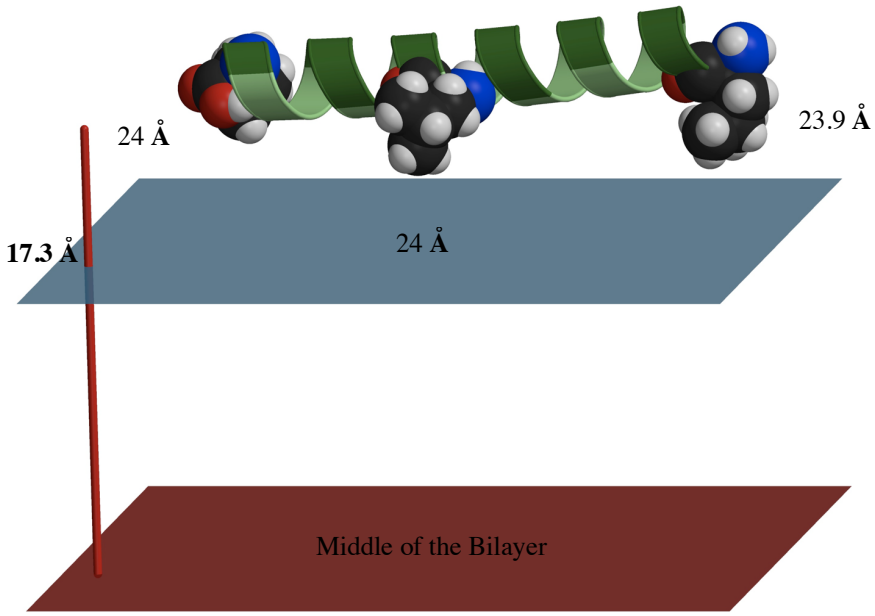

Figure 4.13: 1 to 10 second possible orientations on the bilayer (center of the membrane represented in red, lipid phosphate levels in blue). Insertion angle of 5.4°.

The results of the peptide orientation at the two different concentrations show that at the higher peptide concentration (1 to 10) the peptide is mostly buried between 1.5Å to around 5Å deeper in the membrane than at the lower peptide concentration (**Figures 4.11, 4.12** and **4.13**). There is also a 6% to 20% chance from N-terminal to C-terminal end (**Figure 4.13**) that the peptide would reside in the water region (**Table 4.4** and **4.6**). This may be explained by a couple of possibilities:

1) The peptide is causing such massive curvature on the membrane that the water is filling in the resultant leftover space from the increased negative curvature in the bilayer (see DSC chapter **Figure 2.5**).
2) The concentration of the peptide on the bilayer is so high that the peptides are literally piling on top of one another. The peptide at 1 to 10

concentration is taking up 46% of the lipid bilayer surface. Consequently, it is entirely possible that stacking of the peptides is giving the two different orientations of the peptide along the bilayer.

The water profile for the 1 to 10 sample showed some water penetration into the bilayer system (**Table 4.6**). There are three possible explanations for the water being in the bilayer:

1) The high concentration of the peptide on the bilayer has created a negative curvature on our lipid system. As a result, the bilayer will thin and water will take the place of the thinning membrane, so the water appears to be penetrating the average position of the phosphate group.
2) The high concentration of peptide also brings associated water. So the peptide penetrating the bilayer, will have water around the same depth where the peptide has penetrated the bilayer.
3) Because 3.7% of the water is at 13.5Å from the middle of the bilayer, it could be just a simple case of proton exchange from the $^{2}H_2O$ from the water to the peptide.

Model fitting of the peptide at 1 to 50 and 1 to 10 concentrations, the angle of insertion was calculated by measuring the gradient of a line of best fit of the alpha-carbons. The calculations indicate that the peptide resides on the bilayer with a small angle ranging from 4° to 6.2°. The greater the angle of insertion was associated with the higher peptide concentration. This could be explained by the reasons listed earlier with regards to peptide orientation. Unfortunately, no details on the rotation and torsional angles are available of the peptide; for that

information to be obtained, molecular dynamic simulations of the peptide on a model bilayer system are required to obtain the additional information.

Chapter 5: Conclusion and Further Studies

Summary of results

DSC:

Testing different *cis*/*trans* DOPE mixtures, I found that at 60% *cis* and 50% *cis* DOPE mixtures had a phase transition temperature of 35.7˚C and 40.3˚C respectively. These mixtures were possible starting points for the development and formation of temperature sensitive liposomes.

The introduction of the LS3 peptide into the MLV liposomes decreased the temperature of the phase transition from lamellar to inverse hexagonal phase. The introduction of LS3 at 1 to 25 peptide/lipid concentration (4 mol%) decreased the phase transition temperature from 35.7˚C to 34.4˚C and from 40.3˚C to 37.6˚C.

From my research it seems that the first step in creating temperature sensitive liposomes (between 38˚C and 40˚C) is by using a 50:50 isomeric mixture of *cis*/*trans* DOPE and having a peptide/lipid concentration of 1 to 50 (0.02 mol%).

Summary of results

X-ray diffraction:

The temperature gradient cell experiments showed two features of interest: Both the *cis*/*trans* DOPE and the 1:75 LS3 had no presence of the L_α phase in the sample. The 1:75 LS3 sample had two observed phases in the sample, *Im3m* and H_{II}.

The temperature ramping cell showed that the introduction of LS3 stabilised the inverse hexagonal phase and induced the formation of the bicontinuous cubic phase (*Im3m*).

High peptide concentrations decreased the *d*-repeat in all observed phases upon heating:

Lamellar phase: the *d*-repeat decreased linearly from 61.1Å to 57.9Å.

Inverse hexagonal phase: the *d*-repeat distance decreased from 79.8Å to 67.6Å.

Cubic phase: the *d*-repeat distance actually increased from 20˚C to 40˚C, but above 40˚C the *d*-repeat distance decreased from 165.9Å to 105.8Å.

In general, the introduction of LS3 into the lipid stabilised both the inverse hexagonal and cubic phases as the *d*-spacing increased at lower temperatures. This suggests that the LS3 reduced negative curvature strain on inverse hexagonal and cubic phases. The decrease in *d*-repeat distance in each of the phases upon heating may be the result of increased negative strain on the membrane, where associated water would slowly be eliminated and the phases are more tightly

packed. Heating itself would have increased the instability of the phase, as the lipid molecules movements would have increased disorder within the system.

The peak intensities for each phase represent describes the extent of the phase (amount of phase that is producing the diffraction), where the width of the diffraction peaks is inversely related to the order. The greater the LS3 concentration in the sample indicated an increased amount of H_{II} phase in the samples with increased levels of order in the sample. Higher concentrations of LS3 also showed higher levels of *Im3m* phase in the sample, but this corresponded with a widening of the peaks that indicated that a reduced level of order in the *Im3m* phase.

The most energetically favourable orientation of the peptide on the bilayer, is in descending order of phases, are: Inverse hexagonal > Lamellar > Cubic

Summary of results

Neutron Scattering

I tested the location and orientation of the peptide on the bilayer system at two concentrations: 1 to 50 and 1 to 10.

Small changes in humidity had little effect on the *d*-repeat for the different concentrations.

No LS3 peptide flipping was observed, even at the higher 1 to 10 concentration. It was found that LS3 was located at the hydrophobic/hydrophilic interface at both concentrations. The position of the LS3 on the bilayer was at the phosphate region of the membrane.

The peptide has a slight tilt from 4° to 6.2° with respect to the membrane plane.

The water profile at 1 to 10 concentration showed the majority of the water (96.3%) distributed along the bilayer was 21Å from the middle of the bilayer.

The remaining 3.7% of the water was positioned 13.5Å from the middle of the bilayer.

Discussion

The original intention of the study was to produce a viable temperature sensitive liposome delivery system using the model peptide LS3. Whilst that may have been the case during the DSC experiments, the data provided caused the focus of my project to change to study the effect the peptide had on DOPE lipid structure using X-ray diffraction and neutron scattering after my DSC results.

Using evidence from Chung, (Chung, Lear, & DeGrado., 1992) my original hypothesis stated that LS3 would reside on the membrane surface of a DOPE bilayer, and stabilise the bilayer. With DOPE being categorised as a non-lamellar forming lipid, the interaction of LS3 on the membrane surface was believed to stabilise the lamellar phase by increasing the L_α to H_{II} phase transition temperature, by decreasing the strong negative membrane curvature of the DOPE bilayer system to a flatter lamellar orientation.

After the completion of the DSC experiments, it became clear that the contrary had occurred. The introduction of LS3 to the DOPE bilayer system destabilised the lamellar structure and decreased the L_α to H_{II} phase transition temperature. To understand why this was the case, conducting further studies on the interaction of the peptide on the DOPE bilayers became the main objective of the PhD.

In order to understand why the phase destabilisation would be advantageous from a biological perspective. It is important to remember that PE lipids can make up around 75% of *Escheirchia coli (E.coli)* inner membrane, and it has been postulated that PE lipids are involved in the formation of non-bilayer structures

(Gennis., 2013). Previous studies involving *Acholeplasma laidlawii* and *E.coli* has shown that these bacteria try to keep their membrane lipids near a non-bilayer/bilayer phase transition in order to quickly undergo temporary rearrangement (Morein et al., 1996, Lindblom et al., 1993 and Vikström et al., 2000). The temporary rearrangement may due to cell division (Kruijff., 1997) and the formation of temporary formation of inverted structures involved in membrane fusion and in the movement of lipids and solutes (Darkes et al., 2002, Siegel and Epand., 1997, Ellens et al., 1989 and Epand., 1998). The formation of inverted cubic phases has been observed in the endoplasmic recticulum and parts of the inner mitochondrial membrane (Landh., 1995 and Jouhet., 2013).

My X-ray and neutron experiments were carried out at large-scale scientific facilities. While these facilities allow scientists to access techniques that are not available at their home universities, there are also disadvantages associated with this type of research. These experiments took place at large international scientific centres around the world. Organising the experiments requires the research group to apply for a particular amount of beam-time between 6-12 months in advance. If the application is unsuccessful (rejection can occur because the instrument was oversubscribed during any particular allocation period), the experiment will be delayed for at least another 6 months. Other problems occur that are beyond one's control. The reactor shuts down, radiation leaks along the beam-line, computer software and hardware issues. I have experienced all of these delays, and they have eaten into the experiment time and prevented me from performing more samples and having a greater number of peptide lipid concentrations (specifically with regards to neutron scattering).

X-ray data analysis is an extremely time-consuming affair, for two days of experiment time, a vast amount of data is generated and can take many months to analyse. Once analysed the data showed the structural phases, changes in *d*-repeat with respect to temperature. The results indicate that LS3 stabilises the inverse hexagonal phase at higher temperatures and initiates the formation of cubic phase structures at lower temperatures. Before adding LS3 to the *cis*/*trans* DOPE system, the X-ray data showed no cubic phase formation during temperature ramping. With the addition of increasing concentrations of LS3 to the lipid system, the formation of cubic phases was clearly observed and the *d*-repeat increased for the cubic phase and to a lesser extent to inverse hexagonal and lamellar phases with increasing concentrations of LS3 (~2.5 Å). The inverse hexagonal phase was also observed at higher temperatures with increasing concentrations of LS3. This would suggest that the introduction of LS3 on the lipid system provided thermostability of the inverse hexagonal phase. The evidence tends to suggest that increasing concentration of LS3 decreases the negative curvature because the observed *d*-repeat increased at higher LS3 concentrations. This would make sense if this is the case, as the introduction of the peptide into the lipid system would have associated water and therefore increasing the LS3 concentration would also increase the number of associated water molecules which would increase the *d*-repeat size.

The substantial increase in *d* -repeat with LS3 concentration (~60 Å) is clear, but the relationship between LS3 concentration and *d* -repeat is not linear. Peak cubic d-repeat was observed at 1 to 75 LS3:DOPE at ~165 Å where the *d* -repeat decreased at increasing LS3 levels. The increase in *d* -repeat in this case could be

due to associated water as previously mentioned, or the result of peptide induced expansion into the lipid phase causing the lipid molecules to reorient and creating greater space between the lipid layers. Another possibility could be due to changes in lipid packing due to the LS3/DOPE interactions, in this case LS3 stabilising the cubic phase by decreasing the negative curvature of the lipid system and increasing the *d* -repeat as a result. I think the probability that the increase in *d* -repeat being mainly caused by peptide aggregation is low because the *d* -repeat would have increased in a more linear fashion with increasing concentrations of LS3. The fact that this did not occur suggests that peptide aggregation was not one of the causes of the increase in *d* -repeat.

It is also interesting that the peptide stabilises the inverse hexagonal phase. Currently, I do not have possible explanation why this is the case, but studies have shown that a peptide similar in composition and length (WALP peptide) (Siegel et al. 2006) actually stabilises the inverted cubic phase. However, the major difference between the WALP peptide and LS3 is that WALP is a trans-membrane peptide compared to LS3 that resides on the bilayer surface. The phase transition between the lamellar/cubic phase and lamellar/hexagonal phase is believed to play an important role with regards to membrane fusion and the formation of fusion pores. One of my initial hypotheses stated the LS3 peptide would stabilise the lamellar phase and become unstable after the phase transition to the inverse hexagonal phase. The peptide would be in an unfavourable orientation and would preferentially bind to the negatively charged bacterial membrane. Since I have shown the inverse hexagonal phase is stabilised by LS3, then it can be postulated that the peptide/lipid system can be used to initiate membrane fusion with

bacterial membrane (that has a high % of PE and PS lipids in the membrane) and transfer LS3 peptide into the bacterial membranes via the formation of fusion pores. This could provide an alternative mechanism of delivery for antimicrobial peptides than the one that I proposed previously.

The neutron scattering showed the location of the peptide on the bilayer; using the principles set out by Chen (Chen et al., 2003) and increasing the peptide concentration to 0.1 mol%. My intention was to trigger the pore forming state (I) in my bilayer system and flip the peptide into a trans-membrane orientation. Even at a very high peptide to lipid concentration, initiating pore formation or membrane destabilisation of the lamellar phase did not occur and the peptide remained parallel to the membrane surface. The results showed that the peptide was located like a class A amphipathic peptide which are also located on the surface of the bilayer. So why did LS3 destabilise the lamellar phase by reducing the phase transition temperature and stabilise the cubic phase and inverse hexagonal phase? Traditional class A amphipathic helices have been shown to stabilise the lamellar phase by lying perpendicularly on the hydrophobic/hydrophilic interface, reducing negative strain (Epand et al., 1995, Sato and Feix., 2006, Last et al., 2013). Certain class A amphipathic peptides like aurein 1.2 (Fernandez et al., 2012) and cecropin c1 (Gazit et al., 1996) can induce membrane destabilisation using nonspecific membrane permeabilisation methods. One of the best known is the carpet model (Shai., 2002), where the peptides are absorbed on the membrane surface akin to a detergent. Initially antimicrobial peptides covers the surface of the membrane like a 'carpet' which has the effect of reducing the thickness of the membrane. When the peptide

reaches a critical concentration (which is dependent on the peptide/lipid system), the membrane destabilises and breaks down. Other membrane destabilising mechanisms include the barrel-stave pore and toroidal pores which are shown in **Figure 5.1** (Jäkel et al., 2012).

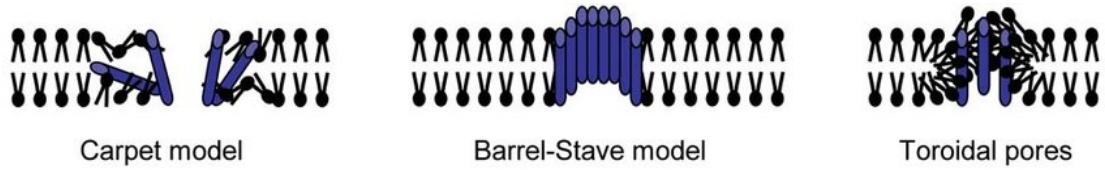

Figure 5.1: Cartoon representation of three main mechanisms of action of antimicrobial peptides. Carpet model shows cationic/hydrophobic peptides that first lie perpendicularly on the membrane surface using electrostatic interactions. Once the peptide covers the membrane like a 'carpet' membrane thickness decreases and at a critical concentration (dependant on the peptide/lipid system) the peptides integrates into the membrane and disrupts membrane stability. Barrel-stave model occurs when the antimicrobial peptide creates a transmembrane channel with the hydrophobic portion of the peptide facing the inside of the pore. The final model, occurs when the membrane cuves into itself causing the formation of a toroidal pore that consists of antimicrobial peptides and the phosphate region (Image taken from Jäkel et al., 2012).

The literature has shown that antimicrobial peptides induced vesicle leakage and membrane fusion has been shown to occur a peptide to lipid molar concentrations higher than 1:50 and it has also been shown that artifacts can be caused at peptide to lipid concentrations above this level (Rausch et al., 2007 and Wimley., 2010). The literature also shows that antimicrobial peptides have been shown to be active at peptide to lipid concentrations between 1:50 and 1:500 when exposed to lipid vesicles (Rausch et al., 2007 and Rathinakumar and Wimley., 2008). In my case, no strong evidence of artifacts was observed at concentrations higher than 1:50 for both X-ray diffraction and neutron scattering. I believe that one of the reasons why LS3 did not flip transmembrane, is because the peptide does not have the same charge distribution like class A peptides but something in between a class A and class L peptide and as the experiments had a lack of an applied

potential difference across the membrane, LS3 did not flip transmembrane to initiate channel formation. Using the preliminary data gathered by the black membrane experiments conducted previously and data shown by Lear and Dieckmann (Lear et al., 1988 and Dieckmann et al., 1999) a potential difference is required for ion channel formation. Previous studies have suggested that pore formation can occur with 3-6 LS3 peptides lining the channel and in one coarse grained model study, pore formation occurred spontaneously using a barrel-stave pore mechanism (Gkeka and Sarkisov., 2008).

Further Studies:

The previous studies in this thesis have shown LS3 destabilising the lamellar phase but stabilising the inverse hexagonal and cubic phases and showing the orientation of LS3 on the membrane having a slight tilt from 4° to 6.2° with respect to the membrane plane. While more structural focused experiments establishing why this is the case can be done with further X-ray diffraction and neutron scattering experiments. Personally, I would want to move the focus of other experimental studies that provide more information of LS3 interacting with a bilayer that has a potential difference applied across it. This is because a potential difference across the membrane seems to be a factor that has not yet been investigated in vivo when investigating LS3 being located in a transmembrane orientation using structural investigative techniques. Multiple molecular dynamic simulation experiments of LS3 have been conducted showing pore/channel formation (Zhong et al., 1998, Dieckmann et al., 1999, Randa et al., 1999, Newns et al., 2000, and Gkeka and Sarkisov., 2008) but there are currently no in vivo structural studies that have been conducted on LS3 interacting with a bilayer that has an applied potential difference across it.

One particular structural study that can be conducted which can investigate the structure and interaction of LS3 on bilayer with an applied potential difference is a neutron reflectometry experiment using a floating bilayer system (Hughes, Goldar, Gerstenberg, Roser, & Bradshaw., 2002). Simply put, a chemically linked monolayer can be attached to a silica substrate and by using a combination of a Langmuir Blodgett and Schaeffer techniques, a monolayer of lipid can be added

one layer at a time to form a floating bilayer system (**Figure 5.2**). Using this setup, it would be possible to add the deuterated LS3 peptide (all leucine residues deuterated if possible). This experimental setup has significant advantages:

Solutions can be controlled by placing chemicals/proteins into the system and allowed to be washed out without disrupting the sample.

Physiologically realistic conditions can be replicated.

A potential difference can be applied across the system.

The last point would be extremely advantages for this experiment as you would be able to see in real time the structural changes of the peptide flipping on the bilayer when it forms an ion channel using the 'voltage gating' mechanism proposed in **Figure 1.19**.

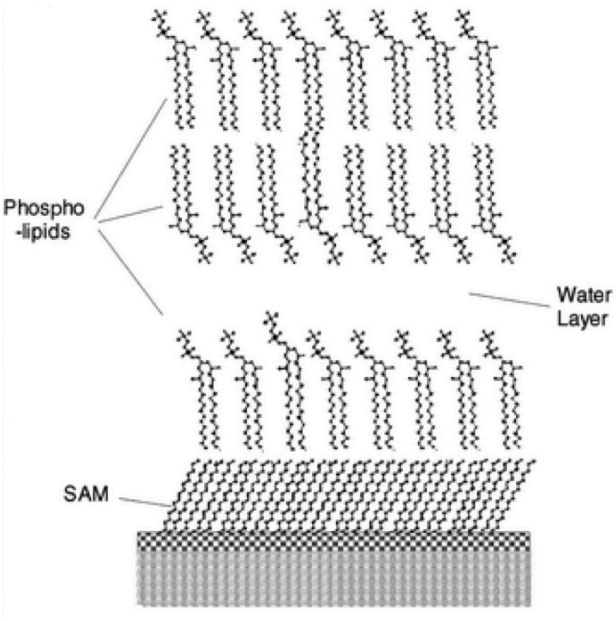

Figure 5.2: Cartoon representation of a floating bilayer system. The chemical linker self assembled monolayer (SAM) is attached to the silicon.. A chemical modified lipid forms a monolayer above the chemical linker. The use of a Langmuir Blodgett dip and Langmuir Schaeffer dip results in the formation of the floating bilayer system. Modified image from (Hughes et al. 2002).

Moving away from structural experiments, I would move the focus of the experiments to see the effect of LS3 on live cultures. In particular, I would like to perform a simple bacterial/fungal culture study to see the effect that LS3 concentration and temperature has on culture growth. Having multiple bacterial cultures (both gram negative and positive) and introducing the LS3/DOPE *cis*/*trans* MLVs to the cultures. They would be incubated at different temperatures over different periods of time to determine if the LS3/liposomes mixtures had an effect on bacterial growth. This would provide insight on whether this potential temperature sensitive liposome is able to transfer LS3 to the bacterial membrane effectively, over the desired temperature range and lastly to determine if the LS3/MLV mixtures are stable/viable over time. Depending on the outcome of the bacteria and fungal culture growth studies, LS3 may also be of interest in oncology treatment. There are studies showing the effects of an amphipathic alpha helical peptides as a cancer treatment (Huang et al., 2012, Papo and Shai., 2003, Schweizer., 2009 and Jäkel et al., 2012). An example of which is $(KLAKLAK)_2$ exhibiting cytotoxicity against various human carcinoma cells (Jäkel et al., 2012). Similar in structure to LS3, $KLAKLAK_2$ is cationic and is known to distort mitochondrial membranes and the peptide has been shown to reduce tumour growth, by specifically inducing apoptosis in cancerous cells. And being able to do further studies determining the potential cytotoxic effects would be my main focus of interest.

References

Albert, A. D., Sen, A., & Yeagle, P. L. (1984). The effect of calcium on the bilayer stability of lipids from bovine rod outer segment disk membranes. *Biochimica et biophysica acta*, *771*(1), 28–34.

Almeida, P.F. & Pokorny, A., 2009. Mechanisms of antimicrobial, cytolytic, and cell-penetrating peptides: from kinetics to thermodynamics. *Biochemistry*, 48(34), pp.8083–93. Available at: http://www.ncbi.nlm.nih.gov/pubmed/19655791.

Amenitsch, H., Rappolt, M., Kriechbaum, M., Mio, H., Laggner, P. and Bernstorff, S., 1998. First performance assessment of the small-angle X-ray scattering beamline at ELETTRA. *Journal of synchrotron radiation*, *5*(3), pp.506-508.

Aubert, E. and Lecomte, C., 2007. Illustrated Fourier transforms for crystallography. *Journal of Applied Crystallography*, *40*(6), pp.1153-1165.

Bailey, A.L., Monck, M.A. & Cullis, P.R., 1997. pH-induced destabilization of lipid bilayers by a lipopeptide derived from influenza hemagglutinin. *Biochimica et biophysica acta*, 1324(2), pp.232–44. Available at: http://www.ncbi.nlm.nih.gov/pubmed/9092710.

Balali-Mood, K., Ashley, R.H., Hauß, T. and Bradshaw, J.P., 2005. Neutron diffraction reveals sequence-specific membrane insertion of pre-fibrillar islet amyloid polypeptide and inhibition by rifampicin. *FEBS letters*, *579*(5), pp.1143-1148.

Bangham, A.D. and Horne, R.W., 1964. Negative staining of phospholipids and their structural modification by surface-active agents as observed in the electron microscope. *Journal of Molecular Biology 8*: 660-668

Brink-van der Laan, E.V.D,, Killian, J.A, & Ben de Kruijff, B.D,, 2004. Nonbilayer lipids affect peripheral and integral membrane proteins via changes in the lateral pressure profile, *Biochimica et Biophysica Acta (BBA)* - Biomembranes, 1666, (Issues 1–2), pp.275-288, ISSN 0005-2736,

Cavallo, L., Kleinjung, J. & Fraternali, F., 2003. POPS: a fast algorithm for solvent accessible surface areas at atomic and residue level. *Nucleic Acids Research*, 31(13), pp.3364–3366. Available at: http://nar.oxfordjournals.org/lookup/doi/10.1093/nar/gkg601 [Accessed April 4, 2014].

Chen, F., Lee, M. & Huang, H.W., 2002. Sigmoidal Concentration Dependence of Antimicrobial Peptide Activities: A Case Study on Alamethicin. *Biophysical Journal*, 82(February), pp.908–914.

Chen, F.-Y., Lee, M.-T. & Huang, H.W., 2003. Evidence for membrane thinning effect as the mechanism for peptide-induced pore formation. *Biophysical Journal*, 84(6), pp.3751–8. Available at: http://www.ncbi.nlm.nih.gov/pubmed/12770881.

Chung, L., Lear, J.D. & DeGrado, W.F., 1992. Fluorescence Studies of the Secondary Structure and Orientation of a Model Ion Channel Peptide in Phospholipid Vesicles. *Biochemistry*, 31(28), pp.6608–16. Available at: http://www.ncbi.nlm.nih.gov/pubmed/1378757.

Chen, X., Sa'Adedin, F., Deme, B., Rao, P. and Bradshaw, J., 2013. Insertion of TAT peptide and perturbation of negatively charged model phospholipid bilayer revealed by neutron diffraction. *Biochimica et Biophysica Acta (BBA)-Biomembranes*, *1828*(8), pp.1982-1988.

Cullis, P.T. and De Kruijff, B., 1979. Lipid polymorphism and the functional roles of lipids in biological membranes. *Biochimica et Biophysica Acta (BBA)-Reviews on Biomembranes*, *559*(4), pp.399-420.

Darkes, M.J. and Bradshaw, J.P., 2000. Real-time swelling-series method improves the accuracy of lamellar neutron-diffraction data. *Acta Crystallographica Section D: Biological Crystallography*, *56*(1), pp.48-54.

Darkes, M.J., Harroun, T.A., Davies, S.M. and Bradshaw, J.P., 2002. The effect of fusion inhibitors on the phase behaviour of N-methylated dioleoylphosphatidylethanolamine. *Biochimica et Biophysica Acta (BBA)-Biomembranes*, *1561*(1), pp.119-128.

De Kruijff, B., 1997. Lipid polymorphism and biomembrane function. *Current opinion in chemical biology*, *1*(4), pp.564-569.

Dieckmann, Gregg R., James D. Lear, Qingfeng Zhong, Michael L. Klein, William F. DeGrado, and Kim A. Sharp. "Exploration of the structural features defining the conduction properties of a synthetic ion channel." *Biophysical Journal* 76, no. 2 (1999): 618-630.

Dowhan, W. and Bogdanov, M., 2002. Functional roles of lipids in membranes. In *New comprehensive biochemistry* (Vol. 36, pp. 1-35). Elsevier.

Ducarme, P., Thomas, a & Brasseur, R., 2000. The optimisation of the helix/helix interaction of a transmembrane dimer is improved by the IMPALA restraint field. *Biochimica et biophysica acta*, *1509*(1-2), pp.148–54.

Ellens, H., Siegel, D.P., Alford, D., Yeagle, P.L., Boni, L., Lis, L.J., Quinn, P.J. and Bentz, J., 1989. Membrane fusion and inverted phases. *Biochemistry*, *28*(9), pp.3692-3703.

Epand, R.M., 1998. Lipid polymorphism and protein–lipid interactions. *Biochimica et Biophysica Acta (BBA)-Reviews on Biomembranes*, *1376*(3), pp.353-368.

Epand, R.F., Schmitt, M.A., Gellman, S.H. and Epand, R.M., 2006. Role of membrane lipids in the mechanism of bacterial species selective toxicity by two α/β-antimicrobial peptides. *Biochimica et Biophysica Acta (BBA)-Biomembranes*, *1758*(9), pp.1343-1350.

Epand, R.M., Shai, Y., Segrest, J.P. and Anantharamiah, G.M., 1995. Mechanisms for the modulation of membrane bilayer properties by amphipathic helical peptides. *Biopolymers: Original Research on Biomolecules*, *37*(5), pp.319-338

Erbes, J., Czeslik, C., Hahn, W., Winter, R., Rappolt, M. and Rapp, G., 1994. On the existence of bicontinuous cubic phases in dioleoylphosphatidylethanolamine. *Berichte der Bunsengesellschaft für physikalische Chemie*, *98*(10), pp.1287-1293.

Ellens, H., Siegel, D.P., Alford, D., Yeagle, P.L., Boni, L., Lis, L.J., Quinn, P.J. and Bentz, J., 1989. Membrane fusion and inverted phases. *Biochemistry*, *28*(9), pp.3692-3703.

Fernandez, D.I.; Le Brun, A.P.; Whitwell, T.C.; Sani, M.A.; James, M.; Separovic, F. The antimicrobial peptide aurein 1.2 disrupts model membranes via the carpet mechanism. *Phys. Chem. Chem. Phys.* 2012, *14*, 15739–15751.

Gawrisch, K. and Holte, L.L., 1996. NMR investigations of non-lamellar phase promoters in the lamellar phase state. *Chemistry and physics of lipids*, *81*(2), pp.105-116.

Gazit, E.; Miller, I.R.; Biggin, P.C.; Sansom, M.S.P.; Shai, Y. Structure and orientation of the mammalian antibacterial peptide cecropin P1 within phospholipid membranes. *J. Mol. Biol.* 1996, *258*, 860–870.

Gennis, R.B. ed., 2013. *Biomembranes: molecular structure and function*. Springer Science & Business Media.

Gkeka, P. and Sarkisov, L., 2009. Spontaneous formation of a barrel-stave pore in a coarse-grained model of the synthetic LS3 peptide and a DPPC lipid bilayer. *The Journal of Physical Chemistry B*, *113*(1), pp.6-8.

Gruner, S.M., 1985. Intrinsic curvature hypothesis for biomembrane lipid composition: a role for nonbilayer lipids. *Proceedings of the National Academy of Sciences*, *82*(11), pp.3665-3669.

Gruner, S.M., 1989. Stability of lyotropic phases with curved interfaces. *The Journal of Physical Chemistry*, *93*(22), pp.7562-7570

Guo, J., Ping, Q., Jiang, G., Huang, L., & Tong, Y. (2003). Chitosan-coated liposomes: characterization and interaction with leuprolide. *International journal of pharmaceutics*, *260*(2), 167–173.

Hallock, K.J., Lee, D.K. and Ramamoorthy, A., 2003. MSI-78, an analogue of the magainin antimicrobial peptides, disrupts lipid bilayer structure via positive curvature strain. *Biophysical journal*, *84*(5), pp.3052-3060.

Haney, E. F., Nathoo, S., Vogel, H. J., & Prenner, E. J. (2010). Induction of non-lamellar lipid phases by antimicrobial peptides: a potential link to mode of action. *Chemistry and physics of lipids*, *163*(1), 82–93.

Harper, P. E., Mannock, D. A., Lewis, R. N., McElhaney, R. N., & Gruner, S. M. (2001). X-ray diffraction structures of some phosphatidylethanolamine lamellar and inverted hexagonal phases. *Biophysical journal*, *81*(5), 2693–2706.

Harroun, T.A., Katsaras, J. and Wassall, S.R., 2008. Cholesterol is found to reside in the center of a polyunsaturated lipid membrane. *Biochemistry*, *47*(27), pp.7090-7096.

Hayashi, H., Kono, K. & Takagishi, T., 1999. Temperature sensitization of liposomes using copolymers of N-isopropylacrylamide. *Bioconjugate Chemistry*, *10*(3), pp.412–8.

Hayashi, H., Kono, K. & Takagishi, T., 1996. Temperature-controlled release property of phospholipid vesicles bearing a thermo-sensitive polymer. *Biochimica et Biophysica Acta*, *1280*(1), pp.127–34.

Hayashi, H., Kono, K. & Takagishi, T., 1998. Temperature-dependent associating property of liposomes modified with a thermosensitive polymer. *Bioconjugate Chemistry*, 9(3), pp.382–9.

Heller, W. T., He, K., Ludtke, S. J., Harroun, T. A., & Huang, H. W. (1997). Effect of changing the size of lipid headgroup on peptide insertion into membranes. *Biophysical journal*, *73*(1), 239–244.

Helfrich, Wolfgang. "Elastic properties of lipid bilayers: theory and possible experiments." *Zeitschrift für Naturforschung c* 28, no. 11-12 (1973): 693-703.

Hickel, A., Danner-Pongratz, S., Amenitsch, H., Degovics, G., Rappolt, M., Lohner, K., & Pabst, G. (2008). Influence of antimicrobial peptides on the formation of nonlamellar lipid mesophases. *Biochimica et biophysica acta*, *1778*(10), 2325–2333.

Hönig, D. and Möbius, D., 1992. Reflectometry at the Brewster angle and Brewster angle microscopy at the air-water interface. *Thin solid films*, *210*, pp.64-68.

Hu, N.J., Bradshaw, J., Lauter, H., Buckingham, J., Solito, E. and Hofmann, A., 2008. Membrane-induced folding and structure of membrane-bound annexin A1 N-terminal peptides: implications for annexin-induced membrane aggregation. *Biophysical journal*, *94*(5), pp.1773-1781.

Huang, Y.B., He, L.Y., Jiang, H.Y. and Chen, Y.X., 2012. Role of helicity on the anticancer mechanism of action of cationic-helical peptides. *International Journal of Molecular Sciences*, *13*(6), pp.6849-6862.

Huang, T., Toraya, H., Blanton, T. & Wu, Y., 1993. X-ray Powder Diffraction Analysis of Silver Behenate, a Possible Low-Angle Diffraction Standard. *J. Appl. Cryst.*, *26*, pp. 180- 184.

Huang, H.W., 2000. Current Action of Antimicrobial Peptides: Two-State Model. *Biochemistry*, *39*(29), pp.8347–8352.

Hughes, AV, Goldar, A, Gerstenberg, MC, Roser, SJ & Bradshaw, J 2002, 'A hybrid SAM phospholipid approach to fabricating a free supported lipid bilayer', *Physical Chemistry Chemical Physics*, vol. 4, no. 11, pp. 2371-2378.

Israelachvili, J.N., Marčelja, S. and Horn, R.G., 1980. Physical principles of membrane organization. *Quarterly reviews of biophysics*, *13*(2), pp.121-200.

Israelachvili, J.N., Mitchell, D.J. and Ninham, B.W., 1976. Theory of self-assembly of hydrocarbon amphiphiles into micelles and bilayers. *Journal of the Chemical Society, Faraday Transactions 2: Molecular and Chemical Physics*, *72*, pp.1525-1568

Jäkel, C.E., Meschenmoser, K., Kim, Y., Weiher, H. and Schmidt-Wolf, I.G., 2012. Efficacy of a proapoptotic peptide towards cancer cells. *in vivo*, *26*(3), pp.419-426.

Jouhet, J., 2013. Importance of the hexagonal lipid phase in biological membrane organization. *Frontiers in plant science*, *4*, p.494.

Kitano, H., Maeda, Y., Takeuchi, S., Ieda, K. and Aizu, Y., 1994. Liposomes containing amphiphiles prepared by using a lipophilic chain transfer reagent: responsiveness to external stimuli. *Langmuir*, *10*(2), pp.403-406.

Klibanov, A.L., Maruyama, K., Torchilin, V.P. and Huang, L., 1990. Amphipathic polyethyleneglycols effectively prolong the circulation time of liposomes. *FEBS letters*, *268*(1), pp.235-237.

Kono, K., Henmi, A. & Takagishi, T., 1999. Temperature-controlled interaction of thermosensitive polymer-modified cationic liposomes with negatively charged phospholipid membranes. *Biochimica et Biophysica Acta (BBA) - Biomembranes*, *1421*(1), pp.183–97.

Koynova, Rumiana & Caffrey, Martin. (2002). An index of lipid phase diagrams. *Chemistry and physics of lipids*. *115*. 107-219. 10.1016/S0009-3084(01)00200-6.

Kulkarni, P.R., Jaydeep, D.Y. & Kumar, A.V., 2011. Liposomes: A novel drug delivery system. *International Journal of Current Pharmaceutical Research*, *3*(2), pp.10–18.

Laggner, P., and M. Kriechbaum. 1991. Phospholipid phase transitions: kinetics and structural mechanisms. *Chem. Phys. Lipids. 57*:121–145.

Landh, T., 1995. From entangled membranes to eclectic morphologies: cubic membranes as subcellular space organizers. *FEBS letters*, *369*(1), pp.13-17.

Langan, P. & Chen, J.C.-H., 2013. Seeing the chemistry in biology with neutron crystallography. *Physical chemistry chemical physics: PCCP*, *15*(33), pp.13705–12.

Last, N.B., Schlamadinger, D.E. and Miranker, A.D., 2013. A common landscape for membrane-active peptides. *Protein Science*, *22*(7), pp.870-882.

Le Pevelen, D.D., 2010. Small Molecule X-Ray Crystallography Theory and Workflow. Encyclopedia of Spectroscopy and Spectrometry (Second Edition). Elsevier Ltd

Lear, J.D., Schneider, J.P., Kienker, P.K. and DeGrado, W.F., 1997. Electrostatic effects on ion selectivity and rectification in designed ion channel peptides. *Journal of the American Chemical Society*, *119*(14), pp.3212-3217. Available at: http://pubs.acs.org/doi/abs/10.1021/ja9629672.

Lindblom, G. & Rilfors, L., 1992. Nonlamellar phases formed by membrane lipids. *Advances in Colloid and Interface Science*, *41*, pp.101–125.

Lindblom, G., Hauksson, J.B., Rilfors, L., Bergenståhl, B., Wieslander, Å. and Eriksson, P.O., 1993. Membrane lipid regulation in Acholeplasma laidlawii grown with saturated fatty acids. Biosynthesis of a triacylglucolipid forming reversed micelles. *Journal of Biological Chemistry*, *268*(22), pp.16198-16207.

Lindner, L.H., Eichhorn, M.E., Eibl, H., Teichert, N., Schmitt-Sody, M., Issels, R.D. and Dellian, M., 2004. Novel temperature-sensitive liposomes with prolonged circulation time. *Clinical Cancer Research*, *10*(6), pp.2168-2178.

Luzzati, V. & Husson, F., 1962. The structure of the liquid-crystalline phases of lipid-water systems. *The Journal of Cell Biology*, *12*, pp.207–219.

Marsh, D., 2013. *Handbook of Lipid Bilayers* 2nd ed., Boca Raton, FL. U.S.A.: CRC Press.

Matsuzaki, K., Sugishita, K.I., Ishibe, N., Ueha, M., Nakata, S., Miyajima, K. and Epand, R.M., 1998. Relationship of membrane curvature to the formation of pores by magainin 2. *Biochemistry*, *37*(34), pp.11856-11863.

Matsuzaki, K., Mitani, Y., Akada, K.Y., Murase, O., Yoneyama, S., Zasloff, M. and Miyajima, K., 1998. Mechanism of synergism between antimicrobial peptides magainin 2 and PGLa. *Biochemistry*, *37*(43), pp.15144-15153.

Meyer, O., Papahadjopoulos, D. & Leroux, J.C., 1998. Copolymers of N-isopropylacrylamide can trigger pH sensitivity to stable liposomes. *FEBS letters*, *421*(1), pp.61–4.

Morein, S., Andersson, A.S., Rilfors, L. and Lindblom, G., 1996. Wild-type Escherichia coli Cells Regulate the Membrane Lipid Composition in a "Window" between Gel and Non-lamellar Structures. *Journal of Biological Chemistry*, *271*(12), pp.6801-6809.

Mueller, P., Rudin, D.O., Ti Tien, H. and Wescott, W.C., 1962. Reconstitution of cell membrane structure in vitro and its transformation into an excitable system. *Nature*, *194*(4832), pp.979-980.

Nath, A., Atkins, W.M. & Sligar, S.G., 2007. Applications of Phospholipid Bilayer Nanodiscs in the Study of Membranes and Membrane Proteins. *Biochemistry*, *46*(8), pp.2059–2069.

Nagle, J.F., 1980. Theory of the main lipid bilayer phase transition. *Annual Review of Physical Chemistry*, *31*(1), pp.157-196.

Newns, D.M., Zhong, Q., Moore, P.B., Husslein, T., Pattnaik, P. and Klein, M.L., 2000. Molecular dynamics study of structure and gating of low molecular weight ion channels. *Parallel Computing*, *26*(7-8), pp.965-976.

Papo, N. and Shai, Y., 2003. New lytic peptides based on the D, L-amphipathic helix motif preferentially kill tumor cells compared to normal cells. *Biochemistry*, *42*(31), pp.9346-9354.

Petrascu, A.-M., Koch, M.H. & Gabriel, A., 1998. A beginners' guide to gas-filled proportional detectors with delay line readout. *Journal of Macromolecular Science*, Part B, *37*(4) pp. 463-483.

Polozov, I.V., Polozova, A.I., Tytler, E.M., Anantharamaiah, G.M., Segrest, J.P., Woolley, G.A. and Epand, R.M., 1997. Role of lipids in the permeabilization of membranes by class L amphipathic helical peptides. *Biochemistry*, *36*(30), pp.9237-9245.

Randa, H.S., Forrest, L.R., Voth, G.A. and Sansom, M.S., 1999. Molecular dynamics of synthetic leucine-serine ion channels in a phospholipid membrane. *Biophysical journal*, *77*(5), pp.2400-2410.

Rappolt, M., Hickel, A., Bringezu, F. and Lohner, K., 2003. Mechanism of the lamellar/inverse hexagonal phase transition examined by high resolution x-ray diffraction. *Biophysical journal*, *84*(5), pp.3111-3122.

Rappolt, M. & Pabst, G., 2008. Chapter 3: Flexibility and Structures of Fluid Bilayer Interfaces. In *Structure and Dynamics of Membranous Interfaces*. pp. 45–81.

Rathinakumar, R. and Wimley, W.C., 2008. Biomolecular engineering by combinatorial design and high-throughput screening: small, soluble peptides that permeabilize membranes. *Journal of the American Chemical Society*, *130*(30), pp.9849-9858.

Rausch JM, Marks JR, Rathinakumar R, Wimley WC. Beta-sheet pore-forming peptides selected from a rational combinatorial library: mechanism of pore formation in lipid vesicles and activity in biological membranes. *Biochemistry*. 2007;46:12124–12139

Regan, L., Degrado W, F., 1988. Characterisation of a helical protein designed from first principles.pdf. *Science*, 241(4868), pp.976–8.

Sa'adedin, F. & Bradshaw, J.P., 2010. A differential scanning calorimetry study of the effects and interactions of antimicrobial peptide LS3 on phosphatidylethanolamine bilayers. *Protein and Peptide Letters*, 17(11), pp.1345–50.

Sato, H. and Feix, J.B., 2006. Peptide–membrane interactions and mechanisms of membrane destruction by amphipathic α-helical antimicrobial peptides. *Biochimica et Biophysica Acta (BBA)-Biomembranes*, *1758*(9), pp.1245-1256.

Schoenborn, B.P., 2010. A history of neutrons in biology: the development of neutron protein crystallography at BNL and LANL. *Acta Crystallographica. Section D, Biological Crystallography*, 66(11), pp.1262–8.

Schweizer, F., 2009. Cationic amphiphilic peptides with cancer-selective toxicity. *European journal of pharmacology*, *625*(1-3), pp.190-194.

Seddon, J.M., 1990. Structure of the inverted hexagonal (HII) phase, and non-lamellar phase transitions of lipids. *Biochimica et Biophysica Acta (BBA)-Reviews on Biomembranes*, *1031*(1), pp.1-69.

Shai, Y. Mode of action of membrane active antimicrobial peptides. *Biopolymers* 2002, *66*, 236–248.

Shearman, G.C., Ces, O., Templer, R.H. and Seddon, J.M., 2006. Inverse lyotropic phases of lipids and membrane curvature. *Journal of Physics: Condensed Matter*, *18*(28), p.S1105.

Siegel, D.P. and Epand, R.M., 1997. The mechanism of lamellar-to-inverted hexagonal phase transitions in phosphatidylethanolamine: implications for membrane fusion mechanisms. *Biophysical journal*, *73*(6), pp.3089-3111

Siegel D. P. (1999). The modified stalk mechanism of lamellar/inverted phase transitions and its implications for membrane fusion. *Biophysical journal*, *76*(1 Pt 1), 291–313.

Siegel, D.P., Cherezov, V., Greathouse, D.V., Koeppe, R.E., Killian, J.A. and Caffrey, M., 2006. Transmembrane peptides stabilize inverted cubic phases in a biphasic length-dependent manner: implications for protein-induced membrane fusion. *Biophysical journal*, *90*(1), pp.200-211.

So, P. T. C., S. M. Gruner, and S. Erramilli. 1993. Pressure-induced topological phase transition in membranes. *Phys. Rev. Lett.* 70:3455–3458.

Templer, R.H., Castle, S.J., Curran, A.R., Rumbles, G. and Klug, D.R., 1999. Sensing isothermal changes in the lateral pressure in model membranes using di-pyrenyl phosphatidylcholine. *Faraday discussions*, *111*, pp.41-53.

Tenchov, B., R. Koynova, and G. Rapp. 1998. Accelerated formation of the cubic phases in phosphatidylethanolamine dispersions. *Biophys. J.* 75:853–866.

Tenchov, B.G., MacDonald, R.C. and Lentz, B.R., 2013. Fusion peptides promote formation of bilayer cubic phases in lipid dispersions. An x-ray diffraction study. *Biophysical journal*, *104*(5), pp.1029-1037.

Thomas, J.L., Barton, S.. W. & Tirrell, D.A., 1994. Membrane solubilization by a hydrophobic polyelectrolyte: surface activity and membrane binding. *Biophysical journal*, 67(3), pp.1101–6.

Tristram-Nagle, S. and Nagle, J.F., 2004. Lipid bilayers: thermodynamics, structure, fluctuations, and interactions. *Chemistry and physics of lipids*, *127*(1), pp.3-14.

Turner, D. C., & Gruner, S. M. (1992). X-ray diffraction reconstruction of the inverted hexagonal (H_{II}) phase in lipid-water systems. *Biochemistry*, *31*(5), 1340–1355.

Tytler, E.M., Segrest, J.P., Epand, R.M., Nie, S.Q., Epand, R.F., Mishra, V.K., Venkatachalapathi, Y.V. and Anantharamaiah, G.M., 1993. Reciprocal effects of apolipoprotein and lytic peptide analogs on membranes. Cross-sectional molecular shapes of amphipathic alpha helixes control membrane stability. *Journal of Biological Chemistry*, *268*(29), pp.22112-22118.

Vikström, S., Li, L. and Wieslander, Å., 2000. The nonbilayer/bilayer lipid balance in membranes: regulatory enzyme in Acholeplasma laidlawii is stimulated by metabolic phosphates, activator phospholipids, and double-stranded DNA. *Journal of Biological Chemistry*, *275*(13), pp.9296-9302.

Wieprecht, T., Dathe, M., Epand, R.M., Beyermann, M., Krause, E., Maloy, W.L., MacDonald, D.L. and Bienert, M., 1997. Influence of the angle subtended by the positively charged helix face on the membrane activity of amphipathic, antibacterial peptides. *Biochemistry*, *36*(42), pp.12869-12880.

Wimley, W.C., 2010. Describing the mechanism of antimicrobial peptide action with the interfacial activity model. *ACS chemical biology*, *5*(10), pp.905-917.

Yatvin, M.B., Kretz W., Horwitz B.A., and Shinitzky M., (1980). pH-Sensitive liposomes: possible clinical implications. *Science, 210*: 1253-1255.

Yeagle, P.L., 2004. The structure of biological membranes. CRC press

Zhong, Q., Moore, P.B., Newns, D.M. and Klein, M.L., 1998. Molecular dynamics study of the LS3 voltage-gated ion channel. *FEBS letters*, *427*(2), pp.267-270.